

UNIVERSITY OF NOVA GORICA
GRADUATE SCHOOL

**PHOTODEGRADATION OF ORGANIC POLLUTANTS IN
AQUEOUS SOLUTIONS CATALYZED BY IMMOBILIZED
TITANIUM DIOXIDE: NOVEL ROUTES TOWARDS HIGHER
EFFICIENCY**

Urh ČERNIGOJ

DISSERTATION

Mentors: doc. dr. Polonca Trebše
doc. dr. Urška Lavrenčič Štangar

Nova Gorica, 2007

ZAHVALA

ŽIVLJENJE je POT. In POT je CILJ.

CILJ je ŽIVETI.

Te vrstice so namenjene vsem, ki soustvarjate mojo pot. Tokrat ne ločujem med dobrimi in slabimi, bližnjimi in daljnimi, domačimi in tujimi, osebnimi in poslovnimi, ker življenje je vseobsegajoče in absolutno. Vsakdo od vas prispeva svoj delež.

Zato: HVALA VSEM.

POVZETEK

Hiter industrijski in ekonomski razvoj v zadnjih 200 letih in zanemarjanje njegovih negativnih vplivov na okolje je med drugim povzročilo tudi onesnaženje površinskih vod z različnimi organskimi in anorganskimi onesnaževali. Zato se v zadnjih desetletjih pojavlja vse večja potreba po čiščenju odpadnih in pitnih vod, pri čemer običajne metode čiščenja ne morejo odstraniti onesnaževal do te mere, da bi očiščena voda lahko ustrezala vse strožjim evropskim standardom, glede čistosti vode. Napredne oksidacijske metode (NOM) predstavljajo skupino tehnik, ki lahko razgradijo sicer kemijsko in mikrobiološko stabilne organske molekule. Namen teh metod je oksidacija in mineralizacija onesnaževal v CO_2 , H_2O , mineralne kisline in anorganske soli. TiO_2 fotokataliza spada v skupino NOM in je predmet intenzivnega raziskovanja v zadnjih 20 letih. V primerjavi z ostalimi NOM-mi ima nekaj očitnih prednosti, na drugi strani pa njene slabosti otežujejo prenos tehnologije iz laboratorija na industrijski nivo. Cilji predstavljenega doktorata so vezani na iskanje rešitev slabosti TiO_2 fotokatalize pri čiščenju organskih molekul v vodnih raztopinah: (1) priprava mezoporoznih tankih plasti iz TiO_2 in karakterizacija njihovih fotokatalitskih aktivnosti v primerjavi s standardnim TiO_2 ; (2) predlog metode za določanje kvantnega izkoristka pritrjenega TiO_2 ; (3) razvoj in izdelava novega laboratorijskega fotokatalitskega reaktorja za pritrjen TiO_2 , ki bi lahko deloval tudi s pomočjo sončne energije; (4) povezava TiO_2 fotokatalize z ozonacijo in preučevanje vpliva ozona na hitrost fotokatalitske razgradnje.

Če želimo doseči učinkovito fotokatalitsko razgradnjo s pomočjo pritrjenega katalizatorja, je potrebno pripraviti tanke plasti z veliko sposobnostjo absorpcije UV fotonov in hkrati z veliko površino in poroznostjo, s čimer povečamo hitrost reakcije med fotonastalimi reaktivnimi intermedii na površini katalizatorja in organskimi molekulami. Tanke TiO_2 prevleke sem pripravil s pomočjo sol-gel metode iz solov, ki so vsebovali titanov tetraizopropoksid kot prekursor. Z dodajanjem raznih neionskih surfaktantov (Brij 56, Pluronic F-127) sem želel ustvariti mezoporozno strukturo v nastalem materialu. Pred nanosom plasti TiO_2 sem preko natrijevega stekla najprej nanesele tanko plast SiO_2 in s tem preprečil neželjeno difuzijo natrijevih kationov v TiO_2 , do katere sicer prihaja med termično obdelavo vzorcev na $500\text{ }^\circ\text{C}$. Iz vseh uporabljenih solov sem pripravil homogene, nerazpokane in prosojne TiO_2 prevleke. Po enem nanosu (potapljanje in žganje) sem dobil tanke plasti, debele med 80 nm (brez surfaktanta) in 300 nm (s Pluronicom F-127). Optične lastnosti prevlek sem ovrednotil z UV-Vis spektroskopijo, kristalno strukturo vzorcev z rentgensko difrakcijo, površinsko morfologijo z mikroskopom na atomsko silo, poroznost materiala pa z merjenjem BET (Brunauer, Emmett in Teller) površine. Anatazna kristalna struktura predstavlja glavno kristalinično fazo v vseh termično obdelanih končnih vzorcih. Boljše absorpcijske lastnosti TiO_2 v UVA področju sem dosegel z večanjem debeline tankih plasti, to je z dodajanjem surfaktanta v sol ali s ponavljanjem ciklov nanašanja in žganja TiO_2 tankih plasti. Prisotnost surfaktanta v solu vpliva tudi na končno površinsko morfologijo vzorcev. Posnetki, dobljeni s pomočjo mikroskopa na atomsko silo, so nedvoumno potrdili, da je površina tankih plasti, pripravljenih brez dodanih surfaktantov, bolj ravna (izračunana hrapavost 0.95 nm) in slabše strukturirana kot površina tankih plasti, pripravljenih s pomočjo surfaktantov, pri katerih je površina bolj strukturirana z jasno izraženimi razmiki med posameznimi nanodelci in z vrednostjo hrapavosti 1.87 nm (z dodanim Pluronicom F-127). Sol-gel postopek, kjer je vključena tudi uporaba surfaktantov, upočasnjuje kristalizacijo anatazne kristalinične faze, kar se odraža tudi na manjših velikostih osnovnih nanodelcev (vse do 10 nm) in posledično verjetno tudi na večji površini vzorca. Posledica dodajanja Pluronica F-127 v sol je tudi 14 krat večja BET površina v primerjavi s površino vzorcev, pripravljenih brez surfaktanta.

Rezultati ovrednotenja tankih plasti TiO_2 , pripravljenega neposredno na natrijevo steklo in kasnejši termični obdelavi pri $500\text{ }^\circ\text{C}$, so potrdili difuzijo natrijevih ionov v polprevodniško plast, kar je posledično pomenilo negativen vpliv na kristalizacijo v anataz, ki je zelo pomemben za učinkovito uporabo TiO_2 kot fotokatalizatorja. S pomočjo rentgenske fotoelektronske spektroskopije smo zasledili relativno visoke koncentracije natrijevih ionov (okrog 5 masnih %) v prevlekah, nanešenih neposredno na natrijevo steklo. Tanke plasti, pripravljene na SiO_2 podlagi, so prikazovale boljše kristaliničnost in monodispergirane nanodelce (kar smo dokazali tako z rentgensko difrakcijo kot z mikroskopom na atomsko silo), večjo absorpcijo sevanja pod 370 nm (UV-Vis spektroskopija) in večjo fotokatalitsko učinkovitost v primerjavi z analognimi prevlekami, nanešenimi na natrijevo steklo. Efekt podlage je bil močnejše izražen pri tankih (manj kot 300 nm) kot pri debelejših nanosih (več kot 500 nm). Večjo debelino sem najenostavneje dosegel z vključevanjem surfaktantov v sol.

Fotokatalitsko aktivnost TiO_2 tankih plasti sem določeval v posebej za to konstruiranem pretočnem fotoreaktorju, napolnjenem z vodno raztopino azo barvila Plazmokorint B. Kot vir UV sevanja sem uporabil Xe svetilko s 355 nm zapornim filtrom, ki je tako prepuščala del UVA sevanja in pa vidno svetlobo. Prevleke sem potopil v obarvano raztopino in "in-situ" spremljal razbarvanje barvila s pomočjo spektrofotometra. Ugotovil sem, da je fotokatalitska učinkovitost pripravljenih prevlek odvisna od uporabe in tipa surfaktanta, debeline nanešene plasti in od vrste podlage. Fotokatalitska aktivnost narašča s številom plasti TiO_2 v vseh primerih. Pri primerjavi različnih prevlek z enakim številom plasti sem opazil, da dodatek surfaktanta Pluronic F-127 v sol pozitivno vpliva na fotokatalitsko učinkovitost. Uporaba omenjenega surfaktanta ima za posledico debelejšo in težje vzorce, kar se odraža na bolj učinkoviti absorpciji UVA sevanja. Pri primerjavi fotokatalitske aktivnosti na enoto mase nanešenega katalizatorja nisem ugotovil nobene razlike med prevlekami, pripravljenimi z ali brez dodanega surfaktanta v sol. To, da je masa TiO_2 najpomembnejši parameter, ki določa fotokatalitsko aktivnost tankih plasti, je nelogičen rezultat, glede na vse dobljene razlike, tako v BET površini kot v ostalih fizikalno-kemijskih lastnostih. Dobljeni rezultati potrjujejo pomembnost natančnih in poglobljenih analiz novo pripravljenih fotokatalitskih materialov, ker prehitro sklepanje in zaključevanje prepogosto vodi do zavajajočih informacij, kar je, še posebej v znanosti, zelo škodljivo.

Evropski standardi za določevanje fotokatalitskih lastnosti materialov trenutno še ne obstajajo, in tudi to je eden izmed razlogov, ki upočasnjuje prenos znanja iz laboratorijev v industrijsko uporabo. Zato so raziskave in sveže ideje na področju standardizacije v fotokatalizi zelo pomembne. Predlagal sem metodo določevanja fotokatalitske aktivnosti pritrjenih fotokatalizatorjev, ki temelji na merjenju fluorescence 7-hidroksikumarina, molekule, ki je eden od produktov reakcije med kumarinom in hidroksilnim radikalom. Metoda je enostavna in zaenkrat zanesljiva. Presenetljivo, razlike v dobljenih kvantnih izkoristkih pri valovni dolžini sevanja 365 nm med Degussa P25 in sol-gel tankimi plastmi so manjše, kot sem pričakoval. Čeprav so bile dobljene hitrosti razgradnje na enoto mase katalizatorja z Degussa P25 prevlekami 5 krat višje v primerjavi s hitrostmi, dobljenimi pri sol-gel prevlekah, je bil izračunan kvantni izkoristek pri Degussa P25 prevlekah samo 2 do 3 krat višji. Rezultate si lahko razlagamo z višjo absorpcijo UVA sevanja Degussa P25 prevlek na enoto mase fotokatalizatorja, kar bi lahko bila posledica boljše kristaliničnosti (več anatazne kristalinične faze) Degusse P25 v primerjavi s sol-gel prevlekami. Pokazal sem tudi, da kvantni izkoristek razgradnje pada z naraščajočo debelino TiO_2 prevlek, ne glede na tip tanke plasti. Pomembna pa je tudi ugotovitev, da določevanje samo kvantnega izkoristka ni primerno za standardizacijo neke fotokatalitske aktivne površine. Glavni problem je izključitev absorpcijskih lastnosti materiala na enoto mase pri računanju kvantnega izkoristka. Zato je vedno potrebno poleg kvantnega izkoristka podati tudi korelacijo med hitrostjo razgradnje in obsevano količino katalizatorja. Za popolno ovrednotenje opisane metode moram v prihodnosti izvesti še vrsto eksperimentov, kjer bi raziskal tudi vpliv pH, fluksa fotonov in koncentracije kumarina na hitrost razgradnje kumarina in na hitrost nastajanja 7-hidroksikumarina.

Glavna slabost fotokatalitskih reaktorjev, ki temeljijo na uporabi suspenzije TiO_2 , je končno ločevanje suspendiranih delcev iz sistema. Če je katalizator pritrjen na trdno podlago v obliki tanke plasti, se omenjenemu problemu izognemo. Ker pa reakcije v fotokatalizi potekajo na mejni površini med trdnim katalizatorjem in raztopino, in ker je le-ta površina v sistemih z pritrjenim katalizatorjem precej manjša kot v suspenzijah, je celokupna hitrost razgradnje ponavadi mnogo nižja v reaktorjih z pritrjenim katalizatorjem. Moj cilj je bil načrtovanje in izdelava laboratorijskega šaržnega reaktorja, ki bi združeval prednosti obeh tipov reaktorjev: (1) veliko razmerje med osvetljeno površino pritrjenega katalizatorja in med volumnom tekočine v reaktorju; (2) visoka stopnja mešanja (turbulentni pogoji); (3) možnost vgradnje reaktorja v posebne zbiralce sončnega sevanja (sestavljene parabolni kolektorji). Takim kriterijem zadošča steklena cev, v kateri je vgrajen vrteč nosilec, na katerem je okrog osrednje osi radialno postavljenih do 12 steklenih ploščic s pritrjenim katalizatorjem (Degussa P25 tanke plasti in prevleke, pripravljene po sol-gel postopku). Za ovrednotenje reaktorja sem spremljal razgradnjo vodnih raztopin 4-klorofenola s tekočinsko kromatografijo visoke ločljivosti. Kot vir UVA sevanja sem uporabil nizkotlačne živosrebrove svetilke s širokim emisijskim vrhom pri 355 nm. Optimalna koncentracija katalizatorja v fotokatalitskih eksperimentih je bila določena okrog 800 mg L^{-1} , ne glede na tip reaktorja (temelječ na suspenziji ali na pritrjenem TiO_2). Ugotovil sem tudi, da je hitrost razgradnje pri konfiguraciji novega reaktorja z 12 uporabljenimi ploščicami 3.8 krat višja v primerjavi s konfiguracijo z dvema pritrjenima

ploščicama, pri čemer je v obeh primerih površinska gostota pritrjenega TiO₂ primerljiva med sabo. Učinkovitost reaktorja s suspendiranim TiO₂ v primerjavi z reaktorjem z 12 ploščicami pritrjenega TiO₂ je le 1.8 krat boljša, kar je zelo vzpodbuden rezultat. Po ovrednotenju reaktorja sem uspešno preizkusil njegovo uporabnost tudi za razgradnjo različnih predstavnikov antibiotikov, fungicidov in pesticidov.

Čeprav so bile določene študije vpliva pH-ja in doze ozona na TiO₂ fotokatalizo že objavljene v znanstveni literaturi, celovita raziskava in pojasnitev vpliva obeh parametrov na učinkovitost fotokatalitske ozonacije (združena fotokataliza in ozonacija) še ni bila opravljena. Kot modelni spojini pri teh raziskavah sem izbral dva predstavnika neonikotinoidnih pesticidov, to je imidakloprid in tiakloprid, ker oba predstavljata veliko grožnjo za vodne ekosisteme in zato je učinkovita metoda razgradnje omenjenih spojin pomembna. V preliminarnih testih stabilnosti sem ugotovil večjo foto- in kemijsko obstojnost tiakloprida v primerjavi z imidaklopridom, zato sem se v nadaljnjih raziskavah posvetil le tiaklopridu. Za oceno primernosti različnih postopkov razgradnje in mineralizacije tiakloprida v vodi pri različnih vrednostih pH-ja in različnih pretokih ozona sem izvedel štiri različne tipe eksperimentov: ozonacijo in pa tri fotokemijske NOM-e (ozonacijo pod vplivom UV sevanja, fotokatalitsko ozonacijo in fotokatalizo). Pri vseh fotokemijskih eksperimentih sem uporabil vir svetlobe, ki oddaja večinoma UVA fotone. Fotokatalitska ozonacija se je pokazala kot najučinkovitejša metoda za razgradnjo tiakloprida, od vseh izvajanih eksperimentov, ne glede na vrednost pH-ja. Opazil sem sinergistični vpliv med ozonom in fotokatalizo v kislem in nevtralnem območju, pri bazičnih pogojih pa je sinergija izginila, kar je lahko posledica samorazpada ozona in pa zmanjšanja adsorpcije ozona na površino katalizatorja. Pri kislih pogojih sem opazil tudi oksidacijo kloridnega aniona v klorat(V), tako pri fotokatalitski ozonaciji kot pri navadni ozonaciji pod vplivom UV sevanja. Z nanašanjem konstant hitrosti razgradenj tiakloprida pri fotokatalitski ozonaciji in ozonaciji pod vplivom UV sevanja v odvisnosti od pretoka ozona sem nedvoumno dokazal sinergijski efekt ozona. Naklon linearnega prilagajanja krivulje eksperimentalnim podatkom v primeru fotokatalitske ozonacije je bil 1.5 krat večji od naklona v primeru navadne ozonacije pod vplivom UV sevanja, do česar ne bi prišlo v odsotnosti sinergije. Linearna odvisnost med hitrostjo razgradnje in pretokom ozona velja do pretokov ozona okrog 1 g h⁻¹, potem pa se hitrost razgradnje pri fotokatalitski ozonaciji počasi ustali.

V doktorski disertaciji sem predstavil in opisal svoje raziskave na področju odstranjevanja organskih molekul iz vode in nekaj načinov doseganja večjih učinkovitosti razgradnje molekul z uporabo TiO₂ fotokatalize. Tu pa se raziskave ne smejo ustaviti in vse opravljeno delo med izvajanjem podiplomskega študija bo dobilo pravo veljavo šele, ko bo pridobljeno znanje prenešeno iz laboratorija v praktično uporabo. Verjamem, da smo že dosegli stopnjo, ko lahko začnemo graditi in kasneje preizkušati pilotno napravo za čiščenje realnih vod, ki bo temeljila na dosežkih, opisanih v tem delu.

SUMMARY

All life forms on Earth depend upon water. The fast industrial development without taking care of all consequences has resulted in serious surface water pollution with organic and inorganic contaminants. There is an increased need for treating the polluted water and conventional wastewater treatment does not always satisfactorily cleanse it according to stricter and stricter European directives. In order to cleanse water of these extra-stable organics, so-called the AOPs have been developed. The aim of these methods is to mineralize the pollutants to CO₂, H₂O and mineral acids and salts. Titanium dioxide photocatalysis belongs to the group of AOPs and has been extensively studied over the last 20 years. Compared to the other methods it has some obvious advantages, but on the other hand there are also some drawbacks which retard its transmission to the industrial scale level. The goals of my PhD research were to overcome some of the most obvious problems in TiO₂ photocatalysis: (1) preparation of mesoporous TiO₂ films and characterisation of its photocatalytic activity compared to standard TiO₂; (2) proposal of a method for evaluating the quantum yield of immobilized TiO₂; (3) development and construction of a new laboratory-scale photocatalytic reactor for immobilized TiO₂, which could be used also in solar applications; and (4) coupling TiO₂ photocatalysis with ozonation and studying the effect of ozone on the kinetics of photocatalytic degradation.

For efficient photocatalysis, it is necessary to prepare TiO₂ films which are capable of harvesting incident light to a great extent, and at the same time films with a high surface area and porosity to increase the rate of reaction between photogenerated species and the pollutants. Thin TiO₂ films were prepared from a titanium isopropoxide precursor by sol-gel processing with or without various nonionic surfactant molecules (Brij 56 or Pluronic F-127). The detrimental effect of interdiffused sodium ions from the glass substrate during heat treatment was prevented by depositing a thin silica barrier layer prior to titania deposition. All used sols resulted in homogeneous and crack-free TiO₂ films with thicknesses from 80 (without Pluronic F-127) to as much as 300 nm (Pluronic F-127) after one dipping and heat-treatment (500 °C) cycle. Optical properties of the films were characterized by UV-Vis spectroscopy, crystalline structures by X-ray diffraction (XRD), porosity by measuring BET (Brunauer, Emmett and Teller) surface and the surface morphology by atomic force microscopy (AFM). The final coating consisted of a dominant anatase crystalline phase in all cases. Adding template to the sol or increasing the thickness of TiO₂ layer by repeating the dipping / heat treatment cycles resulted in higher absorption of UVA radiation. The presence of surfactant in the sol influenced also the morphology of film's surface. The AFM images undoubtedly showed that the surface of the non-templated film was ill-defined and flatter (RMS roughness: 0.95 nm) than the surface of the templated film, which was rougher (RMS roughness: 1.87 nm) and well-structured with clear interstices between the particles. A surfactant-assisted sol-gel process retarded crystallization of the anatase titania films, which resulted in smaller grain sizes (down to 10 nm) and presumably a larger active surface area. The consequence of adding Pluronic F-127 in the sol is also 14 times higher BET surface area compared to the sol without the surfactant.

The results regarding the preparation of the TiO₂ thin films on sodium glass support and heat-treated at 500 °C confirmed that sodium ions impurities had a negative influence on the crystallization of TiO₂, which is otherwise very important for photocatalysis utilizing the semiconducting properties of the material. Relatively high concentrations of sodium ions were proven in films deposited directly on the sodium glass support with X-ray photoelectron spectroscopy analysis. Films on soda-lime glass supports protected with a thin silica barrier layer exhibited better crystallization and monodisperse nanoparticles (XRD and AFM analyses), higher absorption of light below 370 nm (UV-Vis spectroscopy), and higher photocatalytic activity than those films deposited on bare glass supports. The effect of the substrate was more pronounced in thinner films (300 nm) than in thicker ones (1200 nm), which were achieved by adding a template to the sol.

A photocatalytic activity of the as-prepared films was studied in a tailor-made photoreactor filled with an aqueous solution of an azo dye Plasmocorinth B. Xe lamp with 355 nm cut-off filter was used as a light source. The films were immersed in its coloured solution and photobleaching was followed in-situ with the help of UV-VIS spectroscopy. The photocatalytic efficiency of the transparent films obtained by a dip-coating technique was found to depend strongly on the use and type of the surfactant added, on the thickness of the deposited layer and on the type of support. The photocatalytic activity was found to

increase with the number of TiO₂ layers in all cases. However, when comparing different films with the same number of TiO₂ layers, the addition of Pluronic F-127 surfactant in the sol was shown to have a significant positive effect on the photocatalytic activity. The use of this surfactant resulted in thicker and heavier films and consequently in the more efficient absorption of UVA radiation. When comparing the photocatalytic activities per amount of the deposited catalyst, it was found out that there was no difference between templated and nontemplated films. According to the differences in BET surface area and other physico-chemical characteristics of prepared TiO₂ films, it is illogical that the amount of titania is the decisive parameter defining the final photocatalytic activity. These results show the importance of careful and detailed evaluation of the new photocatalytic material, because concluding too fast often leads to misleading information, what is definitely not desired in the scientific world.

There is a lack of standard procedures to evaluate the photocatalytic characteristics of immobilized TiO₂, which hinders the transmission of photocatalysis from the laboratory to the industrial applications. Therefore standardization in photocatalysis has become an important issue. I proposed a method for the evaluation of photocatalytic activity of the immobilized photocatalyst based on the measuring the fluorescence of 7-hydroxycoumarin, which is one of the products between the coumarin and photocatalytically generated hydroxyl radicals. The method seems to be simple and relevant. Surprisingly, the differences in quantum yields at 365 nm between Degussa P25 films and sol-gel processed films were smaller than expected. Although Degussa P25 films showed approximately 5 times higher degradation rates compared to sol-gel processed films with the same amount of the catalyst, the quantum yield of Degussa P25 was only two to three times higher. The phenomena could be explained by higher absorbance of Degussa P25 films per amount of the catalyst, what could be the consequence of its more crystalline structure (higher amount of anatase per amount of TiO₂) compared to my sol-gel films. I also showed that the quantum yields at 365 nm decreased with the thickness of the TiO₂ regardless of the type of the film. But it was also found out that evaluation of the quantum yield is not the only relevant quantity for evaluation of different photocatalytic surfaces. The main problem of calculating the quantum yield is that no information on the absorption characteristics of the material per unit of mass of the catalyst is included within the calculation. Therefore it is always important not only to define the quantum yield, but also to define the correlation between the degradation rate and the irradiated amount of the catalyst. Additional experiments should be done regarding the investigation of the influence of pH, photon flux and concentration of coumarin on the degradation rate and on formation rate of 7-hydroxycoumarin.

The major drawback of slurry-type photoreactors is the final particle-fluid separation for the catalyst recycling. If a catalyst is immobilized on a rigid support as a thin film, such problem is avoided. Unfortunately, as the reaction occurs at the liquid-solid interface, the overall rate is much lower in thin-film reactors than in the corresponding slurry systems. Our goal was to design a laboratory-scale batch photoreactor which would combine the advantages of slurry and immobilized photocatalytic systems: (1) high ratio of illuminated immobilized catalyst surface to the volume of reaction liquid inside the reactor; (2) high degree of mixing; (3) possibility of installing the reactor into the compound parabolic collectors that utilize solar energy. The glass tube with the spinning basket inside (up to 12 glass slides of immobilized catalyst are positioned radially around the central axis) meets these criteria. Degussa P25 TiO₂ or sol-gel produced TiO₂ was immobilized on sodium glass support and the disappearance of 4-chlorophenol in water was monitored by HPLC analysis. Low-pressure mercury fluorescent lamps with a broad maximum at 355 nm were used as an UVA radiation source. The optimal catalyst concentration in the photocatalytic experiments was 800 mg L⁻¹ (regardless of the slurry or immobilized system). It was also found out that the configuration of a novel Carberry type photoreactor with 12 fastened TiO₂ slides shows nearly 3.8 times higher photocatalytic activity compared to the configuration with 2 TiO₂ slides (with the comparable surface density of immobilized TiO₂), serving as an approximation of a classic plain thin-film fixed-bed reactor. I compared immobilized and slurry TiO₂ systems. When 12 slides of immobilized TiO₂ were used, the reaction rate was only 1.8 times slower than in the slurry system, which is a very promising result. Also different members of antibiotics, fungicides and pesticides were efficiently degraded with the help of a novel photocatalytic reactor.

Although some studies concerning the effect of pH and ozone dosage on TiO₂ photocatalysis have already been published, no complete investigation and explanation of the effects of both parameters on photocatalytic ozonation (combination of photocatalysis and ozonation) has been carried out. Aqueous

solutions of neonicotinoid insecticides (thiacloprid and imidacloprid) were chosen as a degradation medium, since they exhibit a high threat for aquatic systems and it is of great importance to find an effective method for their elimination from the environment. In preliminary stability tests, thiacloprid showed higher photo- and chemical stability compared to imidacloprid, therefore its degradation was studied in detail. To assess the suitability of various treatments for degradation and mineralization of thiacloprid in water at different pH values and ozone dosages, I applied ozonation and three different photochemical advanced oxidation processes, namely ozonation under UV radiation, photocatalytic ozonation and photocatalysis. Light source emitting mainly in UVA range was applied in all three processes. The photocatalytic ozonation was found to be the most efficient process irrespective of pH. The synergistic effect of ozone and TiO₂ photocatalysis was noticed at acidic and neutral pH, but the synergism was lost at basic pH, probably due to faster self-decomposition of ozone and nonfavourable adsorption of ozone on titania surface under alkaline conditions. At acidic pH, also the oxidation of chloride anions to chlorate(V) was noticed in photocatalytic ozonation as well as in normal ozonation under UV radiation. By plotting the disappearance rate constants of thiacloprid degradation in photocatalytic ozonation and in ozonation under UV radiation as a function of the flow rate of ozone, the synergistic effect of ozone was undoubtedly proven. The slope of the linear fit in case of photocatalytic ozonation was considerably steeper than in case of normal ozonation under UV radiation, which would not happen in the absence of synergistic effect. The linearity in photocatalytic ozonation system was lost only at very high flow rates of ozone.

Some novel improvements towards achieving higher efficiency of TiO₂ photocatalysis have been shown and described throughout the thesis. In order to implement the research activities performed during my PhD, a transfer to an application scale level would round up the studied topics. I believe that such a stage has been reached, when a photocatalytic pilot plant based on the novel achievements could be designed and applied to the treatment of real waters.

LIST OF CONTENTS

POVZETEK	V
SUMMARY	IX
LIST OF CONTENTS	XIII
LIST OF TABLES	XV
LIST OF FIGURES	XVI
ABBREVIATIONS	XVIII
SYMBOLS	XIX
1 INTRODUCTION	1
2 PROMISING MODERN WATER PURIFICATION METHODS	3
2.1 Overview of advanced oxidation processes (AOPs)	3
2.1.1 H ₂ O ₂ /UV process	4
2.1.2 Photolysis of water	4
2.1.3 Homogeneous photocatalysis	5
2.1.4 Heterogeneous photocatalysis	5
2.1.5 Ozone based AOPs	5
2.2 TiO ₂ photocatalysis	7
2.2.1 Introduction	8
2.2.2 General remarks about titanium dioxide	9
2.2.3 Crystal structure and properties	10
2.2.4 TiO ₂ as a photocatalyst	10
2.2.5 Synthesis of photocatalytically active TiO ₂	11
2.2.5.1 Gas phase methods	11
2.2.5.2 Solution routes	11
2.2.5.2.1 Solution procedures other than sol-gel method (Carp et al., 2004)	11
2.2.5.2.2 Preparing TiO ₂ thin films via sol-gel procedure	12
2.2.6 Primary processes upon bandgap irradiation of TiO ₂ particles	13
2.2.7 Charge transfer mechanism and kinetics	14
2.2.8 Sorption of electron donors and acceptors	15
2.2.9 pH, temperature and photon flux effects on TiO ₂ photocatalysis	16
2.2.10 Formation of H ₂ O ₂ and secondary reactions with activated O ₂ species	17
2.2.11 Evaluation of photodegradation efficiency	17
2.3 Improving the performance of TiO ₂ photocatalysis	18
2.3.1 Structural and morphological aspects	18
2.3.2 Doping	19
2.3.3 Metal coating	19
2.3.4 Composite semiconductors	20
2.3.5 Comparison between TiO ₂ powders and TiO ₂ thin films	21
2.3.6 Photoreactor's engineering	21
2.3.7 Synergistic effects between photocatalysis and other AOPs	24
2.4 Photocatalytic treatment of POPs and heavy metals in water	24
2.4.1 Aliphatic and aromatic hydrocarbons	24
2.4.2 Nonhalogenated aromatic compounds	25
2.4.3 Chlorine-containing compounds	26
2.4.4 Nitrogen containing molecules	28
2.4.5 Degradation of pesticides and dyes	29
2.4.6 Noble metal recovery	30
2.4.7 Potable water applications	30
2.4.8 Solar photocatalytic treatment of real wastewaters	31
2.5 Advantages of TiO ₂ photocatalysis and objectives of the research work	31
3 MATERIALS AND METHODS	33
3.1 Chemicals	33
3.2 Preparation of sols	33
3.3 Deposition and calcination of the films	34

3.3.1	Sol-gel derived films.....	34
3.3.2	Degussa P25 films.....	34
3.4	Characterization of sol-gel derived TiO ₂ films.....	34
3.5	Degradation of organic molecules.....	35
3.5.1	Photocatalytic systems.....	35
3.5.2	Analytical procedures.....	35
4	RESULTS AND DISCUSSION.....	37
4.1	PART 1: Comparison of different characteristics of TiO ₂ films and their photocatalytic properties (Černigoj et al., 2006a, 2006b; Lavrenčič Štangar et al., 2006; unpublished results).....	37
4.1.1	State of the art.....	37
4.1.1.1	Using the surfactants in the preparation of sol-gel derived TiO ₂ films.....	37
4.1.1.2	The effect of sodium glass support on the quality of produced TiO ₂ films.....	38
4.1.1.3	Determination of quantum yields of photocatalytic surfaces.....	38
4.1.2	Experimental section.....	40
4.1.2.1	Preparation of TiO ₂ films.....	40
4.1.2.2	Photocatalytic degradation of an azo dye in water.....	40
4.1.2.3	Photocatalytic degradation of coumarin in water using monochromatic irradiation.....	40
4.1.2.4	Evaluation of quantum yield of different TiO ₂ films.....	41
4.1.3	Results and discussion.....	42
4.1.3.1	Optical properties and porosities of the TiO ₂ films.....	42
4.1.3.2	Structural and morphological properties.....	44
4.1.3.3	Photocatalytic activity.....	47
4.1.3.4	Evaluation of quantum yields of photocatalytically active surfaces.....	50
4.2	PART 2: Evaluation of a novel Carberry type photoreactor for the degradation of organic pollutants in water and studying the effect of ozone on TiO ₂ photocatalysis (Černigoj et al., 2007a, 2007b and unpublished results).....	57
4.2.1	State of the art.....	57
4.2.1.1	Photocatalytic reactors.....	57
4.2.1.2	The influence of ozone on TiO ₂ photocatalysis.....	58
4.2.2	Experimental part.....	60
4.2.2.1	Preparation of the catalyst.....	60
4.2.2.2	Photocatalytic cell and photoreactor.....	61
4.2.2.3	Degradation experiments.....	62
4.2.2.3.1	Evaluation of the CTP.....	62
4.2.2.3.2	Determination of neonicotinoid's stabilities in aqueous solutions in dark.....	62
4.2.2.3.3	Comparison of photocatalysis with other AOPs.....	62
4.2.3	Results and discussion.....	63
4.2.3.1	Photocatalytic degradation of 4-chlorophenol with different reactor's configurations.....	63
4.2.3.2	The influence of spinning on photocatalytic activity.....	64
4.2.3.3	The effect of the amount of TiO ₂ on photocatalytic activity.....	65
4.2.3.4	Optimizing the configuration of the photocatalytic system.....	66
4.2.3.5	Comparison of photocatalytic activities between Degussa P25 and sol-gel thin films.....	67
4.2.3.6	Suitability of the reactor for the degradation of POPs other than 4-chlorophenol.....	68
4.2.3.7	Stability of two neonicotinoid pesticides in aqueous solutions.....	71
4.2.3.8	Degradation of thiacloprid by O ₃ , O ₃ /UV, O ₃ /TiO ₂ /UV and O ₂ /TiO ₂ /UV.....	72
4.2.3.9	Effect of ozone dosage on the degradation of thiacloprid.....	77
5	CONCLUSIONS.....	79
6	REFERENCES.....	81

LIST OF TABLES

Table 1: Some drawbacks and possible solutions of TiO ₂ photocatalysis.....	32
Table 2: Composition of titania sols.....	34
Table 3: The measured masses, calculated surface densities, macroscopic densities and particle sizes of four-layered titania films; calculated RMS roughnesses of single-layered titania films.....	43
Table 4: The calculated half-lives and rate constants of photodecolorisation of aqueous Plasmocorinth B solutions using calcined TiO ₂ films (1 and 4 layers)	48
Table 5: Different parameters of TiO ₂ films, needed for the calculation of quantum yield	51
Table 6: Characteristics of different photocatalytic systems and calculated half-lives of 4-chlorophenol for each configuration.....	60
Table 7: Chemical structures of five treated organic molecules and the results regarding their disappearance and mineralization during photocatalytic and photolytic experiments.....	70
Table 8: Comparison of stabilities of thiacloprid and imidacloprid in aqueous solutions at different experimental conditions	71
Table 9: The influence of pH on formation of nitrate(V). The flow rate of ozone was 0.11 g h ⁻¹	76

LIST OF FIGURES

Figure 1: Scheme of reactions of aqueous ozone. Ozone reacts either directly with a solute <i>M</i> or it reacts with HO ⁻ or M to initiate a radical-type chain reaction (Hoigne, 1998).....	7
Figure 2: Change in the electronic structure of a semiconductor as the number of monomeric units present increases from unity to clusters of more than 2000 (Mills and Le Hunte, 1997).....	8
Figure 3: Band positions of common <i>n</i> -type semiconductors used in photocatalysis and the redox potentials of the H ₂ O/OH ⁻ and O ₂ /HO ₂ ⁻ couple at pH 0 (Mills et al., 1993: 418)	9
Figure 4: Crystal structures of A: rutile; B: anatase; C: brookite	10
Figure 5: A: Schematic presentation of the band energetic model of the overall process of semiconductor photocatalysis for water purification (Mills et al., 1993); B: Band structure in a semiconductor (up) before contact with an electrolyte and (down) in contact with electrolyte (Fox and Dulay, 1993)	13
Figure 6: Secondary reactions with activated oxygen species in photocatalytic mechanism (Hofmann et al., 1995)	17
Figure 7: The effect of metal nanocontacts on photocatalytic processes (Wang et al., 2004)	20
Figure 8: Energy diagram showing the coupling of various semiconductors. Top: Vectorial electron transfer from the light activated semiconductor to the non-activated; Bottom: both semiconductors are activated and vectorial displacement of electrons and holes (Carp et al., 2004)	20
Figure 9: Types of ideal chemical reactors. A: batch reactor; B: mixed flow reactor; C: plug flow reactor; D: batch recirculation reactor	22
Figure 10: Different types of solar photocatalytic reactors; A: PTR; B: TFFBR; C: CPCR (all three Malato et al., 2007); D: DSSR (Bahnemann, 2004).....	23
Figure 11: Initial steps in the photocatalytic degradation of 4-chlorophenol (Theurich et al., 1996).....	28
Figure 12: A: The scheme of continuous flow photocatalytic cell with a thin-film TiO ₂ catalyst deposited on a microscope glass slide: front view (left) and top view of the reactor (right); B: the photos of continuous flow reactor; C: chemical structure of Plasmocorinth B azo dye; D: chemical structure of coumarin; E: chemical structure of 7-hydroxycoumarin (7OHC)	41
Figure 13: A: UV-Vis transmittance spectra of different one-sided TiO ₂ films prepared by high-temperature sol-gel processing; B: The influence of number of TiO ₂ layers on thicknesses of the titania films	42
Figure 14: A: XRD patterns of TiO ₂ film powder samples; B and C: four-layered thin film samples.....	45
Figure 15: AFM 2- and 3D images of the surface of TiO ₂ films; A: C1N, B: C1S and C: D1S.....	46
Figure 16: A: The influence of addition of surfactants in sols on photodecolorisation of Plasmocorinth B solution with one-layered TiO ₂ films deposited on SiO ₂ support. B: The influence of the support on photodecolorisation of Plasmocorinth B solution with different four-layered films.....	49
Figure 17: The influence of irradiated amount of titania on the rate constant for the photodecolorisation of aqueous solution of Plasmocorinth B; SiO ₂ support	49
Figure 18: Optical properties and evaluation of the intrinsic absorption of TiO ₂ films; A: Degussa P25 film; B: C7S film	51
Figure 19: Photocatalytic experiments with coumarin; A: degradation of coumarin, monitored by HPLC-UV detector at 275 nm; B: formation of 7OHC, monitored by HPLC-FLD at 456 nm.....	52
Figure 20: A: A correlation between the formation rates of 7OHC, evaluated with HPLC-FLD, and degradation rates of coumarin, evaluated with HPLC-UV; B: Fluorescence measurements (spectrofluorimeter) of irradiated solution of coumarin; catalyst Degussa P25 P2 film	53
Figure 21: A correlation between formation rates of 7OHC and the absorption (in %) at 365 nm by the TiO ₂ films	53
Figure 22: Calculated Φ_{365} for A: degradation of coumarin; B: formation of 7OHC	55
Figure 23: Top: the photocatalytic cell with the spinning basket inside; A: the spinning basket is placed into the tube with an inner diameter of 40 mm; B: longitudinal section of the spinning basket; C: cross-section of the spinning basket. Bottom: Photos of photocatalytic cell (left), spinning basket with immobilized catalyst (middle) and of the upper part of a photoreactor (right)	61
Figure 24: Photocatalytic degradation of 4-chlorophenol; spinning rate 100 rpm; configurations from Table 6	64

Figure 25: Photocatalytic degradation of 4-chlorophenol; configuration H from Table 6; (□) constant purging with O ₂ during the irradiation, spinning rate 100 rpm; (o) purging with O ₂ for 10 s every 5 min, spinning rate 100 rpm; (Δ) purging with O ₂ for 10 s every 5 min, no rotation	65
Figure 26: Graphical comparison between the most efficient slurry and immobilized configurations	66
Figure 27: The influence of the amount of the irradiated catalyst on half-life of 4-chlorophenol; A: half-life in the range 0-14 min; B: half-life in the range 0-50 min; (□) the configurations from A to E in Table 1; (o) the configurations from F to J in Table 6; (Δ) the configurations from N to R in Table 667	667
Figure 28: Photolytic (A) and photocatalytic (B) degradation and mineralization of aqueous solution of sulfamethoxazole (15 mg L ⁻¹)	69
Figure 29: UV spectra of aqueous solutions (10.5 mg L ⁻¹) of different POPs	69
Figure 30: Degradation of thiacloprid with different AOPs at pH 8.1; A – disappearance of thiacloprid; B – formation of chloride; C – formation of sulphate(VI); D – formation of nitrate(V). The flow rate of ozone was 0.11 g h ⁻¹	72
Figure 31: The influence of pH on disappearance rate constants of thiacloprid (A) and on formation rate constants of chloride (B) and sulphate(VI) (C). The flow rate of ozone was 0.11 g h ⁻¹	73
Figure 32: The influence of pH to the synergistic effect of ozone on O ₂ /TiO ₂ /UV. The flow rate of ozone was 0.11 g h ⁻¹	74
Figure 33: A: Evolution of inorganic anions from thiacloprid solution in deionised water after 25 min and 110 min of irradiation. The flow rate of ozone was 1.4 g h ⁻¹ . B: Evolution of chloride during the O ₃ /TiO ₂ /UV at different pHs and further disappearance of chloride in acidic solution. The flow rate of ozone was 0.11 g h ⁻¹	75
Figure 34: Monitoring of TOC, TN and evolution of nitrate(V) during the O ₃ /TiO ₂ /UV treatment at pH = 11.0. The flow rate of ozone was 1.4 g h ⁻¹	76
Figure 35: The influence of the flow rate of ozone on disappearance rate constants of thiacloprid at pH 8.1.	77

ABBREVIATIONS

AOP = advanced oxidation process
POP = persistent organic pollutant
VUV radiation = vacuum ultraviolet radiation
VOC = volatile organic compound
CB = conduction band
VB = valence band
CVD = chemical vapour deposition
PVD = physical vapour deposition
LH kinetic model = Langmuir-Hinshelwood kinetic model
CPCR = compound parabolic collecting reactor
TFFBR = thin-film-fixed-bed reactor
DSSR = double skin sheet reactor
PTR = parabolic trough reactor
PEG = polyethylene glycol
Si(OEt)₄ = tetraethoxysilane
AcOH = acetic acid
MeOCH₂CH₂OH = 2-methoxyethanol
Ti(OiPr)₄ = titanium(IV) isopropoxide
EAA = ethyl acetoacetate
EO = ethylene oxide
PO = propylene oxide
BET surface = Brunauer, Emmett and Teller surface
7OHC = 7-hydroxycoumarin
PSH = photo-induced superhydrophilicity
CTP = Carberry type photoreactor
O₂/UV = irradiation of oxygenated solutions in the absence of TiO₂
O₃ = ozonation
O₃/UV = ozonation, coupled with UV radiation
O₂/TiO₂/UV = photocatalysis
O₃/TiO₂/UV = photocatalytic ozonation
LD₅₀ = median lethal dose
IC = ionic chromatography
AFM = atomic force microscopy
XPS = X-ray Photoelectron Spectroscopy
TOC = total organic carbon
TN = total nitrogen

SYMBOLS

ε = molar extinction coefficient
 λ = wavelength
 E^0 = standard redox potential
 $h\nu$ = the symbol of a photon of a certain energy
 N = number of monomeric units in the semiconductor particle
 e^-_{aq} = hydrated electron
 E_g = bandgap energy
 K_H = Henry's constant
 e^-_{cb} = conduction band electron
 h^+_{vb} = valence band hole
 e^-_{tr} = trapped electron
 h^+_{tr} = trapped hole
 r_{LH} = rate of product formation
 c = concentration of the substrate
 K = dark adsorption equilibrium constant
 K' = apparent adsorption constant
 k = reaction rate constant
 θ = surface coverage
 Φ = quantum yield
 ζ = photonic efficiency
 ζ_r = relative photonic efficiency
 N_{mol} = number of molecules
 N_{ph} = number of photons
 pH_{zpc} = pH at isoelectric point
 E_{vb} = redox potential of valence band
 T_B = transmittance for a film deposited on the both sides of the glass slide
 T_C = transmittance for a film deposited on the one side of the glass slide
 θ (XRD) = diffraction angle in degree
 β = the full width at half maximum of XRD signal in radians corrected for the instrumental broadening
 K (XRD) = constant (0.9, assuming no crystal distortion in the lattice)
 L = grain size (effective size of coherently scattering domains)
 Φ_p^{abs} = absorbed photon flow at 365 nm
 Φ_{365} = quantum yield at 365 nm
 k' = pseudo first- order reaction rate constant
 k'' = second-order reaction rate constant
 $t_{1/2}$ = half-life of a molecule
 A = absorption
 R = reflectance
 T = transmittance

1 INTRODUCTION

All life forms on Earth depend on water. All terrestrial living beings depend on fresh water. However, over 97 % of the world's water is seawater and as such it does not support life on land. Three-quarters of fresh water are trapped in glaciers and ice caps. Lakes and rivers, the two main sources of drinking water, constitute less than 0.01 % of the total water supply (Baird, 1999: 461). The continued exponential growth in human population has created a corresponding increase in the demand for earth's limited supply of freshwater. At the same time, the fast industrial development and mankind's indifference have resulted in serious surface water pollution with organic and inorganic contaminants.

Protecting the integrity of our water resources is one of the most essential environmental issues of the 21st century. Recent decades have brought increasing concerns for potential adverse human and ecological health effects resulting from the production, use and disposal of numerous chemicals that offer improvements in industry, agriculture, medical treatment and even common household conveniences. Research has shown that many such compounds can enter the environment, disperse and persist to a greater extent than first anticipated. For example, different industrial byproducts are released through regulated and unregulated industrial discharges to water and air resources. Since the release of some chemicals results in an increase of the environmental risk, the mankind's goal should not be to discharge them into the environment but at least treat them in the way that they do not have adverse impacts on the environment into which they are released. Hence a broad field of research emerges, i.e. wastewater technology, which deals with purification of water.

According to the origin of the water from natural cycles and depending on the water quality requirements, the market for water processing mainly covers three important sectors: the treatment technologies of drinking water, wastewater and industrial water. A wide variety of processing routes exist by which water can be treated in order to satisfy different specifications. The detailed design of the appropriate treatment system depends mainly on the raw water composition and on economic considerations.

Conventional wastewater treatment is usually a combination of physical and biological processes designed to remove organic matter from solution (Hammer M. and Hammer M. Jr., 1996: 351). The first step in conventional treatment is a sedimentation process, where the settled and floated organic matter is removed. Secondary treatment is biological treatment. The cultures of microorganisms (activated sludge) metabolize the organic matter from the wastewater resulting in the flocculation of organic colloids. A few municipalities employ tertiary (advanced or chemical) wastewater treatment. In the tertiary treatment, specific chemicals are removed from the partially already purified water before final disinfection. Depending upon the nature of the pollutant, tertiary treatment can include some of the chemical and physical processes, such as adsorption of nonpolar organic molecules onto activated carbon, removal of phosphate by its precipitation as the calcium salt, heavy metal removal by the addition of hydroxide or sulfide, iron removal by aeration at a high pH to oxidize it to its insoluble Fe^{3+} state, desalination by reverse osmosis, electrodialysis or ion exchange.

The conventional purification of drinking water follows similar stages of purification as wastewater treatment, but the quality of outcoming water must meet much more strict standards compared to wastewater treatment not to cause any health and aesthetic problems to the water users (Baird, 1999: 461). Aeration is commonly used as the first step in purification of drinking water to remove dissolved gases, such as H_2S , organosulphur compounds and other volatile organic compounds. Aeration is followed by settling and precipitation of colloidal particles, which is achieved by adding the Al- or Fe-salts, forming gelatinous hydroxides at neutral and alkaline pH values, which physically incorporate the colloidal particles and form a removable precipitate. If the water contains too high concentration of Ca^{2+} and Mg^{2+} , it should be softened by adding Na_2CO_3 or NaOH as the next step of purification. To get rid of harmful bacteria and viruses from drinking water, disinfection is applied as a last step of purification. Chlorination, UVC radiation or ozonation are the most often processes used.

Sectors like the petrochemical, pharmaceutical, textile, agricultural, food and chemical industries all produce waste effluents contaminated with organic compounds, such as aromatics, haloaromatics, aliphatics, dyes, dioxins and a wide range of other polluting materials. Many of these compounds are

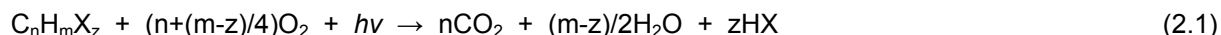
extremely toxic and conventional water purification methods often do not successfully deal with hazardous effluents containing persistent organic pollutants (POPs). On the other hand, drinking water is being increasingly micropolluted by fertilizers, pesticides, thus producing the demand for new and efficient treatment technologies. European directives, especially the Water Framework Directive (Directive 2000/60/EC), Urban Waste Water Directive (91/271/EEC), the Integrated Pollution Prevention and Control Directive (96/61/EC), the Dangerous Substances Directive (67/548/EEC) have all emphasized the importance of developing new effective and environmentally acceptable water treatment technologies (Robertson et al., 2005: 368).

When we have to deal with a new wastewater technology, we have to face out with different kinds of pollutants present in the environment. It is obvious that finding an appropriate method for the efficient removal of all of them at the same time is impossible. An efficient and cheap technique, which would be useful for the removal of a majority of the compounds from diverse group of POPs (fused, aromatic, heterocyclic, halogenated, etc.) would be considered a big success. However, assesment and commercialization of new purification technology is not an easy task. First, we have to evaluate if the system efficiently deals with desired pollutants on the laboratory scale level. For example, if the technique is intended for removal of the POPs from drinking water, the molecules which are often found in drinking water (such as pesticides, drugs, surfactants, colours) are the right choice for testing the suitability of the novel technique. If the degradation rate is too slow to be acceptable for commercial applications, the improvements of the efficiency of the process should be found out prior the commercial application. Only then it is reasonable to design larger systems (pilot plants), where the real water is treated and the possibility of introducing such plants into commercialized products is evaluated.

2 PROMISING MODERN WATER PURIFICATION METHODS

2.1 Overview of advanced oxidation processes (AOPs)

In order to cleanse water of these extra-stable organics, so-called AOPs have been developed. The aim of these methods is to mineralize the pollutants to CO₂, H₂O and mineral acids and salts (2.1).



The underlying oxidative reaction mechanisms are basically imitations of natural processes that take place on Earth. Most AOPs are ambient-temperature processes that use energy to produce highly reactive intermediates of high oxidizing or reducing potential, which then attack and destroy the target compounds. The majority of AOPs involves the generation of significant amounts of the hydroxyl radicals (HO[•]), which is very effective, nonselective oxidizing agent in aqueous solution (E° = 2.80 V). It is the second of the most violent oxidants and can attack virtually all organic compounds. It reacts 10⁶-10¹² times more rapidly than alternative oxidants such as ozone. It has electrophilic properties and its reactions with appropriate substrate molecules are kinetically controlled, usually exhibiting very high second order rate constants, which are often close to the diffusion-controlled limit. The hydroxyl radical can initiate the oxidation of a molecule by three possible mechanisms (Legrini et al., 1993):

- Extraction of a hydrogen atom from the organic molecule. The products are water and a reactive organic radical (2.2).



- Electron transfer to hydroxyl radicals constitutes another mechanism of oxidative degradation (2.3).



- Addition to one atom of a multiple bond as it often happens in aromatic structures (2.4).



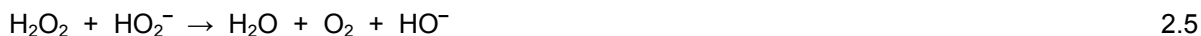
Since the generation of OH[•] radicals is a relatively expensive process and as the total destruction of the pollutant is not always required, AOPs are especially useful in two cases: (i) as a pre-treatment to transform recalcitrant pollutants in more biodegradable compounds; or (ii) as a post-treatment, to polish waters before their discharge to the receptor bodies. The main idea of the combination is the use of a more expensive technology only in the first or final step of the treatment, to reduce costs (Litter, 2005: 330).

Many innovative technologies have been proposed for treating liquid or gaseous wastes and are currently under intensive investigation, for example catalytic oxidation (Levec and Pintar, 1995), sonolysis (Ince et al., 2001), X-ray irradiation (Chitose et al., 2003), Fenton chemistry (Gogate and Pandit, 2004) and many other remediation technologies. A lot of them involve also UV radiation energy as an important step in synthesis of OH[•] radicals, because UV energy often appreciably increases the reaction rate of AOPs in comparison with the same technology in the absence of illumination. The photo-activated chemical reactions are characterized by a free radical mechanism initiated by the interaction of photons of a proper energy level with the molecules or chemical species present in the solution, in absence or presence of the catalyst. The UV spectral range is usually divided into four regions: UVA or near-UV radiation with wavelengths (λ) between 315 and 400 nm; UVB radiation (280 nm < λ < 315 nm); UVC radiation (190 nm < λ < 280 nm); and vacuum ultraviolet (VUV) radiation (λ < 190 nm). As a source of the photons, high-pressure mercury or xenon arc lamps, with good emission in the near-UV range, can be used. Some applications require UVC irradiation and in this case germicide lamps are easily available. Sunlight irradiation may be used in some applications, but it must be taken into account that only 3-5 % of UV radiation is present in the solar spectrum. If solar light can be used, a cosequent saving of electrical power

will be achieved. AOPs, based also on usage of UV radiation, are called photochemical AOPs (Legrini et al., 1993). Some of the photochemical AOPs and ozonation based AOPs are shortly described below.

2.1.1 H₂O₂/UV process

Hydrogen peroxide (H₂O₂) is a weak acid, a powerful oxidant ($E^0 = 1.78$ V at pH 0) and an unstable compound that disproportionates with a maximal rate at the pH of its pK_a (2.5) (Litter, 2005: 335). H₂O₂ has been widely used in the removal of low levels of pollutants from wastewaters (chlorine, nitrites, sulphites, hypochlorites) and as a disinfectant (Neyens and Baeyens, 2003). However, low reaction rates make its use in the treatment of high levels of refractory pollutants ineffective.



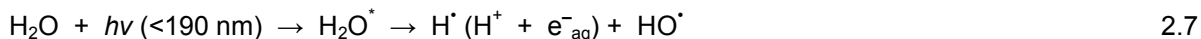
The oxidizing power of H₂O₂ can be sensibly improved by cleavage of O-O bond, generating HO· radicals. The mechanism most commonly accepted for the photolysis of H₂O₂ is the cleavage of the molecule into hydroxyl radicals with a quantum yield of two HO· radicals formed per quantum of radiation absorbed (2.6). Wavelengths lower than 280 nm must be used to efficiently cleave the O-O bond in H₂O₂, therefore only low- or medium-pressure mercury lamps are suitable for this process. The rate of photolysis of aqueous H₂O₂ has been found to be pH dependent and increases when more alkaline conditions are used. This might be primarily due to the higher molar absorption coefficient of the peroxide anion at 253.7 nm.



The use of H₂O₂ as an oxidant brings a number of advantages in comparison to other methods of chemical or photochemical water treatment: commercial availability of the oxidant, thermal stability and storage on-site, infinite solubility in water, no mass-transfer problems associated with gases and simple operation procedure. On the contrary, there are also some obstacles. The rate of oxidation of the contaminant is limited by the rate of formation of hydroxyl radicals and H₂O₂ has a small molar absorption coefficient at 253.7 nm ($\epsilon = 18.6 \text{ M}^{-1} \text{ cm}^{-1}$) and even smaller above this value (Legrini et al., 1993). The solar spectrum is consequently useless for H₂O₂ photolysis. Besides low ϵ of H₂O₂, also other species can absorb photons in UVC range and they can act as radiation filters. High concentrations of H₂O₂ would theoretically solve the problem of its low absorption characteristics, but this is not valid, because H₂O₂ acts as a sink for generated HO· radicals at high concentrations.

2.1.2 Photolysis of water

The homolysis of water molecules by VUV radiation leads to the formation of hydrogen atoms and hydroxyl radicals as major primary species (2.7). In addition, small amounts of hydrated electrons (e^-_{aq}) are generated which are immediately trapped by dissolved molecular oxygen with the formation of superoxide radical anions ($\text{O}_2^{\cdot-}$). Similarly, hydrogen atoms are immediately transformed into hydroperoxyl radicals (HO_2^\cdot) by fast reaction with dissolved O₂ (Oppenlander, 2003: 126). In aerated solutions, HO_2^\cdot and ($\text{O}_2^{\cdot-}$) are rapidly generated from the primary active species (2.8 and 2.9). The generated oxidants (HO^\cdot , HO_2^\cdot and $\text{O}_2^{\cdot-}$) and reductants (H^\cdot , e^-_{aq} , HO_2^\cdot and $\text{O}_2^{\cdot-}$) make possible simultaneous reductions and oxidations in the chemical system.



The important advantage of VUV process is that there is no need for additional chemicals or catalysts besides water and an appropriate lamp, generally xenon excimer lamp with $\lambda_{\text{exc}} = 172$ nm. On the other

hand, these lamps are expensive and therefore VUV process is only in the research stage of development for water treatment. The other drawbacks of VUV process are (i) expensive, transparent reactor material (special quartz glass) and (ii) that absorption of radiation occurs in very thin film of treated solution due to high absorption coefficients of water and organic pollutants at λ below 190 nm.

2.1.3 Homogeneous photocatalysis

Fenton's well-known experiments at the end of the 19th century demonstrated that solutions of H₂O₂ and Fe²⁺ salts were able to oxidize tartaric and malic acids as well as other organic compounds (2.10) (Fenton, 1894). At pH below 3, the reaction system is autocatalytic, because Fe³⁺ decomposes H₂O₂ in O₂ and H₂O through a chain mechanism, simultaneously reducing the Fe³⁺ to Fe²⁺ (Litter, 2005: 344). But the back reaction is much slower compared to 2.10 and in the presence of an excess of peroxide, the concentration of Fe²⁺ is small in comparison with that of Fe³⁺ and the whole reaction is slower if no additional Fe²⁺ is added.



Homogeneous photocatalytic AOPs in aqueous phase are mainly based on the photo-Fenton reaction (2.10, 2.11) using Fe²⁺ salts and H₂O₂ in mildly acidic solutions (pH between 2.5 and 5). These processes utilize the photoreduction of produced Fe³⁺ ions and its complexes. In contrast to the Fenton reaction, Fe²⁺ ion recycles continuously by irradiation of Fe³⁺-H₂O complexes and therefore it is not depleted during the course of the oxidation reaction. The dominant Fe(OH)²⁺ complex absorbs in the UV/Vis range below 400 nm, therefore also the solar UV radiation could be efficiently applied. Iron concentrations can be orders of magnitude lower than in the conventional Fenton reaction. Iron salt must be eliminated after the treatment by neutralization and precipitation of Fe(OH)₃, as in classic Fenton processes. The quantum yield of Fe²⁺ photoproduction is relatively low (0.14 at 313 nm), however it could be drastically enhanced by photolysis of the highly photosensitive ferrioxalate complex ([Fe(C₂O₄)₃]³⁺) with quantum yield 1.24 at 300 nm (2.12) (Oppenlander, 2003: 124). The absorption of ferrioxalate complex extends from UV part also to the visible domain to λ below 500 nm. Solar light can be used and that makes the technology very attractive from the economical point of view.



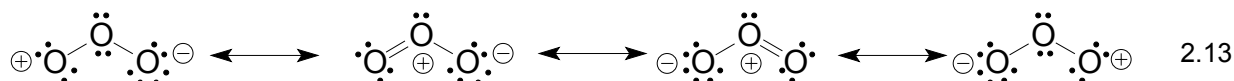
The main disadvantages of photo-Fenton reaction are using H₂O₂, maintaining accurate acidic pH during the reaction and removal of iron salts and remaining H₂O₂ after the process.

2.1.4 Heterogeneous photocatalysis

As a difference to homogeneous photocatalysis, in the heterogeneous photocatalysis two phases are present. Usually the solid, semiconductor catalyst (TiO₂, ZnO, CdS etc.) is insoluble in water. It is commonly assumed, that superoxide radical anions and hydroxyl radicals are the primary species formed after photogeneration of the electron/hole pair of a semiconductor catalyst in the presence of water and air. A detailed overview of photocatalysis is presented in Chapter 2.2.

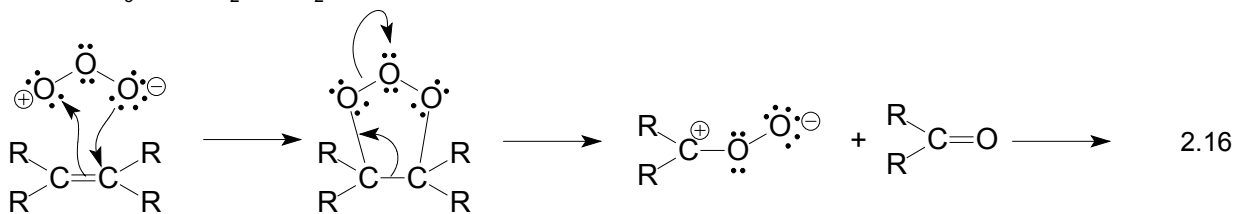
2.1.5 Ozone based AOPs

Ozone is a gaseous molecule at standard conditions with melting point at -193 °C. It is a singlet diradical in its ground state. Its structure has been described as a resonance hybrid of four canonical forms of dipolar character that mark a continuous scale (2.13). It is moderately soluble in water with the value of Henry constant $K_H = 100 \text{ atm} (\text{mol L}^{-1})^{-1}$ at 20 °C (Hoigne, 1998).



Ozonation is widely and successfully applied for many types of oxidative water treatments. Its chemical effects can be described by considering the sequences of highly selective direct reactions of molecular ozone (standard redox potential $E^0 = 2.07$ V at pH 0) and the reactions of the more reactive OH^\cdot radicals which are always produced from decomposed ozone in aqueous systems. For water treatment processes ozone is typically produced on-line in an ozone generator fed with dried air or oxygen. Typically ozone is formed by a silent electrical discharge in an air gap between two electrodes separated by a dielectric. The electrodes are connected to a high voltage generator which supplies a peak voltage in the 10 to 30 kV range. To transfer the ozone into the aqueous phase, the ozone-containing gas is diffused into a counterflow of water via porous plates or turbine-type diffusers located at the bottom of contact columns. The residual ozone is generally destroyed by thermal or thermal/catalytic process (Hoigne, 1998).

Ozone reacts with reactants primarily with its terminal electrophilic O-atoms. The most often described types of reactions of aqueous ozone are electron-transfer reactions, for example reaction between hydroperoxide anion and ozone (2.14), oxygen-atom transfer reactions, for example reaction between hydroxide anion and ozone (2.15) and ozone addition reactions, for example reaction between alkene and ozone (2.16).



Ozone molecule is not stable in aqueous solution. By reactions with HO^- , or solutes or reactions on surfaces such as on activated carbon, some ozone is consumed and often transformed into products such as hydrogen peroxide (H_2O_2) or HO_2^\cdot . A model that is composed of a chain of well-studied individual reactions is represented in Figure 1 (Hoigne, 1998). As represented by this model, the radical-type chain reactions are initiated by reactions that lead to the production of radicals that act as chain carriers. O_3 reacts apparently faster at higher pH where (i) many solutes show a higher degree of dissociation and form anions that are more reactive species for reacting with electrophilic ozone; (ii) the concentration of hydroxide anions is higher and the decomposition of ozone is accelerated due to the reaction with them.

Besides producing the HO^\cdot radicals from ozone in aqueous solution with increasing the pH, also the UV radiation accelerates the decomposition of ozone, generating different reactive oxygen species including H_2O_2 and HO^\cdot radicals. Aqueous ozone has ϵ_{max} of $3150 \text{ M}^{-1} \text{ cm}^{-1}$ at 258 nm and the broad absorption band extends up into the UVB region (Hoigne, 1998). If the aqueous ozone is exposed to UV radiation of a wavelength below 310 nm, it is very efficiently photolysed to form an excited O atom which adds to H_2O forming H_2O_2 (2.17 and 2.18). At this point two different types of reaction can occur. (i) One is H_2O_2 based degradation, which was already described in Chapter 2.1.1. (ii) On the other hand we must consider that deprotonated H_2O_2 (i.e. HO_2^-) transfers, in a fast reaction, an electron to ozone resulting in O_3^- and HO_2^\cdot species (already described with eq. 2.14) that act as chain carriers for the succeeding radical-type chain reactions. This mechanism is more favorable with the increase of pH, where more H_2O_2 is deprotonated.

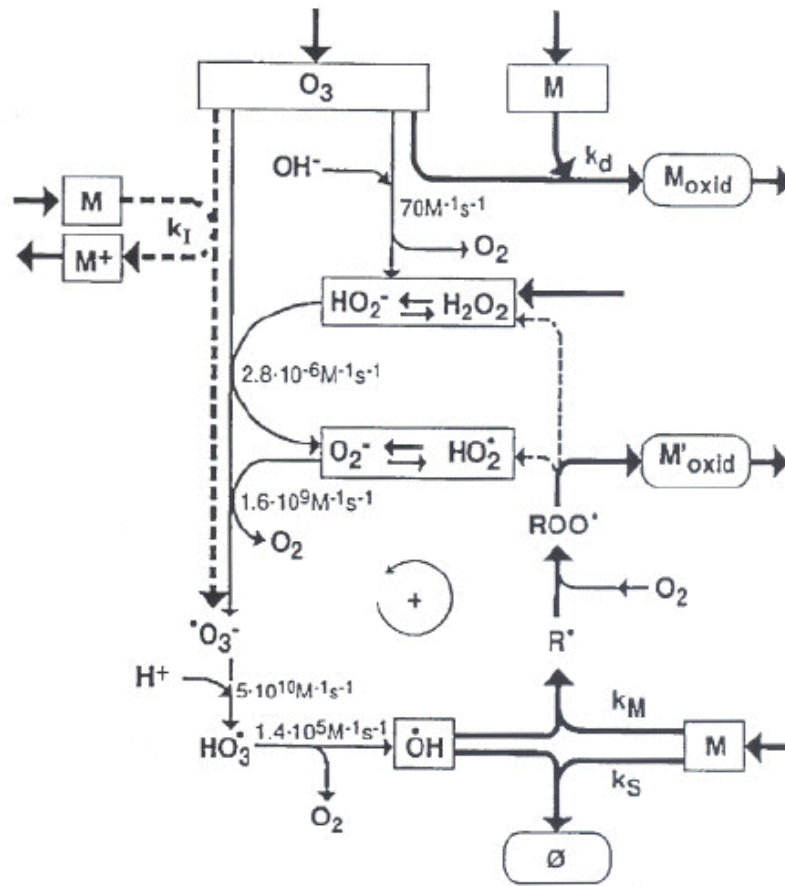


Figure 1: Scheme of reactions of aqueous ozone. Ozone reacts either directly with a solute M or it reacts with HO^- or M to initiate a radical-type chain reaction (Hoigne, 1998)



Instead of producing H_2O_2 indirectly via O_3/UV process, often H_2O_2 is added to ozonation system and such process is called Perozone. Such process is expensive but it is even more efficient than only ozonation.

To conclude, the ozone degradation rate is higher in alkaline solutions and also the addition of H_2O_2 accelerates the reaction. Additional advantage is a higher absorption of UV radiation compared to H_2O_2 absorption. Disadvantages of ozone based processes are expensive generation of ozone and wasteful sources of energy (UV lamps). Ozone is also a poisonous chemical with aggressive odor and must be destroyed before releasing it into the environment.

2.2 TiO_2 photocatalysis

Using expensive chemicals and light sources in some AOPs are obstacles, which can not be successfully solved despite the new technologies and new development. O_3 or H_2O_2 are poisonous chemicals and must be eliminated after the AOPs, increasing their costs additionally. Fenton and photo-Fenton reactions are limited by very narrow range of suitable pH conditions. The heterogeneous photocatalysis theoretically solves majority of the above mentioned problems without adding the new ones. The majority of the research work, which I have done during my PhD education, is closely related to TiO_2 photocatalysis. This

is the reason why all aspects of photocatalysis are described in detail separately in the subsequent chapters.

2.2.1 Introduction

The term photocatalysis implies the combination of photochemistry with a catalyst. Both radiation and catalyst are necessary to achieve or to accelerate a chemical reaction. Heterogeneous photocatalysis employs semiconductors as catalysts. A principle of a semiconductor physics is indicated in Figure 2. As the number of monomeric units (N) in a particle increases, the energy necessary to photoexcite the particle decreases. In the limit when $N > 2000$, it is possible to end up with a particle which exhibits the band electronic structure of a semiconductor, in which the highest occupied energy band (the valence band - VB) and the lowest unoccupied energy band (the conduction band - CB) are separated by a bandgap E_g , a region devoid of energy levels in a perfect crystal (Mills and Le Hunte, 1997). The interaction of a photon with an energy $h\nu$ greater or equal to the E_g of a semiconductor produces the electron/hole pair. The excited electron is transferred to the reducible specimen, at the same time that the catalyst accepts electron from the oxidizable specimen, which occupies the hole.

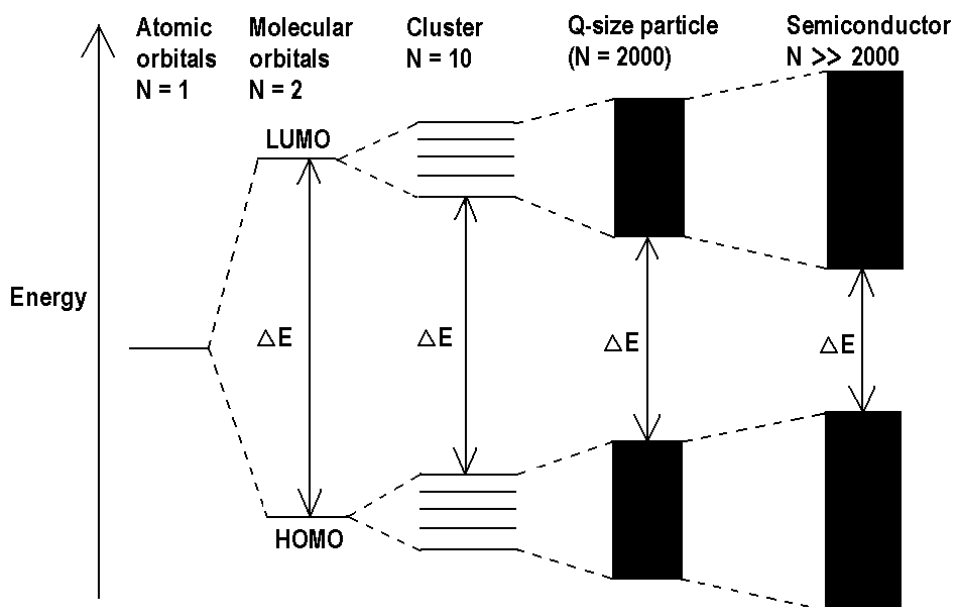


Figure 2: Change in the electronic structure of a semiconductor as the number of monomeric units present increases from unity to clusters of more than 2000 (Mills and Le Hunte, 1997)

Besides catalyst and a proper radiation no additional chemicals or expensive processes are necessary. The process may use atmospheric oxygen as the oxidant, it can be carried out under ambient conditions and there are already a lot of inexpensive photocatalysts available today (TiO_2 , ZnO , WO_3 , etc.). However, the biggest problem of the photocatalysis nowadays is low quantum efficiency of generation of reactive species, capable of oxidation or reduction of organic molecules. New development in the research field of photocatalysis might improve this to the degree that photocatalysis will be soon economically acceptable for specific applications.

As it was already mentioned, many different inorganic semiconductors have photocatalytic properties. It is not usually recognized that many examples of semiconductor photocatalysis had already been reported in the literature by the early part of the last century. For example, ZnO had attracted a great deal of attention at the turn of the 20th century as a photosensitizer for the decomposition of organic compounds (Perret, 1926). Many other materials have also been tested as photocatalysts, i.e WO_3 , V_2O_5 , ZnS , SrTiO_3 , but all the listed semiconductors are far less attractive for environmental applications than TiO_2 (Pirkanniemi and

Sillanpaa, 2002). The ability of a semiconductor to undergo photoinduced electron transfer to an adsorbed molecule is governed by the bandgap energy positions of a semiconductor and the redox potential of the adsorbates. The energy level at the bottom of CB is the reduction potential of e^- , on the contrary, the top of the VB determines the oxidizing ability of h^+ (Figure 3). TiO_2 has an $E_g = 3.2$ eV, this means that it absorbs radiation below 390 nm, therefore it is able to utilize UV radiation from solar spectrum. Additionally, VB potential of TiO_2 lies above the redox potential of water oxidation and the CB potential lies below the redox potential of reduction of oxygen (Figure 3). TiO_2 is also biologically and chemically inert, photostable, largely available and inexpensive, what are its additional advantages in comparison to the other photocatalysts.

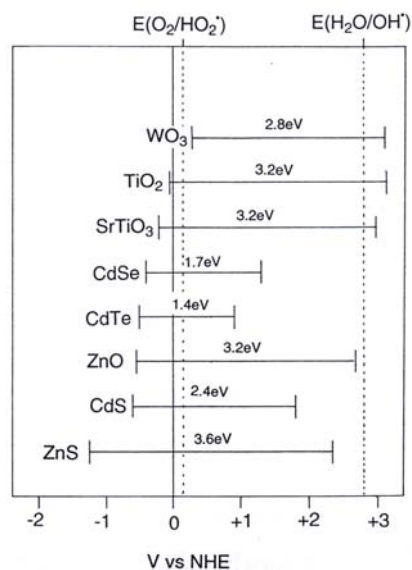


Figure 3: Band positions of common n-type semiconductors used in photocatalysis and the redox potentials of the H_2O/OH^- and O_2/HO_2^- couple at pH 0 (Mills et al., 1993: 418)

2.2.2 General remarks about titanium dioxide

Titanium dioxide belongs to the family of transition metal oxides. In the beginning of the 20th century, industrial production started with TiO_2 replacing toxic lead oxides as pigments for white paints. At present, the annual production of TiO_2 exceeds 4 million tons (Carp et al., 2004). It is used as a white pigment in paints, plastic and paper, which represent the major end-use sectors of TiO_2 . The consumption of TiO_2 as a pigment increased in the last few years in a number of minor end-use sectors such as textiles, food (it is approved by EU legislation as food coloring), leather, pharmaceuticals (tablet coating, toothpastes, as a UV absorber in sunscreen creams).

It is manufactured by either sulphate or chlorine process. In the sulphate process, ilmenite (a $FeTiO_3$ mineral) is transformed into iron- and titanium sulphates by reaction with sulphuric acid. Titanium hydroxide is precipitated by hydrolysis, filtered and calcinated at 900 °C. The chlorine process uses rutile (one of four polymorphs found in nature), which is either excavated or produced in a crude quality from ilmenite. The rutile is reacted with chlorine to produce titanium tetrachloride, which is purified and reoxidized, yielding very pure TiO_2 .

Besides its usage as a white pigment and as a photocatalytic material, TiO_2 has received a great deal of attention also in research and industrial fields. As a result of its high refractive index, it is used as anti-reflection coating in silicon solar cells and in many thin-film optical devices (Carp et al., 2004). It is utilized as a gas sensor for the determination of O_2 and CO concentrations due to the dependance of the electric conductivity on the ambient gas composition. It is used also in catalytic reactions, for example for selective reduction of NO_x to N_2 , for decomposition of volatile organic compounds (VOCs), for H_2 production by gas

shift production, for CO oxidation by O₂, for H₂S oxidation to S etc. Rutile is investigated as a dielectric gate material for MOSFET devices as a result of its high dielectric constant. In batteries, the anatase structure is used as an anode material in which lithium ions can intercalate reversibly. Other photochemical and photophysical applications include photolysis of water, light-induced superhydrophilicity, gas purification systems, production of solar cells, photocatalytic sterilization, photocatalytic cancer treatment etc. (Fujishima et al., 2000).

2.2.3 Crystal structure and properties

There are three polymorphs of TiO₂ found in nature, i.e.: anatase (tetragonal), brookite (orthorhombic) and rutile (tetragonal) (Carp et al., 2004). The structures of rutile, anatase and brookite can be discussed in terms of (TiO₆⁶⁻) octahedra (Figure 4). The three crystal structures differ by the distortion of each octahedral and by the assembly patterns of the octahedral chains. Anatase can be regarded to be built up from edge-sharing octahedra, on the contrary, rutile is built up from corner-sharing octahedra. Thermodynamic calculations based on calorimetric data predict that rutile is the most stable phase at all temperatures and pressures up to 60 kbar (Carp et al., 2004). The small differences in the Gibbs free energy (4-20 kJ mol⁻¹) between the three phases suggest that the metastable polymorphs are almost as stable as rutile at normal pressures and temperatures. Also kinetically, anatase transformation into rutile at room temperature is so slow that the transformation practically does not occur. At a macroscopic scale, the transformation reaches a measurable speed for bulk TiO₂ at $T > 600$ °C.

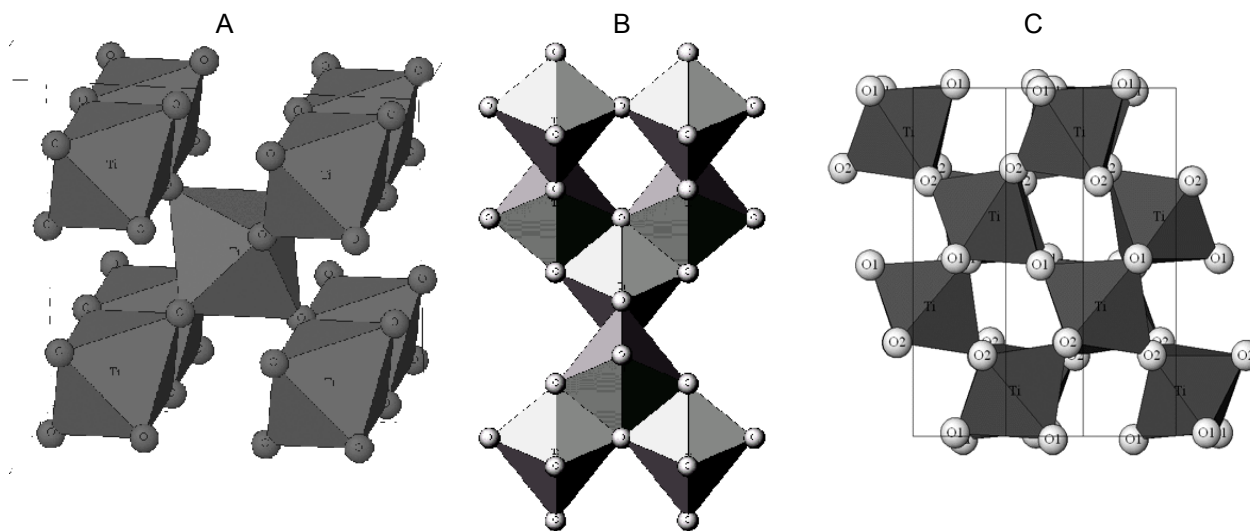


Figure 4: Crystal structures of A: rutile; B: anatase; C: brookite

2.2.4 TiO₂ as a photocatalyst

TiO₂ was used as a photocatalyst for degradation of organic molecules in aqueous solutions for the first time in 70's (Pruden and Ollis, 1983). Mostly it is used in a powder form. The powder is suspended in aqueous solution of pollutant and the slurry is then irradiated. One commercially available product, widely used as a standard in photocatalytic applications, is Aeroxide® P25 TiO₂, manufactured by Degussa through the high temperature (higher than 1200 °C) flame hydrolysis of TiCl₄ in the presence of hydrogen and oxygen. The product is nonporous 99.5 % TiO₂ (anatase: rutile = 70: 30), with surface area of 50 ± 15 m² g⁻¹ and an average particle diameter of 21 nm.

Both common crystal structures, anatase and rutile, are used as photocatalyst, with anatase showing a greater photocatalytic activity for most reactions. This is not in accordance with bandgap energies for bulk

material, where rutile has a value $E_g = 3.02$ eV, anatase, on the other hand, $E_g = 3.20$ eV, what corresponds to 410 and 384 nm absorption thresholds, respectively. It has been suggested that the increased photoreactivity of anatase is due to its slightly higher Fermi level, higher capacity to adsorb oxygen and higher degree of hydroxylation of the surface (Tanaka et al., 1991).

2.2.5 Synthesis of photocatalytically active TiO_2

TiO_2 can be prepared in the form of powder, crystals or thin films. Both powders and films can be built up from crystallites ranging from a few nanometers to several micrometers. It should be noted that nanosized crystallites tend to agglomerate, but many novel methods lead to nanoparticles without the need to additionally deagglomerate them (Carp et al., 2004).

2.2.5.1 Gas phase methods

Gas phase methods can be chemical or physical (Yoshiya et al., 2002: 44). The main techniques are:

1. Chemical vapour deposition (CVD). Compounds, ranging from metals to composite oxides, are formed from a chemical reaction or decomposition of a precursor in the gas phase and the product is then deposited on a surface of a substrate. CVD method is a widely used to coat large surfaces in a short span of time.

2. Physical vapour deposition (PVD). Films are again formed from the gas phase, but here without a chemical transition from precursor to product. This is possible only with substances that are stable in the gas phase. The most commonly employed PVD method is thermal evaporation, in which a material is evaporated from a crucible and deposited onto a substrate.

3. Spray pyrolysis deposition (SPD). SPD is an aerosol deposition technique for thin films and powders related to CVD. The main differences are that in spray pyrolysis: (i) an aerosol is formed from a precursor solution instead of a vapour; (ii) the aerosol is directly focused onto the substrate in most cases, while diffusion is a dominant process in CVD; (iii) the heated substrates are at ambient pressure, while in CVD, the set-up is commonly under reduced pressure.

4. There are also several other sophisticated thin film techniques based on vapour-phase deposition, such as sputtering, molecular beam epitaxy, ion implantation and dynamic ion beam mixing. Although these methods have the merit to control the film growth and the feasibility to obtain pure materials, they are energy intensive and involve high temperatures (Carp et al., 2004).

2.2.5.2 Solution routes

For some applications, especially for the synthesis of thin films, liquid-phase processing is one of the most convenient and utilized methods of synthesis. This method has the advantage of control over the stoichiometry, producing homogeneous materials, allowing formation of complex shapes, and preparation of composite materials. The main disadvantages are often expensive precursors, long processing time, presence of carbon as an impurity, etc.

2.2.5.2.1 Solution procedures other than sol-gel method (Carp et al., 2004)

1. Solvothermal methods. These methods employ chemical reactions in aqueous (hydrothermal method) or organic media (solvothermal method) under self-produced pressures at low temperatures (usually under 250°C). Generally, a subsequent thermal treatment is required to crystallize the final material.

2. Precipitation methods. These involve precipitation of hydroxides by the addition of an alkaline solution to a raw material followed by calcination to crystallize the oxide. The drawback is a difficult control of particle size and size distribution, as fast precipitation often causes formation of larger particles instead of nanoparticles.

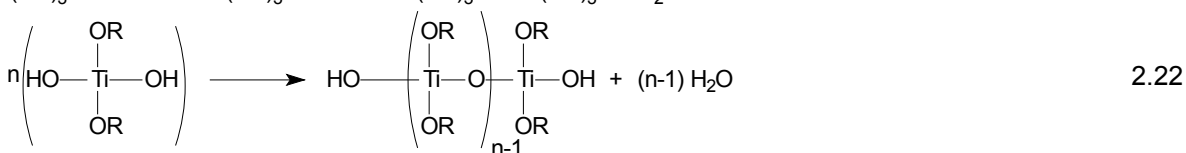
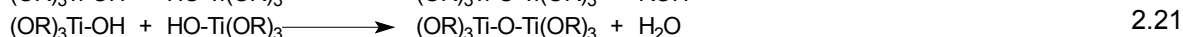
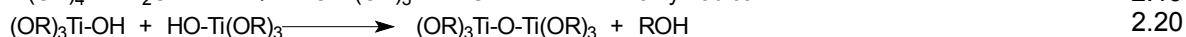
3. Combustion synthesis. It leads to highly crystalline fine/large area particles. The synthetic process involves a rapid heating of a solution containing redox mixtures. During combustion, the temperature reaches about 650 °C for a short period of time making the material crystalline. Since the time is short, particle growth of TiO₂ and phase transition to rutile is hindered.

4. Electrochemical synthesis. It can be used to prepare advanced thin films such as epitaxial, superlattice, quantum dot and nanoporous ones. Use of inorganic titanium salts is always accompanied by difficulties due to high tendency of the salts to hydrolyze. Non-aqueous solutions represent an option to overcome this problem.

2.2.5.2.2 Preparing TiO₂ thin films via sol-gel procedure

Sol gel process is among all other processes often used because of its relatively low cost and flexible applicability to wide range of size and shape of substrate.

In the sol-gel process (Brinker and Scherer, 1989: 2), precursors (starting compounds) for preparation of a colloid consist of a metal or metalloid element surrounded by various ligands. Precursors are often metal alkoxides, for example, common precursor for titanium oxide is titanium isopropoxide. Metal alkoxides are popular precursors because they react readily with water. The reaction is called hydrolysis and is presented in equation 2.19. Two partially hydrolyzed molecules can link together in a condensation reaction (2.20, 2.21). By definition, condensation liberates a small molecule, such as water or alcohol. However, hydrolysis and condensation can be exothermic and violent, particularly in the case of transition metal alkoxides and usually they lead to undesirable routes. Therefore stabilizing agents can be added into the sols (acetic acid, ethyl acetoacetate...), which prevent the process of precipitation by decreasing the rate of the hydrolysis and condensation reactions. In such case stable sols (colloidal solutions) are obtained.



Condensation reactions can continue to build larger and larger metal-containing molecules by the process of polymerization (2.22). When cross-linked polymers with an average size of several nanometers are formed, the sol is obtained. The final result of condensation/polymerization reactions is a gel, consisted of a three dimensional titania network that extends throughout the solution.

The dip coating process can be used to deposit thin films from the sol. The essential point of dip coating is pulling out the substrate from the vessel containing the sol with the constant speed. Dip coating process can be divided into four stages: immersion, deposition, drainage and evaporation. The xerogel films are produced after the solvent evaporates out of the thin film.

The last step in preparation of the films is annealing. Most gels are amorphous, even after drying, but many crystallize when heated. If the objective of the processing is to produce a pore-free ceramic, it is necessary to heat the gel to a high enough temperature to cause sintering. Sintering is a process of collapse of pores driven by surface energy. In TiO₂ photocatalysis crystallization is a desired process

(anatase is photocatalytically active, amorphous phase is not), but sintering not (porous films have higher active area than nonporous).

2.2.6 Primary processes upon bandgap irradiation of TiO₂ particles

Figure 5A represents schematically the processes occurring in photocatalysis upon bandgap irradiation of a semiconductor particle. The process of a generation of electron/hole pair is presented also with the equation 2.23, where e^-_{cb} represents a CB electron and h^+_{vb} a positive hole in the VB of the semiconductor. After their generation both CB electrons and VB holes migrate to the surface of the semiconductor particle. Contact between the semiconductor and the electrolyte establishes a Schottky barrier. The electric field of this barrier induces spatial separation between electrons and holes in opposite directions, causing the bands to bend at the solid-liquid interface. The Fermi level of the semiconductor then moves to equilibrate with the potential of the redox couple (Figure 5B). Charge carriers are driven to surface trapping sites either by diffusion or by migration induced by the space-charge gradient (Fox and Dulay, 1993). The transit time needed by these charge carriers to reach the surface is in the range of picoseconds (Robertson et al., 2005: 370).

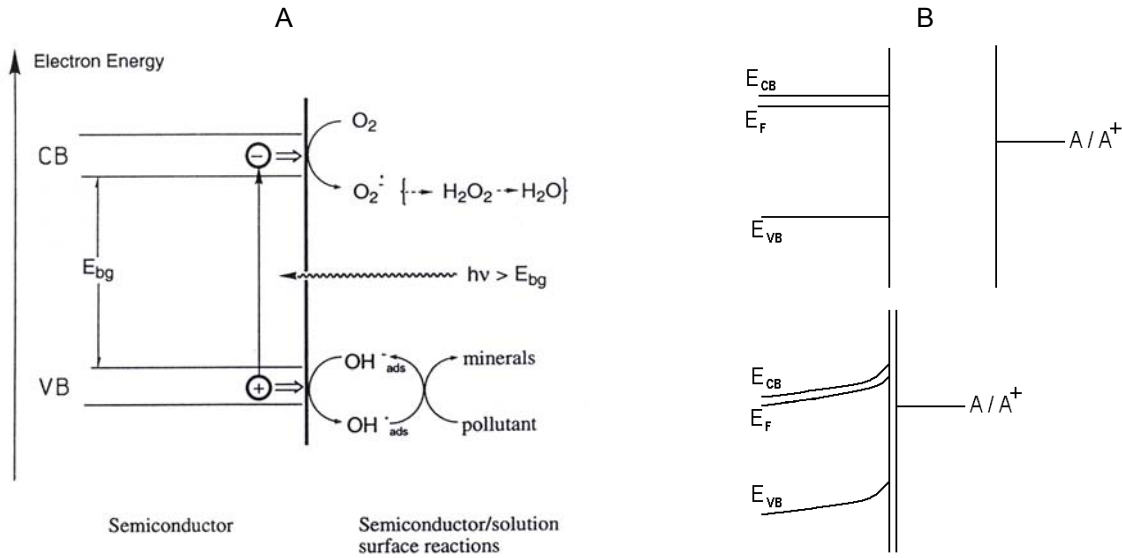
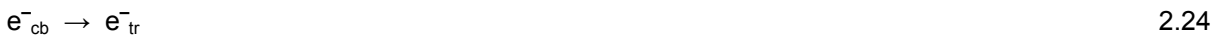


Figure 5: A: Schematic presentation of the band energetic model of the overall process of semiconductor photocatalysis for water purification (Mills et al., 1993); B: Band structure in a semiconductor (up) before contact with an electrolyte and (down) in contact with electrolyte (Fox and Dulay, 1993)

Reaching the surface these charge carriers are trapped in the subsurface and surface states of the particle (2.24 and 2.25), where e^-_{tr} and h^+_{tr} represent the trapped electron and hole, respectively. In a picosecond study by Serpone et al. (1995) on TiO₂ colloid solutions of varying diameters it was observed that spectra of trapped electrons as well as of trapped holes are fully developed after a laser pulse of 30 ps.



Generally it is assumed that Ti(IV) cations at the surface of the TiO₂ particle are reduced by the light-induced electrons forming Ti(III) cations which can be considered to be intrinsic surface states localized

about 0.1 eV below the CB edge, i.e., within the bandgap. (Robertson et al., 2005: 370). It is also assumed that the CB electrons are trapped in surface or bulk Ti(III) sites with different energies (Serpone et al., 1995). The chemical nature of the trapped holes has not been completely clarified yet. But all the research work on this area proposed the reduction of oxygen, either the oxygen from surface bound hydroxyl group or the subsurface oxygen anion. Bahnemann et al. (1997) proposed at least two different sites for holes on the surface of the TiO₂ particle: energetically deep and shallow traps. While both types of trapped holes will recombine with the trapped electrons within the first 200 ns after their generation, only holes excited thermally from the shallow traps have the chance to migrate to the energetically more deep traps. It is assumed that deeply trapped holes are chemically equivalent to surface-bound hydroxyl radicals.

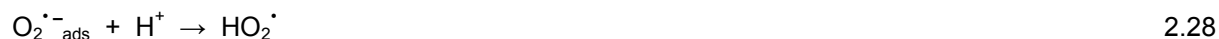
All mentioned charge carriers formed upon absorption of irradiation can recombine in a radiative or nonradiative way according to reaction 2.26. Unlike metals, semiconductors lack a continuum of interband states to assist recombination of the electron/hole pair. This assures an electron/pair lifetime sufficiently long to allow these species to participate in interfacial electron transfer. However, the majority of electron/hole pairs in TiO₂ photocatalysis recombines according to reaction 2.26, thus lowering the quantum yield for the oxidation of organic or inorganic molecules.



The recombination kinetics was studied by rapid depletion of the transient absorption spectra during laser flash photolysis studies (Serpone et al., 1995). Absorption decay for the 2.1 nm sols was found to be a simple first-order process, and electron/hole recombination was 100 % complete by 10 ns. For the bigger particles (13.3 and 26.7 nm) second-order biphasic kinetics was obtained: the decay times of the fast components decrease with the increase in particle size. 10 ns after the excitation pulse, about 90 % or more of the photogenerated electron/hole pairs have recombined such that the quantum yield of photooxidations must be 10 % or less. On the contrary, Ohko et al. (1997) reported very high quantum yield values (more than 20 %) for 2-propanol oxidation on a TiO₂ film in ambient air under very low irradiation intensity, where recombination losses are small and the coverage of the adsorbed organic compound is high.

2.2.7 Charge transfer mechanism and kinetics

In most experiments and applications with TiO₂ photocatalyst, O₂ is present to act as the primary electron acceptor. Usually the electrons trapped as Ti(III) are transferred to O₂ adsorbed at the semiconductor surface yielding O₂^{•-} and in the next step, depending on the pH, also deprotonated HO₂[•] (2.27 and 2.28) (Peterson et al., 1991).



Besides the electron transfer from the semiconductor to adsorbed O₂ also the direct transfer to an organic molecule is possible. This type of photocatalytic reaction, yielding an organic radical anion, has been found to occur with some organic compounds, such as tetrachloromethane, several nitroaromatic compounds, etc. (Robertson et al., 2005: 374). Different decay kinetics and evolution of the transient absorption spectra of TiO₂ colloidal solutions upon bandgap irradiation have been observed depending upon the presence of O₂, air or N₂. In every case, a biphasic decay of the transient absorption signal was observed. Following the fast initial decay, the remaining 20-40 % of the original signal height decayed much more slowly. While in the presence of N₂ this portion of the signal appeared to be stable even over a period of 200 ms, its decay rate increased with increasing O₂ concentration. However, this process is a really slow and in many cases could be the rate-limiting step in photocatalytic processes.

A significant number of papers propose that the photocatalytic oxidation of organic or inorganic compounds may occur by either indirect oxidation via a surface-bound hydroxyl radical (i.e. a trapped hole at the particle surface) or directly via the valence-band hole before it is trapped either within the particle or at the particle surface. It is not the intention of the thesis to review all the studies on this topic, but anyway, a few examples are presented in next paragraphs.

In the experiments of SCN⁻ oxidation, direct hole transfer was proven in the study conducted by Colombo and Bowman (1996) using femtosecond time-resolved diffuse reflectance spectroscopy. They found out that interfacial charge transfer of an electron from the SCN⁻ effectively competes with electron/hole recombination on an ultrafast time scale. Mao et al. (1991) observed that trichloroacetic acid and oxalic acid are oxidized primarily by VB holes on TiO₂ via a photo-Kolbe process. It should be noted that these compounds also have no H atoms available for abstraction by HO[•] radicals. Some researchers (Ishibashi et al., 2000) claim that holes are more important than HO[•] radicals regardless the type of the molecule. They found that the measured quantum yield values that could be attributed to a reaction involving HO[•] radicals are several orders of magnitude smaller than those that could be attributed to reactions involving holes.

On the contrary, the majority of the other researchers believe that the direct charge transfer to the organic molecule requires that the scavenging molecules are adsorbed on the TiO₂ surface prior to the adsorption of a photon. Otherwise, this reaction could not compete with the normal hole-trapping reactions (2.26). Similar conclusions were obtained also by Villarreal et al. (2004), who proposed a kinetic model for distinguishing between direct and indirect interfacial hole transfer on TiO₂ particles. Their model emphasizes that an isoenergetic, indirect hole transfer mechanism prevails in the case of nonspecific adsorption of dissolved pollutant species, while direct hole transfer takes place inelastically under specific adsorption. In the case of specific adsorption, direct and indirect hole transfer coexist if both surface-bound pollutant species and water molecules compete for hole capture.

A good example for differences in both mechanism was obtained by degradation of acetate (Robertson et al., 2005: 376). Hydroxyl radicals attack acetate ions mainly at the methyl group according to 2.29, producing glycolate (CH₂OHCOO⁻), formate (HCOO⁻), formaldehyde (H₂CO) and glyoxilate (CHOCOO⁻) as the stable products in the presence of O₂ (2.30), while direct oxidation of acetate in Kolbe decarboxylation (one-electron oxidation) leads to formation of H₂CO, methanol (CH₃OH), dimethylperoxide (H₃COOCH₃), hydroperoxymethane (H₃COOH) and HCOO⁻ in the presence of O₂ (2.31 and 2.32). When comparing these results with photocatalytic oxidation of acetate, the CH₂OHCOO⁻ and CHOCOO⁻ were found only in alkaline suspensions. Their formation could be an evidence for the photocatalytic oxidation of acetate via hydroxyl radicals. This is obtained only in alkaline suspensions, where TiO₂ is negatively charged and consequently there is no specific adsorption of acetate anions which would prefer direct hole transfer.



An additional support of hydroxyl radicals as reactive species is the observation that the rate of chlorinated ethanes correlates with the C-H bond strengths of the organics, which indicates that H atom abstraction by HO[•] is an important factor in the rate-determining step for oxidation (Mao et al., 1991).

2.2.8 Sorption of electron donors and acceptors

Interfacial electron transfer is kinetically competitive only when the relevant donor or acceptor is preadsorbed before photoactivation. Surely in aqueous metal oxide suspensions, hydroxyl groups or

water molecules can serve the role of surface-bound traps for the photogenerated hole, forming a surface-adsorbed hydroxyl radical. There is also firm evidence that many organic substrates can themselves act as adsorbed traps for the photogenerated hole.

The importance of substrate preadsorption on a given photocatalyst can be probed by the use of Langmuir-Hinshelwood (LH) kinetic model modified to accommodate reactions occurring at a solid-liquid interface. This model assumes that (i) at equilibrium, the number of surface adsorption sites is fixed; (ii) only one substrate may bind at each surface site; (iii) the heat of adsorption by the substrate is identical for each site and is independent of surface coverage; (iv) there is no interaction between adjacent adsorbed molecules; (v) the rate of surface adsorption of the substrate is greater than the rate of any subsequent chemical reactions; (vi) no irreversible blocking of active sites by binding to product occurs. With these assumptions, the surface coverage θ is related to the initial concentration of substrate c and to the dark adsorption equilibrium constant K (2.33). The rate of product formation r_{LH} can then be written as a single-component LH kinetic rate expression (2.34), where k is the apparent reaction rate constant occurring at the active site on the photocatalyst surface and K' is apparent adsorption constant. If the LH model is valid, the K and K' should be the same. The linearity of a plot of $1/r_{LH}$ versus $1/c$ tests the validity of the LH model (Fox and Dulay, 1991).

$$\Theta = K \times c / (1 + K \times c) \quad 2.33$$

$$r_{LH} = -dc / dt = k \times K \times c / (1 + K \times c) \quad 2.34$$

Many photocatalytic reactions show good linearity in such plots (Kaur and Singh, 2007). Unfortunately, this fit cannot be taken as a solid proof of preadsorption since an identical analytical formulation of the rate law is obtained even for reactions occurring entirely within a homogeneous phase (Turchi and Ollis, 1990). Additionally, photocatalysis routinely involves the initial generation of reactive intermediates such as free electrons, holes and HO^\cdot radicals. The reactivity of the latter toward reactants in the solution or adsorbed on the surface is such that we cannot expect reactant adsorption to be equilibrated. With other words, the dark adsorption equilibrium constant (K) from 2.33 should not be the same as the apparent adsorption constant (K') in the rate equation (2.34). Several papers have explored the influence of both radiation intensity and reactant concentration on the values of k and K' (Emeline et al., 2000). In contrast, the usual LH model presumes the dependence of the intensity only through the k . Discordances of such kinds have resulted in a pseudo steady state hypothesis (Ollis, 2004). The pseudo steady state hypothesis (i) yields rate equations in which both the reaction rate constant (k) and the apparent binding constant (K') depend on radiation intensity raised to the same exponent and that (ii) this dependence requires that the adsorption equilibrium constant on catalytic sites could not be the same as apparent binding constant in the rate equation.

2.2.9 pH, temperature and photon flux effects on TiO_2 photocatalysis

The particle size, surface charge and band edge positions of TiO_2 are influenced by pH (Siffert and Metzger, 1991). If shifting the redox potential of the band edges dominated the reactivity of the TiO_2 particles, then lower rates of substrate oxidation would be observed at high pH values since the VB edge decreases by 59 mV for each increasing unit of pH. Nonetheless, changes in rate of photocatalytic activity from one end of the pH range to the other are usually small, often less than 1 order of magnitude (Haque et al., 2006) and it is not always that rates of oxidation are enhanced with decreasing of pH. More important parameter regarding the determination of a photoreactivity at different pH values is amphoteric character of TiO_2 and consequently a surface sorption. The isoelectric point (pH_{zpc}) for TiO_2 in water is about $\text{pH} = 6$ and positive surface charge is expected at lower pH and negative charge is predicted at higher pH values (2.35 and 2.36). This implies that the adsorption of relatively nonpolar pollutants is enhanced at a pH value close to pH_{zpc} . This implies, that interactions with cationic electron donors and electron acceptors will be favoured at $\text{pH} > pH_{zpc}$ conditions, while anionic electron donors and acceptors will be favoured at $\text{pH} < pH_{zpc}$. For example, with TiO_2 powders suspended in aqueous silver nitrate solution, the rate of photoproduction of O_2 and elemental Ag was affected by the pH. The observed pH

dependence was attributed to surface-charge dependence of Ag^+ adsorption: a decrease in pH led to protonation of TiO_2 which inhibited Ag^+ adsorption to the surface (Fox and Dulay, 1991).



Like most photoreactions, photocatalytic reactions are not dramatically sensitive to minor variations in temperature. Thus, the potentially temperature-dependent steps, such as adsorption, desorption, surface migration, and rearrangement do not appear to be rate determining in this case (Haque et al., 2006).

There are two regimes of the photocatalytic reaction with respect to the UV-photon flux. They comprise a first-order regime for fluxes up to about 25 mW cm^{-2} in laboratory experiments and a half-order regime for higher intensities. In the former regime, the e^-/h^+ pairs are consumed more rapidly by chemical reactions than by recombination reactions, whereas in the half-order regime, the recombination is dominant.

2.2.10 Formation of H_2O_2 and secondary reactions with activated O_2 species

H_2O_2 is formed on illuminated TiO_2 surfaces in the presence of air via O_2 reduction by a CB electron in the presence of a suitable electron donor (2.27, 2.28 and 2.37). H_2O_2 could theoretically be formed also via reaction between two surface-bound hydroxyl radicals, but it was shown by Hoffman et al. (1994) and Fujishima et al. (2000) that the primary formation of H_2O_2 occurs via the reduction of adsorbed O_2 . H_2O_2 is another source of reactive oxygen species and as such has a positive effect on the kinetics of the oxidation of organic molecules. The mechanism of the oxidation by H_2O_2 is presented in detail in Chapter 2.1.1. The secondary processes, which take place after the charge transfer of electron/hole pairs to the reaction medium, are summarized and illustrated in Figure 6.

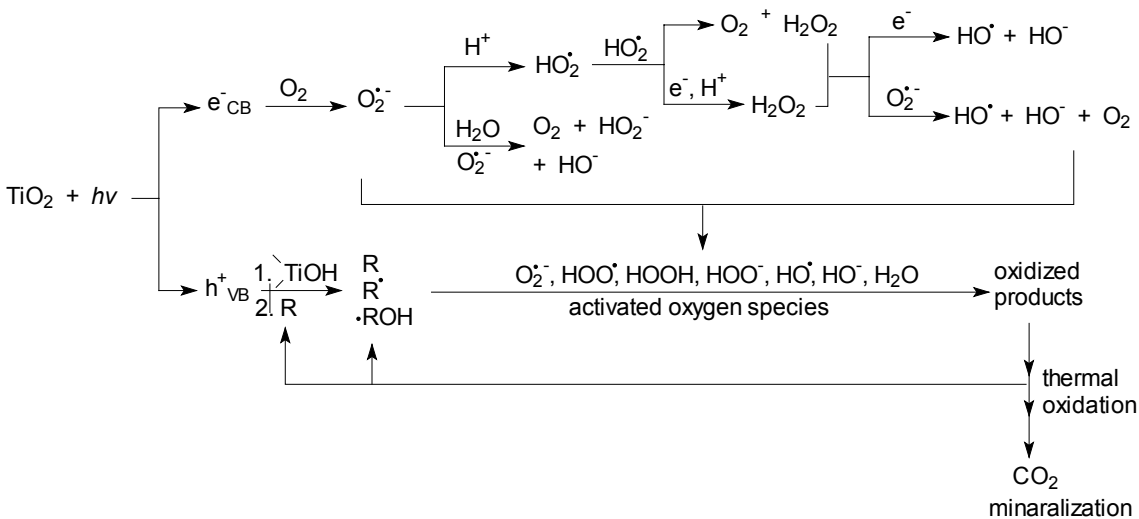


Figure 6: Secondary reactions with activated oxygen species in photocatalytic mechanism (Hofmann et al., 1995)

2.2.11 Evaluation of photodegradation efficiency

The evaluation of photocatalytic efficiencies of different catalysts are usually presented as percentage of degradation, degradation rate, or half-life. However, because of different experimental factors, these data

are difficult to compare. Although there are numbers of different ways of defining the efficiency of the photocatalyst to degrade an organic molecule, the only absolute measure is overall quantum yield ($\Phi_{overall}$) (Serpone, 1997). It is defined as the ratio between the number of molecules (N_{mol}) undergoing an event and the number of photons (N_{ph}) absorbed by the reactant (in our case by the photocatalyst) (2.38).

$$\Phi_{overall} = N_{mol} (\text{mol s}^{-1}) / N_{ph} (\text{einstein s}^{-1}) = \text{rate of reaction} / \text{rate of absorption of photons} \quad 2.38$$

Examination of the Φ of the photodegradation of phenol for different photocatalyst materials (suspensions) under the same conditions shows a nine-fold variation between the lowest value ($\Phi = 2.8\%$ for Hombikat UV-100) and the highest ($\Phi = 25\%$ for Fluka AG) (Serpone et al., 1997). Such variations may be due to several factors: (i) differences in the crystalline phase of TiO_2 ; (ii) differences in the sizes and shapes of the particles; (iii) differences in the density of OH^- groups on the particle surface and in the number of water molecules hydrating the surface; (iv) differences in the number and nature of trap sites both in the lattice and at the surface; (v) the adsorption/desorption characteristics of each surface, which may vary according to the nature of the photocatalyst material and also the nature of the organic substrate.

The rate of absorption is difficult to evaluate as a result of absorption, transmission and scattering of the semiconductor particles. On the contrary, $\Phi_{overall}$ does not depend only on material physical and chemical characteristics, but also on many other parameters, such as intensity and the wavelength of the irradiation, the amount of the catalyst, the nature and concentration of the organic molecules, concentration of O_2 etc. The method, which tries to avoid the inherent difficulties encountered in the precise evaluation of the number of photons absorbed by the photocatalyst, difficulties with utilization of different light sources, different reactor geometries and other unspecified factors by referring all the results to an equivalent experiment carried out under identical conditions for a standard process, is defined as the photonic efficiency (ζ) (Serpone, 1997). ζ describes the number of reactant molecules transformed or product molecules formed divided by number of incident photons, at a given wavelength, inside the front window of the photocatalytic cell (2.39).

$$\zeta = N_{mol} (\text{mol s}^{-1}) / N_{ph} \text{ incident inside reactor cell (einstein s}^{-1}) \quad 2.39$$

Many researchers in the field use polychromatic light sources, such as Xe lamps, low and medium pressure Hg lamps, blacklight tubes. Using these light sources without the monochromator, also a value for ζ cannot be calculated and, under these circumstances, we can calculate the formal quantum efficiency, which is defined as rate of reaction divided by incident light intensity (Mills and Le Hunte, 1997). But the rate of photocatalytic reaction depends on many parameters, including the reactor geometry, nature and concentration of the semiconductor and substrate, the concentration of O_2 , radiation intensity, temperature, pH, the presence of competitive interfering species and stirrer speed, therefore the values of ζ and formal quantum efficiency obtained by one research group may be very different from those obtained by another.

2.3 Improving the performance of TiO_2 photocatalysis

2.3.1 Structural and morphological aspects

In addition to the crystallite transformation obtained by high-temperature calcination, crystallite growing and serious sintering are observed with increasing the temperature of calcinations, leading to the drastic decrease in surface area. The photocatalytic activity is not necessarily dependent on catalyst surface area, but rather on the availability of active sites (Sclafani and Hermann, 1996). The amount of the surface-adsorbed water and hydroxy groups is related to the crystallite form and surface area. Anatase is more active than rutile in adsorbing water and hydroxy groups and this is probably the main reason of higher photocatalytic efficiency of anatase compared to rutile (Ding et al., 2000).

A large surface area can be determining factor in certain photodegradation reactions, as a large amount of adsorbed molecules promotes the reaction rate. However, powders with large surface area are usually

associated with low crystallinity and large number of crystalline defects, which favour the recombination of electrons and holes leading to a poor photoactivity (Saadoun et al., 1999). A balance between surface area and crystallinity must be found in order to obtain the highest photoactivity.

Particle size is an important parameter for photocatalytic efficiency, since the predominant way of electron/hole recombination may be different depending on the particle size (Zhang et al., 1998). It is well known that in the nanometer-size range, physical and chemical properties of semiconductors are modified compared with bulk. Small variations in particle diameters lead to great modifications in the surface/bulk ratio, thus modifying the significance of volume and surface electron-hole recombinations. When the crystallite dimension of a semiconductor particle falls below a critical radius of approximately 10 nm, the charge carriers appear to behave quantum mechanically (Hoffmann et al., 1995). The wave function of the charge carriers spreads over the whole semiconductor particle: thus the charge carriers do not need to diffuse to accomplish reactions with species present on the surface and, as a consequence, it is possible to obtain quantum yields approaching unity. One of the predicted effects of quantization is an increase in E_g and therefore a blue shift in the absorption edge with decreasing the particle size. Consequently the redox potential of photogenerated holes and electrons in quantized semiconductors will be enhanced. The increased driving force in size-quantized systems are expected to increase the rate constant of charge transfer in the normal Marcus region. Thus, the use of size-quantized semiconductor particles may result in increased photoefficiencies for systems in which the rate-limiting step is charge transfer (Nosaka et al., 1990). The positive effects of increased overpotentials (i.e. difference between E_{vb} and E_{redox}) on quantum yields can be offset by unfavorable surface speciation and surface defects due to the preparation method of size-quantized semiconductor particles.

2.3.2 Doping

Doping the semiconductor with various transition metal ions may lead to an enhanced efficiency of the photocatalytic systems. The photophysical mechanism of doped semiconductors is not always understood. Among others, unsolved problems relate to the surface structure and to the contribution of the charge carriers. But the total induced alteration of the photocatalytic activity is made up from the sum of changes which occur in (i) the light-absorption capability of the photocatalyst; (ii) adsorption capacity of the substrate molecules; (iii) interfacial charge transfer rate (Carp et al., 2004).

Many papers deal with the effect of doping species incorporated in TiO₂ films on their photocatalytic activity. In 2001, several groups reported visible-light-sensitive TiO₂ powders and thin films. Subsequently, nitrogen-doped TiO₂ has attracted considerable attention (Hashimoto et al., 2005). Yellow and transparent nitrogen-doped TiO₂ thin films can be fabricated by sputtering a Ti or TiO₂ target in a gas flow that contains N₂O or N₂. Compared with the conventional TiO₂, nitrogen-doped TiO₂ has better absorption characteristics in visible, but at the same time also the recombination of UVA generated electrons/holes is higher, therefore the final result is its decreased photocatalytic activity.

Doping effect can beneficially influence separation of electron-hole pairs. Li et al. (2004) published the results of the study, where PW₁₁O₃₉⁷⁻/TiO₂ composite films were prepared and then used towards azo-dye degradation. Much higher photocatalytic activity was achieved with such composite film. Effect of doping on the photocatalytic activities of Mo/TiO₂ films was studied by Yang et al. (2004). Sonawane et al. (2004) reported the results of preparation and photocatalytic activity of Fe/TiO₂ films. Another metal oxide used for doping TiO₂ films was WO₃ (Rampaul et al., 2003). Many other metal oxides and metals were also used for doping into or deposited on TiO₂ films (Carp et al., 2004), but the details on this topic are not relevant to my dissertation.

2.3.3 Metal coating

If the redox potential of the metal is higher than that of TiO₂, electrons are removed from the TiO₂ particles in the vicinity of each metal particle. This results in formation of a Schottky barrier at each metal-semiconductor region, which leads to a decrease in electron/hole recombination, as well as to an efficient

charge separation (Yoshiya et al., 2002: 30). As a consequence of the improved separation of electrons and holes, metal deposition on the TiO₂ surface enhances photocatalytic reactions by accelerating the transfer of electrons to dissolved O₂ (Figure 7).

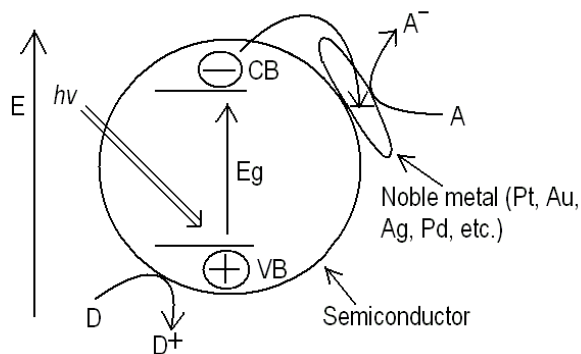


Figure 7: The effect of metal nanocontacts on photocatalytic processes (Wang et al., 2004)

Photodeposition is the most commonly used technique in obtaining metals deposits on TiO₂ and involves the reduction of metal ions by CB electrons, while the anodic process is represented by the oxidation of water by VB holes. The deposition of metals can be either beneficial or detrimental for photocatalytic degradation in aqueous solution, depending on an amount of loaded metal, chemical nature of the pollutant and chemical nature of the metal. (Hu et al., 2003).

2.3.4 Composite semiconductors

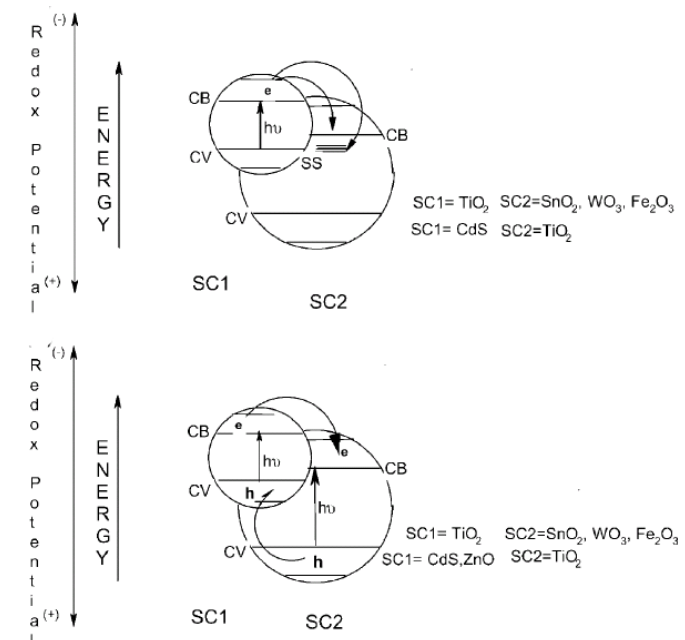


Figure 8: Energy diagram showing the coupling of various semiconductors. Top: Vectorial electron transfer from the light activated semiconductor to the non-activated; Bottom: both semiconductors are activated and vectorial displacement of electrons and holes (Carp et al., 2004)

The coupling of two semiconductors, possessing different energy levels for their corresponding CB and VB, provides an approach to achieve more efficient charge separation, an increased lifetime of the charge

carriers and an enhanced interfacial charge transfer to adsorbed substrates. Two different cases can be distinguished: first only one semiconductor is illuminated and the second is non-activated (Figure 8, top), or both are illuminated (Figure 8, bottom) (Carp et al., 2004).

A proper placement of the individual semiconductors (i.e. convenient energy levels of the coupled photocatalyst) and optimal thickness of the covering semiconductor are crucial for efficient charge separation. Undoubtedly, the geometry of the particles, surface texture and particle size also play a significant role in the interparticle electron transfer (Shang, 2004).

2.3.5 Comparison between TiO₂ powders and TiO₂ thin films

When estimating the advantages and disadvantages of powdered and immobilized forms of TiO₂, it must be again summarized, what controls the photocatalytic activity of a semiconductor. Three basic parameters are (Yoshiya et al., 2002: 30) (i) light absorption properties of the material; (ii) rate of reduction and oxidation of the molecule by photogenerated holes and electrons; (iii) rate of electron – hole recombination.

According to all described parameters, aqueous suspensions of TiO₂ powders are usually preferred over immobilized photocatalyst, because the fixation of TiO₂ on solid supports reduces its photocatalytic activity due to (i) reduction of active surface; (ii) mass-transfer limitations; (iii) presence of foreign cationic impurities (Si⁴⁺, Na⁺, Fe³⁺ etc.) in a deposited layer (as a consequence of the thermal treatment necessary to improve photocatalyst adhesion), which increases the electron/hole recombination. On the contrary, there are problems associated with implementation of TiO₂ suspensions in a large scale level due to inconvenient, time-consuming and expensive particle-fluid separation after the photocatalytic process.

Therefore there is a need to immobilize the photocatalyst onto an appropriate support, but simultaneously to overcome the problems associated with the immobilization: (i) increasing the specific catalyst area per volume of pollutant solution and simultaneously not decreasing the crystallinity of the material; (ii) increasing the adsorption capacity and surface area of the photocatalyst; (iii) influencing the selectivity of the photocatalytic reaction (Carp et al., 2004).

2.3.6 Photoreactor's engineering

The complex field of photochemical engineering is governed by the reaction system, the lamp technology and by chemical engineering. Suitable photoreactor concepts can only be obtained by an appropriate combination of these three aspects. The engineering of photochemical reactor systems for the applications of AOPs refers to the basic principles of chemical reaction engineering, however, it has to take into account the particular concepts of photochemical engineering, which include the following substantial issues: (i) specific excitation of the reactive species; (ii) total absorbance of electromagnetic radiation to avoid unnecessary losses; (iii) radiation losses by reflection and scattering should be minimized; (iv) optimal oxygen saturation of the aqueous phase; (v) convergence of lamp and reactor geometry and the spatial separation between the lamp and the reaction mixture; (vi) efficient cooling of the lamp; (vii) precise description of the radiation distribution within the reactor volume considering the heterogeneity of the photochemical process; (viii) combination of this spatially defined energy absorption with the classical mass and energy system balances allows the description of the photoreactor/photochemical system (Oppenlander, 2003: 240).

Classical chemical reaction engineering provides mathematical concepts to describe the ideal or real mass balances and reaction kinetics of commonly used reactor types that include discontinuous batch, mixed flow, plug flow, batch recirculation systems and staged or cascade reactor configurations (Levenspiel, 1996: 90). The different reactor types are shown schematically in Figure 9. All these reactors are amenable to photochemical reaction engineering. Many commercial photochemical reactor systems make use of the batch recirculation mode for the treatment of highly contaminated wastewaters of limited

volume. On the other hand, cascades of photoreactor modules allow the gradual treatment of contaminated water streams with a very high photon flow in total.

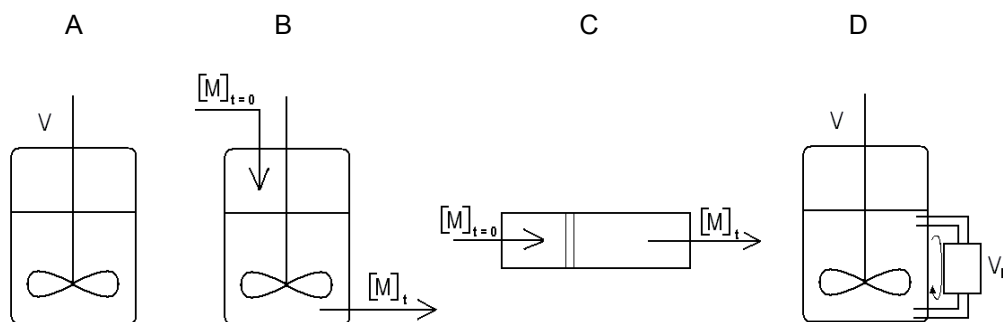


Figure 9: Types of ideal chemical reactors. A: batch reactor; B: mixed flow reactor; C: plug flow reactor; D: batch recirculation reactor

Based on the manner in which the photocatalyst is used all photocatalytic reactor configurations fall under two main categories regarding the shape of the solid phase (photocatalyst). The solid phase could be dispersed or stationary. Dispersed phase photoreactors may be operated with the catalyst particles and the fluid phase agitated by mechanical or other means. Depending on the means of agitation, the photoreactors resembles slurry or fluidized bed reactors. In numerous investigations, an aqueous suspension of the catalyst particles in immersion- or annular-type photoreactors has been used. On the contrary, the photocatalyt particles are immobilized onto a fixed transparent surface, such as the reactor wall or a fibre mesh, or are supported on particles, such as glass ceramic beads, that are held in fixed positions in the photoreactor (Mukherjee and Ray, 1999).

Several factors impede the efficient design of a photocatalytic reactor (Mukherjee and Ray, 1999). The problem of scaling up multiphase photocatalytic reactor is considerably more complex than that of scaling up conventional chemical reactors or homogeneous reactors. The need to utilize a solid catalyst makes the entire problem quite complicated as another phase is added to the system. In fact, in a photocatalytic reactor, besides the conventional reactor complications, such as reactant-catalyst contact time, flow patterns, mixing, mass transfer, reaction kinetics, catalyst installation, temperature control, an additional engineering factor related to the illumination of the catalyst becomes relevant. The high degree of interaction between the transport processes, reaction kinetics and light absorption leads to a strong coupling of physicochemical phenomena. When looking from the perspective of reactor design of a TiO_2 photocatalytic reactor, three main problems are present. First, TiO_2 is mostly used in a powder form for photocatalytic experiments (Topalov et al., 2004), where the final particle-fluid separation for the catalyst recycling can be inconvenient, time-consuming and expensive. This problem is avoided if TiO_2 is immobilized on a rigid support as a thin (nano- or micro-scale) film. But then the second problem arises because of the immobilization of the catalyst. Since the reaction occurs at the liquid-solid interface, only a part of the catalyst is in contact with the reactant. Hence, the overall rate may be limited to mass transport of the pollutant to the catalyst surface (Mukherjee and Ray, 1999). The third issue is that besides the requirement for a good contact between reactants and catalyst, it is also necessary to achieve efficient exposure of the catalyst to irradiation through the whole interior of the reactor (Ray and Beenackers, 1998). Different types of reactors for photocatalytic detoxification of water have already been proposed for laboratory and pilot-plant scale usage, but detailed review is provided in Chapter 4.2.1.1.

The artificial generation of photons required for the detoxification of polluted water is the most important source of costs during the operating of photocatalytic wastewater treatment plants. This would suggest that use of sunlight would be an economically and ecologically sensible light source. There are four main types of the solar photocatalytic reactors, while from which one is based on concentrating solar collectors (parabolic trough reactor or PTR), the other three are based on non-concentrating (one-sun) collectors of solar energy, namely (i) thin-film-fixed-bed reactor (TFFBR), (ii) compound parabolic collecting reactor (CPCR) and (iii) double skin sheet reactor (DSSR) (Robertson et al., 2005: 411). The PTR concentrates the parallel rays of the UV solar spectrum by a factor of 30-50 with the help of parabolic collector (Figure

10A). Because only parallel radiation can be focused on reaction pipe, which is located in the focal line of the collector, all diffuse radiation falling on the collector is lost for photocatalysis (Malato et al., 2002). Such system also needs a sun-tracking system to follow the sun. One of the first solar reactors, not applying a light-concentrating system and thus being able to utilize the diffuse as well as the direct portion of the solar UV irradiation for the photocatalytic process, was the TFFBR (Goslich et al., 1997) (Figure 10B). The most important part of the TFFBR is a sloping plate coated with a photocatalyst and rinsed with the polluted water in a very thin film. The main disadvantage of this type of the reactor is its low compactness and laminar flow, which presents mass transfer problems.

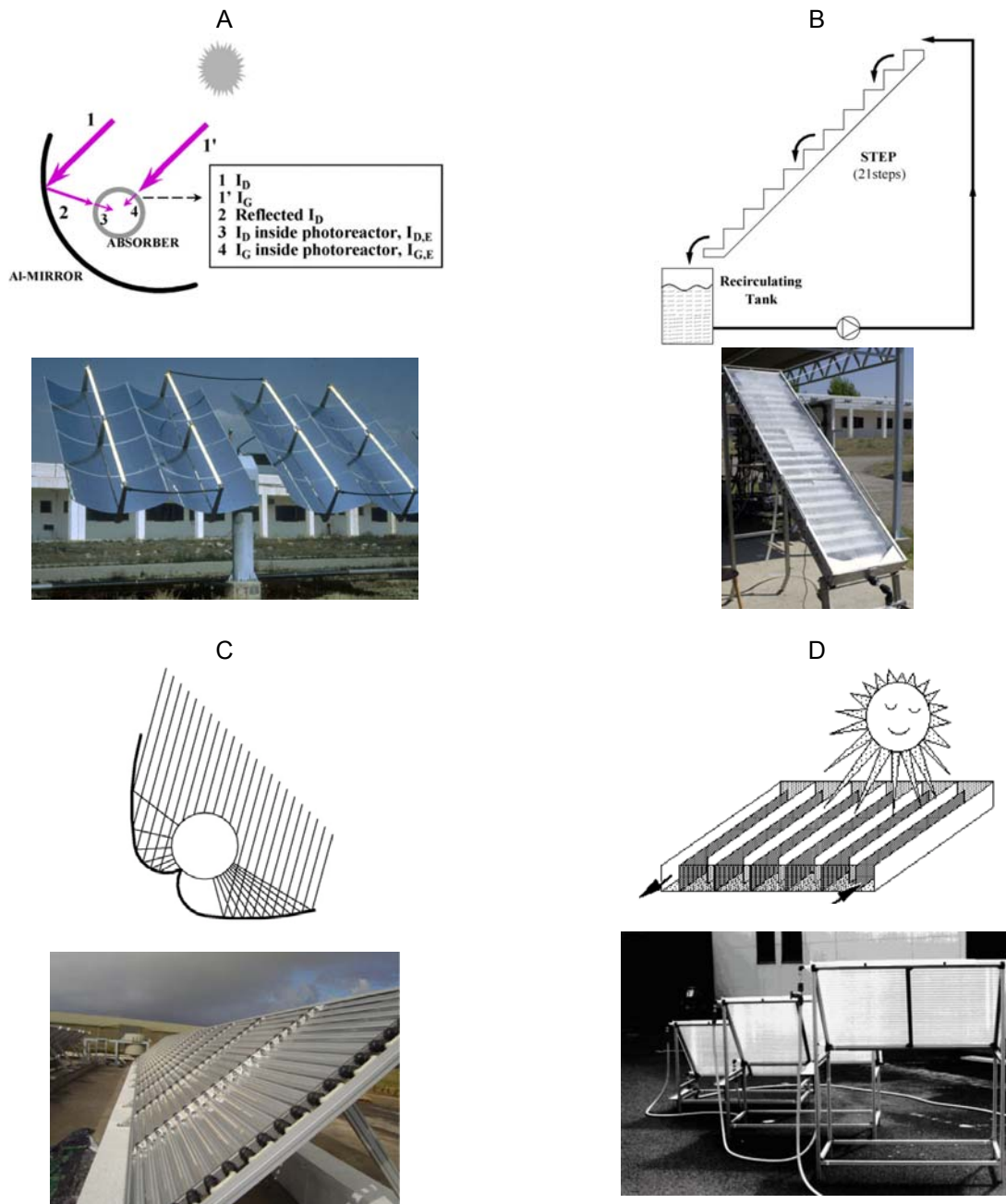
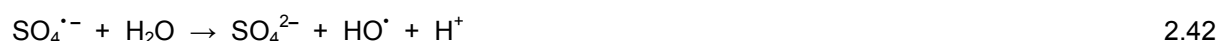


Figure 10: Different types of solar photocatalytic reactors; A: PTR; B: TFFBR; C: CPR (all three Malato et al., 2007); D: DSSR (Bahnmann, 2004)

A CPCR is a trough reactor without light concentrating properties. It differs from a PTR by the shape of its reflecting mirrors. On the other hand, the CPCR reflector consists of two half circular profiles side by side, and a parabolic continuation at both outer sides of the circles (Figure 10C). The focal line is located closely above the connection of the two circles. This geometry enables radiation entering from almost any direction to be reflected into the focal line of the CPCR, i.e., most of the diffuse radiation entering the module can also be employed for the photocatalytic reaction. Moreover, a CPCR must not necessarily track the sun due to its geometry (Malato et al., 2002). DSSR consists of a flat and transparent structured box made of Plexiglas® (Bahnmann, 2004) (Figure 10D). The suspension containing the model pollutant is pumped through the channels. The system can utilize both the direct and the diffuse portion of the solar irradiation.

2.3.7 Synergistic effects between photocatalysis and other AOPs

Inorganic oxidants such as O₃ (Agustina et al., 2005), H₂O₂, S₂O₈²⁻, BrO₃⁻ (Muneer and Bahnmann, 2002) have been proposed to increase the efficiency of TiO₂ photocatalysis due to (i) an increase in the number of trapped electrons, which prevents recombination; (ii) the avoidance of problems caused by low O₂ concentration; and (iii) the generation of more HO· radicals or other strongly oxidizing radicals which may enhance the photocatalytic degradation of pollutants, according to the following reactions (2.40, 2.41, 2.42) (Carp et al., 2004). Coupling ozonation with TiO₂ photocatalysis is presented in detail in Chapter 4.2.1.2.



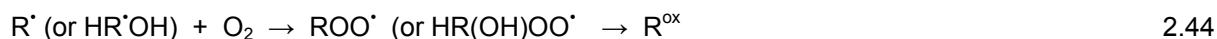
2.4 Photocatalytic treatment of POPs and heavy metals in water

The first complete mineralisation of an organic compound in water by photocatalysis was reported by Pruden and Ollis (1983). Using TiO₂ photocatalyst, the complete destruction of several halogenated hydrocarbons including trichloroethane, methylene chloride, chloroform and tetrachloromethane was achieved. Since then, thousands of scientific papers have been published regarding the photocatalytic elimination of organic and inorganic compounds (Carp et al., 2004; Mills and LeHunte, 1997). Photocatalytic oxidation of organic compounds is of considerable interest for environmental applications and in particular for the control and eventual destruction of hazardous wastes. The complete mineralization to CO₂, H₂O, and associated inorganic components such as HCl, HBr, SO₄²⁻, NO₃⁻, of a variety of aliphatic and aromatic chlorinated hydrocarbons via heterogeneous photooxidation on TiO₂ has been reported (Robertson et al., 2005: 385). The general classes of compounds that have been degraded, although not necessarily completely mineralized by semiconductor photocatalysis include alkanes, haloalkanes, aliphatic alcohols, carboxylic acids, alkenes, aromatics, haloaromatics, polymers, surfactants, pesticides and dyes. In subsequent subchapters a short review of the mechanism and elimination of the most important classes of organic compounds are presented.

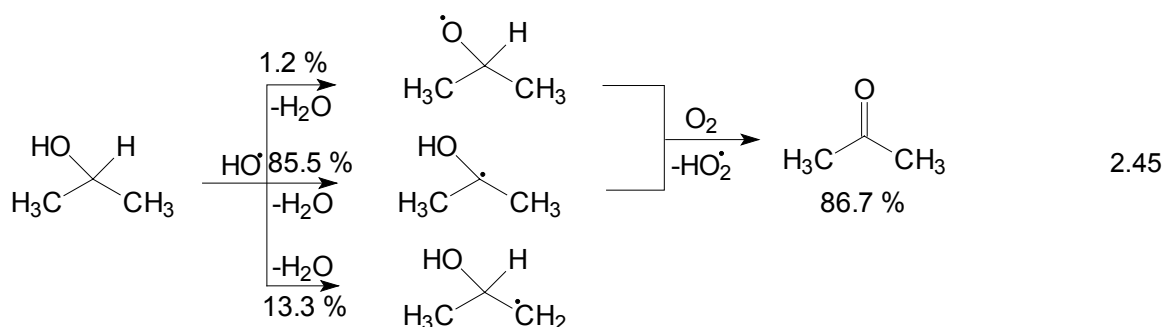
2.4.1 Aliphatic and aromatic hydrocarbons

The first step in degradation of aliphatic hydrocarbons (RH) is an abstraction of hydrogen by HO· radical or electrophilic addition of HO· to an unsaturated C-C bond, which results in the generation of carbon-centered radical (R· or HR·OH) (2.43). R· reacts in a bimolecular reaction with dissolved O₂ to produce peroxy radicals (ROO·) (2.45). ROO· undergoes a variety of molecular rearrangements and/or elimination reactions until the final oxidation products (R^{ox} = aldehydes, ketones, alcohols, H₂O₂, aliphatic peroxide) are formed (2.44). In reality, these oxidation products are interfering with hydroxyl radical attack on RH

and hence they are complicating the product spectrum considerably. Additionally, the $\text{HCO}_3^{\cdot-}$ and $\text{CO}_3^{\cdot-}$ radicals may introduce selective oxidation reactions into the degradation cycle (Oppenlander, 2003: 172). Aliphatic ketones and aldehydes undergo similar oxidation reactions as aliphatic hydrocarbons in the presence of a source of hydroxyl radicals (Stefan and Bolton, 1999).



Despite the fact that HO^{\cdot} radicals are very reactive and unselective oxidants, significant selectivities of hydrogen abstraction reactions still exist with respect to different types of hydrogen atoms bound in a specific substrate. So, primary H atoms contribute a smaller fraction to the overall rate constant of hydrogen abstraction than secondary or tertiary H atoms (Hoigne, 1998). An interesting example of selectivity with respect to hydrogen abstraction by hydroxyl radicals is demonstrated in the scheme 2.45 (Asmus et al., 1973). The HO^{\cdot} radical mainly abstracts a H atom from the secondary C atom and only a minor pathway goes through the abstraction of primary or hydroxyl H atom.

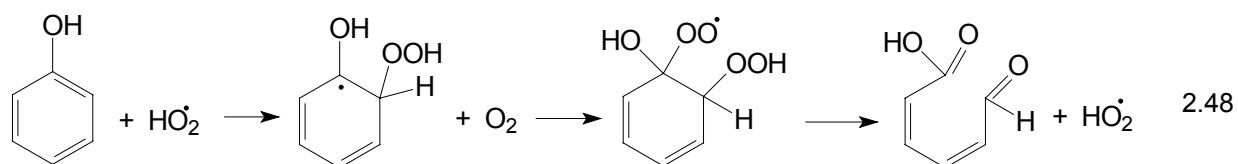
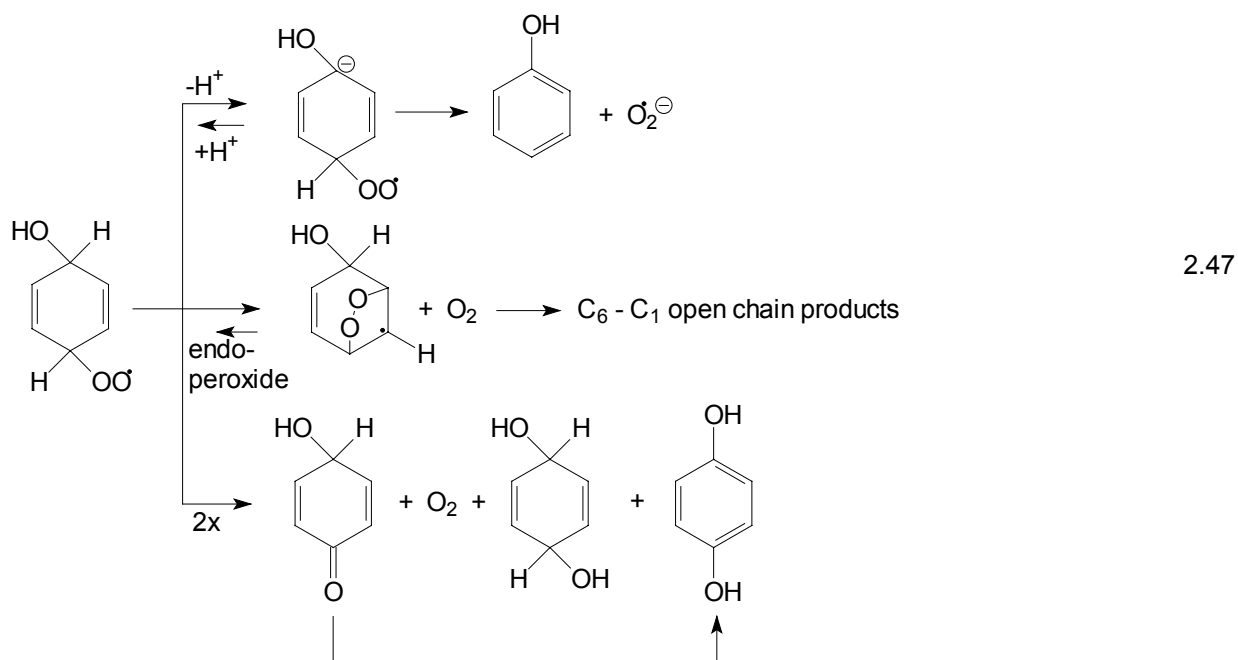
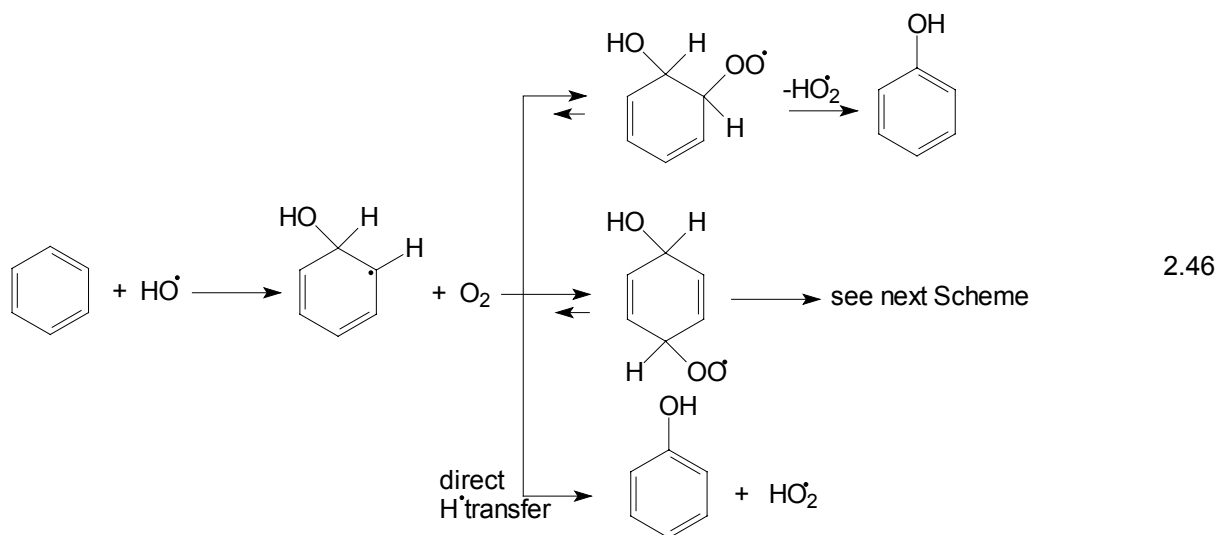


2.4.2 Nonhalogenated aromatic compounds

The degradation of aromatic compounds in water by HO^{\cdot} radicals is even more complex than in case of aliphatic. Benzene and its derivatives react rapidly with HO^{\cdot} radicals to yield cyclohexadienyl-type radicals, which immediately add dissolved O_2 to the ortho or para position with respect to the HO functional group (2.46). The reactions of the resulting para-peroxy radicals with 1,4-cyclohexadienyl structure are outlined in 2.47 (Oppenlander, 2003: 172). The endoperoxide that is produced via intramolecular O_2 radical addition to a double bond of the molecule is mainly responsible for the formation of open chain products with six or less carbon atoms. The HO_2^{\cdot} radicals which are formed after interfacial electron transfer to O_2 or during the decomposition reactions can add to phenol as shown in 2.48. Subsequent reaction with O_2 and elimination of HO_2^{\cdot} finally leads to the formation of open chain product, which is afterwards again attacked by HO^{\cdot} and/or other reactive oxygen species leading to the ultimate products of CO_2 and H_2O .

Of course, the mechanism of phenol degradation is different if the HO^{\cdot} radical is the initiator of its degradation. In such case, the first step is the electrophilic addition of HO^{\cdot} radical to aromatic C=C bond.

Polyaromatic hydrocarbons are generated by a range of industrial activities ranged from town gas generation to activities of the oil and gas industry. These compounds can be very persistent and are often resistant to biodegradation. Semiconductor photocatalysis has been successfully applied to the destruction of a wide range of these chemicals, although not surprisingly the decomposition rates are significantly slower than that observed for simpler compounds (Ireland et al., 1995). From isolated by-products it was proposed that HO^{\cdot} radical attack was the primary mechanism of the degradation process.

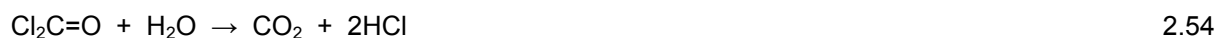


2.4.3 Chlorine-containing compounds

Volatile chlorine-containing compounds like trichloroethene, tetrachloroethen, 1,3-dichlorobenzene, 2-chloro-, 4-chloro-, and 2,4-dichlorophenol are widely used as industrial solvents and precursors in organic synthesis in chemical industry. These chemicals are usually toxic, mobile and very persistent in the environment. The stability of C-Cl bond in halohydrocarbons is responsible for their toxicity and persistence in biological environment. The C-Cl bond is actually inert against HO[•] radical attack. This is probably the reason that halogenated aromatic and aliphatic compounds represent the most

comprehensively studied class of compounds for which photocatalytic water treatment has been applied. Complete photocatalytic dechlorination (reduction) of many chlorinated compounds tends to be rather slow towards the mineralization of organic carbon to CO₂. Moreover, when organochlorine compounds undergo oxidation, they may produce other organochlorine compounds that may be more toxic than the parent molecule itself.

Trichloromethane and dichloromethane react with relatively low rate constants via H atom abstraction (Kormann et al., 1991) (2.49 – 2.54). However, unsaturated chlorinated hydrocarbons react very fast with HO[•] radicals by electrophilic addition. The HO-adduct radicals rapidly eliminate HCl with formation of the carbonyl functional group, and the remaining C-radicals add O₂.



The decomposition of halogenated hydrocarbons can be initiated also by CB electrons (reductive pathway), not only by VB holes (oxidative pathway). However, the redox potential of CB electron of TiO₂ is not sufficiently negative to be a versatile reducing agent. But for perhalogenated hydrocarbons, such as tetrachloromethane, the CB reduction pathway is the only possible way of destruction. The reduction of CCl₄ is strongly dependent on the presence of electron donors (D = methanol, ethanol etc.), which reduce the undesired recombination of photoexcited electron-hole pairs. Therefore, the following reactions (2.55 and 2.56) should proceed concurrently on the TiO₂ surface to maximize the photoreduction efficiency (Choi and Hoffmann, 1995).



Theurich et al. (1996) studied the degradation of 4-chlorophenol. Hydroxyl radical attack to the unsaturated aromatic C=C bond is believed to be also here the primary oxidation step. The first mechanistic steps for the photocatalytic destruction of 4-chlorophenol are presented in Figure 11 (Theurich et al., 1996). Cl is released from the organic molecules as a (i) Cl[•] atom as a consequence of a direct photochemical excitation of 4-chlorophenol and homolytic cleavage of C-Cl bond or (ii) Cl⁻ anion as a consequence of HCl elimination. Similar mechanism has been proposed also for the destruction of other chlorophenols.

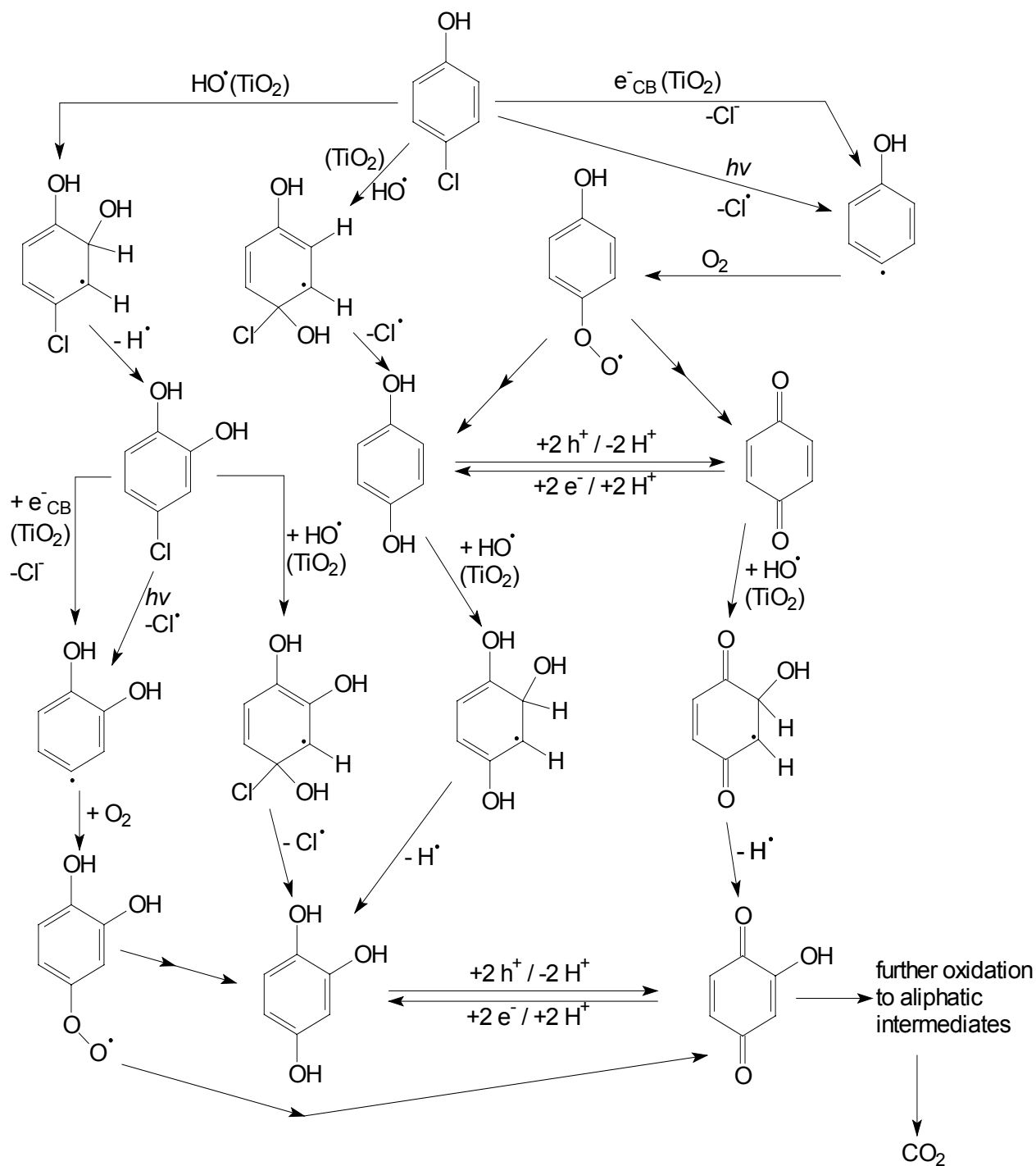
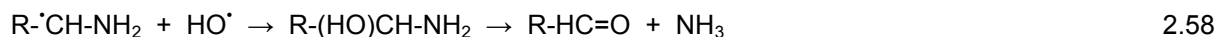


Figure 11: Initial steps in the photocatalytic degradation of 4-chlorophenol (Theurich et al., 1996)

2.4.4 Nitrogen containing molecules

The final oxidation state of nitrogen after the mineralization of nitrogen-containing compounds depends on several factors. The most important are the nature of the initial organic compound and the experimental conditions (pH, O_2 concentration, loading, nature of catalyst, irradiation time). NH_4^+ cation is very slowly oxidized to NO_3^- (Nohara et al., 1997). Primary amino group or amide group are in TiO_2 photocatalyzed

oxidations predominantly converted to the NH_4^+ ions. It is proposed that α -carbon adjacent to the primary amine is initially oxidized to promote the scission of the N-C bond (2.57 and 2.58). Nitrate ions are likely formed via generation of hydroxylamino groups. The chemical structure of the substrate influences the proportion of these ions formed (Nohara et al., 1997).



The mechanism of ring opening for pyridine is analogous to that of the aromatic ring in photocatalytic oxidation of benzene. In slightly aerated, acidic TiO_2 solutions, the photocatalytic degradation of nitrobenzenes, aniline, nitrosophenols, phenylhydroxylamine (Piccinini et al., 1997), nitrophenols, aminophenols (Maurino et al., 1997) yields quantitative formation of CO_2 , whereas nitrogen is converted both through oxidative and reductive pathways into nitrate and ammonium ions.

Nitrogen is qualitatively converted to molecular N_2 in azo dyes (containing $-\text{N}=\text{N}-$ double bond) (Karkmaz et al., 2004). HO^\bullet radical attacks the azo linkage-bearing C-carbon. The resulting adduct breaks down to form phenyldiazonium radical and hydroxylated aromatic compound. The phenyldiazonium radical breaks down to produce N_2 and phenyl radical (2.59 and 2.60).



2.4.5 Degradation of pesticides and dyes

A wide variety of pesticides is nowadays introduced into water systems from various sources such as industrial effluents, agricultural runoff and chemical spills. It is estimated that less than 1 % of all pesticides used in agriculture actually reaches air or water (Carp et al., 2004), what still represents a concerning amount due to their high toxicity even at very low concentrations. A large volume of literature has been published on the photocatalytic degradation of pesticide pollutants in the last 15 years (Devipriya and Yesodharan, 2005). In most cases, total mineralization was observed for all pesticides at longer irradiation times. An exception is s-triazine herbicide, which during degradation forms highly stable cyanuric acid (2,4,6-trihydroxy-1,3,5-triazine) towards the oxidative attack, but is fortunately non-toxic (Konstantinou et al., 2001).

In most photocatalytic degradation experiments of pesticides, at least some of the degradation products have been identified. However, mechanistic studies leading to the formation of such products are relatively few. The effect of many parameters such as the presence of salts and other natural organic matter in the water is also not clearly understood. The employment of oxidative degradation for the degradation of pesticides leads sometimes also to more toxic intermediate compounds. Only monitoring the degradation efficiency of the process is therefore not enough to evaluate the usefulness of the process (Bavcon Kralj et al., 2007). Studies on the use of solar radiation as the source of energy for the degradation process have yielded encouraging results and the solar photocatalytic treatment is already at the pilot plant level and in one case also at the industrial level.

Considering the volume and chemical composition of the discharged effluent, the textile dyeing and finishing is one of the major pollutants in industry (Correia et al., 1994). Commercial dyestuffs all derive their colour from the relatively complex chromophore system, which they contain. A necessary criterion for their successful use is that they shall be highly stable in light and washing processes, and also stable against microbiological attack. For these reasons it cannot be expected that dyestuff, in general, will be easily degraded when entering the aqueous environment. Therefore the photocatalytic decolorization of municipal wastewater contaminated with textile dyes was studied already in 80's and 90's (Davis et al. 1994).

Still nowadays several studies concern the photocatalytic treatment of aqueous wastes containing single or mixed azo dyes. Some of the reported studies were mainly focused on the examination of the primary process of decolorization (Arabatzis et al., 2003; Stathatos et al., 1999), whereas less attention has been paid to a detailed analysis of the reaction mechanism (Stylidi M. et al., 2002; Karkmaz et al., 2004).

2.4.6 Noble metal recovery

Heavy metals are generally toxic for human beings since they accumulate in the body. They can be removed from industrial waste effluents as small crystallites deposited on the photocatalyst according to 2.61 (Herrmann, 2005). The redox potential of the cation metal couple must be higher than the flat band potential of the semiconductor. Because of their favorable redox potentials, only noble metals can be photodeposited. From an application point of view, the recovery of silver from photographic baths seems the most promising issue, provided that the legislation towards Ag-containing discharge water becomes more strict.



2.4.7 Potable water applications

In recent years scarcity of safe drinking water has become a significant challenge to the existence of many communities throughout the world with the Middle East and Southern Europe experiencing particular problems. In addition to different harmful microorganisms in polluted water, cyanotoxins present serious problems to the water industry as existing technologies are not always effective in the removal of such compounds. TiO₂ photocatalysis has been proven to be rather effective in removal of a wide range of chemicals and microbiological pathogens from potable water supplies (Robertson et al., 2005: 395).

Humic acids are naturally occurring compounds and must be removed prior to the distribution of water since not only they colour the water, but may solubilise pesticides. The effectiveness of TiO₂ photocatalysis has been confirmed by different researchers (Wiszniewski et al., 2004). Cyanobacterial toxins produced and released by cyanobacteria in freshwater around the world are well documented (Lawton et al., 1999). Microcystins are the most common of the cyanobacterial toxins found in water, as well as being the ones most often responsible for poisoning animals and humans. Lawton et al. (1999) reported a rapid photocatalytic degradation of microcystin to 7 UV-detectable compounds, 6 of which did not undergo further degradation. Anyway, photocatalytic process removed any residual toxicity from the water together with potential tumour promoting activity.

Modern research in the field aimed at supplying microbe-free water has placed particular emphasis on minimization of costs. To date, numerous studies have been carried out demonstrating the germicidal effects of TiO₂ photocatalysis (Sichel et al., 2007). Some authors suggest that the cell membrane is the primary site of attack by reactive HO· radicals (Maness et al., 1999). They reported results that can be explained by peroxidation of the polyunsaturated phospholipid component of the lipid cell membrane leading to a loss of essential cell functions, e.g., respiratory activity, and in the end, to cell death. Anyway, at the present time, the photochemical mechanism of the TiO₂ biocidal action remains largely unclear. In order for TiO₂ photocatalysis to be accepted as a reliable water disinfection method, a residual effect of treatment is necessary after initial treatment has taken place. Additionally, proper evaluation of the illumination standardization parameters used for photocatalytic treatments is obviously a critical step. In this sense, Rincon and Pulgarin (2004) proved that the solar UV dose necessary to reach a target disinfection level is not a good system efficiency indicator. They therefore proposed a new parameter, 'effective disinfection time', defined as a treatment time necessary to avoid bacterial regrowth after 24 h (or 48 h) in the dark after phototreatment.

2.4.8 Solar photocatalytic treatment of real wastewaters

Despite its obvious potential for the detoxification of polluted water, there has been very little commercial or industrial use of photocatalysis as a technology so far. Several years ago, according to a review by Goswami (1997), only two engineering-scale demonstrations, one for groundwater treatment in the USA and one for industrial wastewater treatment in Spain had been published. But more installations have recently been erected, mainly based on non-concentrating collectors. Dillert et al. (1999) have treated biologically pretreated industrial wastewater from the Volkswagen AG factories in Germany and Brasil. The results of the experiments, which were performed using DSSRs were so promising that a pilot plant was installed in Wolfsburg factory. A pilot plant using TFFBR has been built at the site of a textile factory in Tunisia (Bahnemann, 2004). A full-size demonstration photocatalytic plant based on CPCRs was erected at the facilities of HIDROCEN (Madrid), where TiO_2 suspensions are used as a photocatalyst. Since late 1999, this plant (including the catalyst separation unit) has been operating with all its capacities (Malato et al., 2007).

When the aim of a disinfection system is to provide drinking water, the catalyst might be immobilized on a robust, inert support that allows the catalyst to be irradiated, avoiding post-treatment separation of the catalyst. Vidal et al. (1999) published the first study on a TiO_2 solar photocatalysis pilot plant for water disinfection. Very recent work has studied improvement of solar disinfection using supported TiO_2 on flexible resistant materials, in the shape of cylinders, pills, balls, etc. One example is TiO_2 deposited on fiberglass inserted in a tubular photoreactor in a CPC (Fernandez-Ibanez et al., 2005). The most recent applications of water disinfection by TiO_2 photocatalysis are development of a solar reactors to decontaminate and disinfect small volumes of water. Field tests with the final prototypes were carried out in 2005 to validate operation under real conditions. Water from the feed tank is pumped through illuminated tubes in a CPC and the electricity for the pumping is provided by a solar panel (Navntoft et al., 2007).

2.5 Advantages of TiO_2 photocatalysis and objectives of the research work

An overview on TiO_2 photocatalysis has been presented: from the basic mechanistic aspects toward the present and possible future application of TiO_2 photocatalysis for wastewater and drinking water treatment. According to Chapter 2, some advantages of TiO_2 photocatalysis over the other AOPs could be summarized.

- Low cost and high chemical stability of TiO_2 .
- It needs only O_2 and UV photons for the activation. Also the solar energy could be used as source of UV photons.
- It can be applied to the systems with very low concentrations of highly toxic pollutants.
- Ions, generally present in water, do not decrease its activity considerably.
- Total mineralization for many organic compounds could be achieved.
- Other decontamination methods could be efficiently combined with TiO_2 photocatalysis thus increasing its efficiency.
- TiO_2 photocatalysis works at room temperature, therefore no additional input of thermal energy is necessary.

All listed benefits keep the photocatalysis as one of a promising AOPs for some special industrial applications. In order to improve its applicative value, its main drawbacks must be solved efficiently. The main disadvantages and the possible solutions for the problems are summarized in Table 1.

According to the presented problems, **the goals of my PhD research** were:

- preparation of fixed, mesoporous TiO_2 and characterisation of its photocatalytic activity compared to standard TiO_2 ;
- proposal of a new method for evaluating the quantum yield of immobilized TiO_2 ;
- development and construction of a new laboratory-scale photocatalytic reactor for immobilized TiO_2 , which could be used also in solar applications;

- coupling of TiO₂ photocatalysis with ozonation and studying the effect of ozone on the kinetics of photocatalytic degradation.

Table 1: Some drawbacks and possible solutions of TiO₂ photocatalysis

<i>DRAWBACKS</i>	<i>POSSIBLE SOLUTIONS</i>
<i>No standardized measurements of photocatalytic activities of different materials</i>	<i>Proposing a simple and reliable method for defining a quantum yield of chosen material</i>
<i>Slow complete mineralization of organic matter</i>	<i>(i) Concentrating on partial detoxification of hazardous pollutants, improving the selectivity of photocatalytic action toward specific molecules; (ii) improving the mineralization with other decontamination methods</i>
<i>Use of UV photons and consequently (i) necessity for the treated waters to be transparent in this spectral region; (ii) a small part of solar spectrum is in UV region</i>	<i>Preparing TiO₂ with improved photocatalytic activity in the broader spectral region, i.e. improved absorption characteristics in the Vis region</i>
<i>Problems with the separation of TiO₂ slurries after the photocatalysis</i>	<i>Fixation of TiO₂ on different supports without losing its photocatalytic activity due to lower catalyst/water interface</i>
<i>Underdeveloped photocatalytic engineering</i>	<i>Development of new types of photocatalytic reactors, which could beneficially use artificial as well as solar radiation</i>

3 MATERIALS AND METHODS

3.1 Chemicals

The chemicals used in this study were used as purchased: acetonitrile (HPLC grade), tetraethoxysilane ($\text{Si}(\text{OEt})_4$), 65 % nitric(V) acid, sulphuric(VI) acid, methanol, ethyl acetate, acetone and sodium dihydrogenphosphate from J. T. Baker, sodium chlorate(V), potassium oxalate, titanium(IV) isopropoxide ($\text{Ti}(\text{OiPr})_4$), sodium carbonate, sodium bicarbonate and 2-methoxyethanol ($\text{MeOCH}_2\text{CH}_2\text{OH}$) from Fluka, ammonium acetate, Plasmocorinth B and zinc powder from Merck, Pluronic F-127, sulfathiazole, sulfamethoxazole from Sigma, disodium hydrogenphosphate, 1,10-phenanthroline, acetic acid (AcOH), polyoxyethylene(10) cetyl ether (Brij 56), 7-hydroxycoumarin (7OHC) and 4-chlorophenol from Aldrich, sodium thiosulphate, potassium iodide, sodium hydroxide, ferrous sulphate(VI), sodium sulphate(VI), hydrochloric acid, sodium nitrate(V), sodium nitrate(III), ethanol, ethyl acetoacetate (EAA), sodium chloride, sodium acetate, ferric chloride hydrate, sodium bromide, lead(II) nitrate(V), coumarin from Riedel-de Haen and myclobutanil from LKT Laboratories.

Pure thiacloprid and imidacloprid were obtained from commercial technical products Calypso SC 480 (Bayer) and Confidor 70 WG (Bayer), respectively, following the procedure by Obana et al. (2003). Acetone (2 x 25 mL) was added to the dry commercial product (5 g). The suspension was filtered after 2 minutes of mixing. Acetone was removed by rotary evaporator. The dry solid residue was suspended in deionised water (50 mL) and then neonicotinoid molecules were extracted with ethyl acetate (3 x 20 mL). One half of ethyl acetate was evaporated, the white crystals precipitated. The suspension was cooled in the refrigerator for 15 min and then the solid was separated from the solvent and recrystallized from pure ethyl acetate. The purity of the obtained crystals was confirmed by ^1H NMR spectra of both molecules and by measuring the melting points. The obtained melting point of thiacloprid was 131.5 – 132.6 °C (131.3 – 132.7 °C for analytical standard, purchased by Riedel-de Haen), while for imidacloprid it was 140.5 – 142.1 °C (139.9 – 141.9 °C for analytical standard, purchased by Riedel-de Haen).

All aqueous solutions of the organic pollutants were prepared by using highly pure water ($< 18 \text{ M}\Omega \text{ cm}^{-1}$) from the NANOpure system (Barnstead).

3.2 Preparation of sols

SiO_2 sol: $\text{Si}(\text{OEt})_4$ was dissolved in ethanol ($n(\text{ethanol})/n(\text{Si}(\text{OEt})_4) = 6.6$). Separately 11.5% solution of nitric(V) acid was prepared by dissolving concentrated (65%) nitric(V) acid in water ($n(\text{Si}(\text{OEt})_4)/n(\text{HNO}_3) = 3.2$). After ten minutes both solutions were mixed together and the resulting sol was used after ageing at room temperatures for two hours. The sol was unstable and therefore it was always freshly prepared.

TiO_2 sols: $\text{Ti}(\text{OiPr})_4$ was added to AcOH ($n(\text{AcOH})/n(\text{Ti}(\text{OiPr})_4) = 1$) or to EAA ($n(\text{EAA})/n(\text{Ti}(\text{OiPr})_4) = 1$) during constant stirring. The prepared solution was dissolved in $\text{MeOCH}_2\text{CH}_2\text{OH}$ ($n(\text{MeOCH}_2\text{CH}_2\text{OH})/n(\text{Ti}) = 12.7$ (for U and R films) or 13.6 (for C and D films)) after 5 minutes. The resultant alkoxide solution was stirred at room temperature for solvolysis and condensation reactions at least for three hours. After using, the sol was kept in the refrigerator. It was conditioned at room temperature for at least one hour before the next use.

The procedure for the preparation of the sols with added surfactants was basically the same as described above. The only difference was that the surfactant, either Brij 56 (average molar mass = 683 g mol^{-1}) or triblock copolymer Pluronic F-127 with structural formula $\text{EO}_{97}\text{PO}_{69}\text{EO}_{97}$, where EO represents the ethylene oxide block and PO represents the propylene oxide block (average molar mass = $126000 \text{ g mol}^{-1}$), was dissolved in the sol after the addition of $\text{MeOCH}_2\text{CH}_2\text{OH}$. The practical quantities of particular chemicals, used for different TiO_2 sols preparation, are given in Table 2.

Table 2: Composition of titania sols

Symbol of titania sol	Ti precursor - Ti(OiPr) ₄ (mL)	Complexing agent (mL)	Solvent - MeOCH ₂ CH ₂ OH (mL)	Molar ratio (n(Ti):n(complexing agent):n(solvent))	Surfactant (g)
U	8.96	AcOH 1.74	30.4	1:1:12.7	/
R	8.96	AcOH 1.74	30.4	1:1:12.7	Brij 56 7
D	8.96	EAA 3.94	32.4	1:1:13.6	/
C	8.96	EAA 3.94	32.4	1:1:13.6	Pluronic F-127 4.7

3.3 Deposition and calcination of the films

3.3.1 Sol-gel derived films

At first the SiO₂ films were deposited on clean glass slides by a single dipping with a withdrawal speed of 10 cm min⁻¹. The substrates coated with gel films were left at room temperature in air for 30 min and then they were calcined at 500 °C for 30 min. The bare soda-lime glass or as-prepared silica films on soda-lime glass were used as substrates for the deposition of titania films. They were deposited with a pulling speed of up to 10 cm min⁻¹ from a TiO₂ sol and similarly heat-treated at 500 °C for 30 min. The thicknesses of the TiO₂ films were increased by repeating the dipping and heat-treatment cycles. The amount of the catalyst on a glass slide was determined by weighing.

3.3.2 Degussa P25 films

Additionally, a series of different types of immobilized TiO₂ layers were prepared on glass slides by sedimentation from aqueous suspension of TiO₂ P25 (10 g L⁻¹) for different times, with additional drying and annealing at 500 °C for 15 min. The amount of the catalyst on a glass slide was determined by weighing.

3.4 Characterization of sol-gel derived TiO₂ films

Thicknesses of TiO₂ films deposited from sols U, R, D and C on bare and SiO₂-precoated sodium glass by 1, 3 and 5 coating-heating cycles have been measured. For this purpose, a part of the coating was removed from the substrate by a reaction of zinc powder and concentrated hydrochloric acid until the sharp step was obtained between the substrate and the intact TiO₂ film. Thicknesses of titania films were measured with a Talysurf profilometer (Taylor – Hobson). The amount of deposited TiO₂ films was measured by weighing. The average value was taken from measurements of a number of identical films. The macroscopic density was then calculated from the amount of TiO₂ and its volume (thickness multiplied with the geometrical area of the substrate covered by titania film).

Absorption spectra (340 - 400 nm spectral range) of clean and calcined both-sided TiO₂ films deposited on two different supports were recorded on HP 8453 UV-Vis spectrophotometer. Bare sodium glass or sodium glass protected with SiO₂ layer were used as a blank. The band gap energies were calculated and estimated from UV-transmittance spectra of the titania films according to Sreemany and Sen (2004) and Abdel-Aziz et al. (2006).

Surface topography of TiO₂ films was evaluated by atomic force microscopy (AFM) on CP-II scanning probe microscope (Veeco) in non-contact mode at constant force in air. The tip was also a Veeco product (model RFESPA-M).

Dry and clean four-layered TiO₂ films, deposited from sols U, R, D and C on bare sodium glass and on SiO₂-precoated sodium glass have been used for X-ray diffraction analysis. Also so called “film powders” were used in XRD analysis to obtain diffractograms with higher intensities of peaks. “Film powders” were obtained by mechanical scratching of number of already calcined C4 films away from their substrates. XRD analysis of the films and “film powders” was performed on a Philips PW1710 automated X-ray diffractometer using the graphite monochromatized Cu K α radiation in the step-by-step mode.

Nitrogen sorption measurements were performed on a Micrometrics accelerated surface and porosity analyzer (ASAP 2020). The “film powders” were used instead of immobilized films. The “film powders” for sorption measurements were obtained by mechanical scratching a number of C and D films away from their substrates before thermal treatment. Sufficient amount of the powder sample was then calcined for 1 hour at 500 °C.

The surface and in-depth composition of different C and D films, prepared both on soda-lime glass or on soda-lime glass precoated with SiO₂ layer, were analyzed by X-ray Photoelectron Spectroscopy (XPS) on a Perkin-Elmer Φ 5600ci spectrometer.

3.5 Degradation of organic molecules

3.5.1 Photocatalytic systems

The photocatalytic systems used during my research work differed considerably between each other. Therefore the details of the developed photocatalytic systems and the details of the evaluation of the efficiencies of titania films toward the degradation of organic molecules are described separately in Chapters 4.1.2 and 4.2.2.

3.5.2 Analytical procedures

Absorption spectra (200 - 400 nm spectral range) of pure aqueous solutions of organic molecules (10.5 mg L⁻¹) were recorded on HP 8453 UV-Vis spectrophotometer.

The fluorescence of the irradiated aqueous solution of coumarin was determined for an aliquot (3 mL) of each irradiated sample using a Perkin Elmer MPF-3L instrument with excitation and emission bandwidths both at 4 nm. Excitation wavelength was at 332 nm, the maximum of the emission wavelength was at 456 nm.

The ionic chromatography (IC) equipment consists of Shimadzu LC-10Ai pump with conductivity detector (Shimadzu CDD-6A). The separation of chloride, nitrate(III), nitrate(V), chlorate(V) and sulphate(VI) anions were run on Dionex AS4A-SC anion column (250 mm x 4.6 mm). Mixture of sodium carbonate and sodium bicarbonate in water (1.8 : 1.7 mM) with the flow rate of 1.5 mL min⁻¹ was used as a mobile phase. The injection volume was 100 μ L. In the experiments where hydrochloric acid was used as a pH modifier, the concentration of chloride generated from neonicotinoid insecticides was obtained by subtracting the initial chloride concentration from the chloride concentration at certain time of degradation.

Acidified irradiated samples (35 mL) were analyzed by measuring the TOC and TN values on Shimadzu TOC-V_{C_{PN}} + TNM-1 analyzer. The analyses were based on ISO 8245 standard.

HPLC analysis of coumarin and 7-hydroxycoumarin (7OHC) solutions: The HPLC analyses were made on a Spectra-Physics chromatograph, coupled with UV (Spectra-Physics SP8450) and fluorescence detector (Shimadzu RF-530). The chromatographic separations were run on the Eclipse XDB-C8 column (Zorbax, 150 mm x 4.6 mm, 3.5 μm) using a 68:32 isocratic mixture of aqueous acetic acid (1 %) and methanol as the mobile phase. The flow rate was 1.0 mL min^{-1} . The injection volume was 50 μL . The elution of coumarin was monitored by UV detector at 275 nm, while 7OHC (Figure 12E) was monitored by a fluorescence detector with the excitation wavelength at 332 nm and emission wavelength positioned at 456 nm. The calibration curves were performed for the aqueous solutions of coumarin and 7OHC.

HPLC analysis of 4-chlorophenol solutions: The HPLC equipment consists of a HP 1100 Series chromatograph, coupled with a DAD detector. The chromatographic separations were run on a C18 Hypersil ODS column (Supelco, 150 mm x 4.6 mm, 5 μm) using a 70:30 mixture of 10 mM aqueous $\text{NH}_4\text{OOCCH}_3$ solution and acetonitrile as the eluent in the first 5 min, then it was changed into a 45:55 mixture by applying a linear gradient between 5 and 10 min. The eluent flow rate was 1.0 mL min^{-1} . Injection volume was 30 μL . The compound elutions were monitored by the DAD detector at 228 nm.

HPLC analysis of other organic molecules: The HPLC analyses were made on a HP 1100 Series chromatograph, coupled with DAD detector. The chromatographic separations were run on a C18 Merck column (Purospher STAR, 250 mm x 4.6 mm, 5 μm) using a 85:15 mixture of aqueous ammonium acetate (10 mM) and acetonitrile as the eluent in the first 4 min, then it was changed into a 30:70 mixture by applying a linear gradient between 4 and 16 min. The flow rate was 1.0 mL min^{-1} . The injection volume was 10 μL . The compounds elutions were monitored by DAD detector at belonging UV absorption maxima. The calibration curves were performed for the aqueous solutions of all analyzed parent compounds.

4 RESULTS AND DISCUSSION

4.1 PART 1: Comparison of different characteristics of TiO₂ films and their photocatalytic properties (Černigoj et al., 2006a, 2006b; Lavrenčič Štangar et al., 2006; unpublished results)

4.1.1 State of the art

4.1.1.1 Using the surfactants in the preparation of sol-gel derived TiO₂ films

A large number of studies have been made in the last ten years to immobilize the catalyst on a rigid support via different deposition techniques, such as CVD or PVD, spray pyrolysis, sol-gel technique etc. Sol-gel process is among all other processes most frequently used because of its relatively low cost, mild and ambient atmosphere reaction conditions, homogeneity at a molecular level, as well as flexible applicability to a wide range of size and shape of substrates (deposition on optical fibers (Peill et al., 1997), spherical ceramic balls (Dionysios et al. 2004), glass rods (Ray and Beenackers, 1998) etc.).

For efficient photocatalysis, it is necessary to prepare TiO₂ films that are capable of harvesting incident radiation to a great extent, and at the same time films with a high surface area and porosity to increase the rate of reaction between photogenerated species and the pollutants. For many applications including photocatalysis a nanostructured titania film is preferable to one which is dense or compact. Numerous reports have appeared on highly porous titania film structures either with large pores (Liu et al., 2005) or ordered mesopores (Crepaldi et al., 2003; Alberius et al., 2002; Yu et al., 2004). The film structure and morphology could be tailored through the variation of the sol-gel processing conditions and the use of structure directing agents, i.e. templates. Their role is to create porosity, smaller particles, and a larger surface area of the material. The most often used templates belong to the polyethylene glycol (PEG) or a group of triblock copolymers with the chemical composition poly(ethylene oxide)-poly(propylene oxide)-poly(ethylene oxide).

Ordered mesoporous inorganic films were prepared by different research groups worldwide. Yun et al. (2003) succeeded in preparing transparent, crack-free mesoporous TiO₂ thin films, deposited on sodium glass slides by using a triblock copolymer Pluronic P-123 as a template under strongly acidic conditions. The mesostructure of prepared films was greatly dependent on the synthesis conditions. Photocatalytic activity of the films was not investigated. There are several other reports of preparing mesostructured titania thin films using surfactant Pluronic P-123 via sol-gel procedure (Kartini et al., 2004; Bosc et al., 2006). Bosc et al (2006) reported the synthesis of hexagonal and cubic mesoporous anatase TiO₂ from titania sol containing different triblock copolymers and efficient photocatalytic degradation of toluene in a gas phase with the mesoporous TiO₂ itself and even better with the mesoporous TiO₂ coupled with WO₃. Porous TiO₂ thin films were synthesised from a sol-gel system using PEG as a template (Bu et al., 2004). The porous structure of TiO₂ thin films was found to depend significantly on the synthesis conditions.

Guillard et al. (2004) studied the correlations between physical properties and photocatalytic efficiencies of TiO₂ films. It was shown that the presence of a polymer (polyethylene glycol) in the initial sol-gel solution decreased the TiO₂ crystallite size and strongly increased the initial porosity and the transparency of the film. The use of a viscous solvent in sol-gel solutions also reduced the number of dip coatings necessary to obtain a sufficient film thickness and induced the higher porosity of the material, while the optical characteristics were unchanged. They also showed that whatever the additives were used in the sol-gel solution, TiO₂ film thickness was found to be the main parameter influencing the photocatalytic efficiency. Having the same thickness, smaller crystallite sizes favoured the photocatalytic efficiency. Additionally, no correlation between porosity and photocatalytic efficiency of TiO₂ film was found.

4.1.1.2 The effect of sodium glass support on the quality of produced TiO₂ films

The photocatalytic efficiency of titania films is affected by additional factors such as the presence of cations (Na⁺, Ca²⁺) which may diffuse from the glass support in the interior of the film during its sintering (Yu et al., 2001), and have been found to have a detrimental effect on the photocatalytic activity (Guillard et al., 2002; Yang et al., 2004). In this regard, various explanations were given, such as: (i) Na⁺ ions raise the temperature of anatase formation and increase the particle size (Nam et al., 2004), they inhibit anatase crystallization and cause agglomeration of TiO₂ particles (Lavrenčič Štangar et al., 2006); (ii) they promote the recrystallization of the anatase to rutile (Trapalis et al., 2003); (iii) they perturb the crystallinity of TiO₂ (Guillard et al., 2002), prevent the formation of the anatase phase and produce recombination centers of photogenerated electron-hole pairs (Paz and Heller, 1997); (iv) they produce either sodium titanate (Na₂O·xTiO₂) or a brookite phase (Kuznetsova et al., 2005); (v) they cause bonding or a shift of the oxygen anions resulting in the partial reduction of Ti(IV) to Ti(III) (Yu et al., 2001); and finally (vi) they adsorb CO₂ in air to form carbonate and cause the increase in the carbon amount (Yu et al., 2002). To reduce the migration of cationic impurities into the active film we covered the soda-lime glass substrates with a thin silica film made by a sol-gel route prior to depositing the titania film via the high-temperature processing route (Černigoj et al., 2006a, 2006b).

4.1.1.3 Determination of quantum yields of photocatalytic surfaces

Regarding the determination of quantum yield (Φ), such studies are mostly connected with some mechanistic studies in the scientific literature and are not intended as proposals for evaluation of photocatalytic activities of different TiO₂ materials (Du and Rabani, 2003; Ishibashi et al., 2000; Wang et al., 2004; Bettoni et al., 2004). Therefore there are still no standards to evaluate the self-cleaning performances of photocatalytically active surfaces. Standardization in photocatalysis has become an important issue. A relative photonic efficiency (ζ_r) as a standard measure for different TiO₂ materials and different organic substrates was proposed already by Serpone (1997) and this protocol was suggested also to the Commission on photochemistry under the IUPAC (Serpone and Salinaro, 1999; Salinaro et al., 1999). The ζ_r is defined as a rate of disappearance of a substrate divided by a rate of disappearance of a standard molecule and should be therefore related to an acceptable standard process, a standard photocatalyst material and a standard secondary actinometer in photocatalyzed process (Serpone, 1997) (4.1). Ultimately, these ζ_r values can be converted into photochemically defined Φ , once a Φ_{stand} for a given photocatalyst and a given substrate (in their case phenol) has been determined (4.2)

$$\zeta_r = \text{rate of disappearance of substrate} / \text{rate of disappearance of phenol} \quad 4.1$$

$$\Phi = \zeta_r \times \Phi_{stand} \quad 4.2$$

Mills and Le Hunte (1997) argued that there was no advantage of this methodology compared with the classical measurement of the Φ , since Φ_{stand} would vary enormously with different reaction conditions, and a value would have to be determined for each set of specific reaction conditions (this task is not less difficult than the measurement of Φ). There is also a danger in quoting ζ_r values, since a ζ_r value of much greater than unity would be taken as an indication of a very efficient photochemical process, which it may not be. For example, a ζ_r value of 2 for a process under test indicates simply that it is twice as fast as the degradation of phenol carried out under the same reaction conditions; however, it provides no indication of how efficient the process is with respect to harvesting the incident photons.

Evaluation of photocatalytic activities of TiO₂ slurries is out of scope of my PhD and is far more difficult task than the evaluation of TiO₂ films (Minero and Vione; 2006). Despite this and the fact that a large number of supported photocatalysts prepared in the last years, not many attempts have been made to quantify the activity of immobilized materials in terms of standardized parameters such as photonic efficiencies. There are many different methods that can be used to determine the activity on photocatalytic surfaces. The photocatalytic destruction of the thiazine dye, methylene blue, is probably the most extensively studied application for dye destruction (Houas et al., 2001). It is commonly used as a standard molecule in demonstration experiments of photocatalysis as it provides an excellent visual representation

of the process. Anyway, it is a tricky standard molecule, because it also undergoes simultaneous reduction to a colourless leuco dye, what is not a photocatalytically initiated process (Yan et al., 2006). Additionally, testing methods based on decolorisations of different dyes are based on the relative comparison of photoefficiency of the probe to photoefficiency of the standard under constant conditions, which leads to a problem how to guarantee constant conditions that may differ among laboratories.

The other techniques include those based on photo-oxidation of organic films (such as stearic acid (Minabe et al., 2000) and contact angle changes (Mills et al., 2002). Stearic acid forms solid films when deposited under ambient conditions on TiO₂ surface under test. The photocatalytic destruction of such solid compounds are of practical interest since they provide a reasonable model compound for the type of solid organic films that often deposit on exterior glass surfaces. On the contrary, this could be one disadvantage of mentioned method, because it resembles the conditions achieved in gaseous photocatalysis. For three-dimensional systems, such as wastewater treatment by TiO₂ surfaces, a different method should be proposed. Recently, an alternative test based upon a colour change of a dye in water has been presented by Evans et al. (2007). The formulation comprises the redox dye resazurin (a sacrificial electron donor), glycerol and a polymer (hydroxy ethyl cellulose), all dissolved in water. Whether wet or dry, upon irradiation of the ink on a photocatalytic surface, the photogenerated holes oxidize the glycerol and the electrons reduce the blue resazurin to the pink resorufin. The test is quick and comparison of photoactivity when determined using the dye and stearic acid tests indicates a good correlation. But still, the drawback of all three mentioned methods is their relativity. They are not absolute methods and a standard photocatalytic surface (i.e. Degussa P25 for slurries) must be evaluated first. Mills et al. (2003) proposed commercially available Pilkington ActivTM self-cleaning glass as such standard photocatalytic surface. Although not as active as a film of P25 TiO₂, ActivTM vastly superior mechanical stability, very reproducible activity and widespread commercial availability make it suitable and necessary exchange for P25 TiO₂.

Another, more quantitative and absolute approach for evaluating the photocatalytic surfaces is based on a measurement of the rate of the hydroxyl radical generation by oxidation of methanol, 2-propanol etc. Measurements lead to useful results for the comparison of the photoactivity of different materials, independently on the specific degradation mechanism of the selected pollutants. Marugan et al. (2006) evaluated the photonic efficiency for the hydroxyl radical generation on several silica-supported TiO₂ photocatalysts. The study has been carried out using methanol as hydroxyl radical scavenger. Methanol was chosen because previous studies (Wang et al., 2002) have demonstrated the possibility of using high concentrations of methanol to quantify the complete hydroxyl radical production from the photogenerated holes at the semiconductor surface.

Generation of HO[·] radicals are quantitatively detected also by using specific fluorescent probes. These are molecules, which upon the reaction with the substrate, give highly fluorescent products. There are few known fluorescence probes for detection of HO[·] radicals, i.e. sodium terephthalate, 1,3-cyclohexanedione, fluorescein, 4-(9-anthroyloxy)-2,2,6,6-tetramethylpiperidine-1-oxyl etc. (Gomes et al., 2005). Coumarin is a poorly fluorescent molecule that has been known to form many different products by reaction with hydroxyl radical, among the others also very fluorescent 7-hydroxycoumarin (7OHC) (Lout et al., 2005). Newton and Milligan (2006) showed in their radiolysis experiments that the yield of generation of 7OHC is around 4.7 % per generated HO[·]. One advantage of using coumarin as the probe is that 7OHC fluoresces in the visible spectral range.

According to the overview of the literature, we firstly decided to prepare different types of sol-gel derived TiO₂ films, with or without the addition of different templating agents into the sol. The physical and chemical properties of as-prepared thin films were then evaluated by different techniques. Additionally, the photocatalytic efficiencies of the material were evaluated. Within this, also a simple continuous flow photocatalytic reactor was developed. In the next step the physico-chemical characteristics of films were correlated with the photocatalytic activities. In the last step of Part I, the development of a method for evaluation of quantum yields for photocatalytic surfaces, which is based on formation rates of 7OHC (HO[·] radicals) by a fluorescence detection is presented.

4.1.2 Experimental section

4.1.2.1 Preparation of TiO₂ films

Transparent titania films were made by sol-gel processing and deposited by the dip-coating technique on both sides of the soda-lime glass slides (dimensions of 25 mm × 70 mm) with or without a silica protecting layer. The barrier glass-protecting SiO₂ and active TiO₂ films were prepared from the SiO₂ sol and corresponding TiO₂ sols (U, R, D and C). The procedure for preparation of these sols and the procedure of deposition and calcination of films is described in detail in Chapter 3.2 and Chapter 3.3.1, respectively. The names of the samples are composed of three characters: (1) U, R, D or C = the symbol of titania sol, (2) 1 to 9 = number of dipping-heating cycles, and (3) N = deposited on bare glass support or S = deposited on glass support with a thin silica barrier film.

Beside sol-gel derived films also non-transparent Degussa P25 films were deposited on soda-lime glass slides (dimensions of 25 mm × 70 mm) as it is described in detail in Chapter 3.3.2. The names of the samples are composed of two characters: (1) P denotes Degussa P25; (2) numbers from 1 to 7 denote progressive amounts of TiO₂.

4.1.2.2 Photocatalytic degradation of an azo dye in water

A continuous flow reactor (Figure 12A and B) was constructed for the experiments on the photocatalytic activity of the films deposited on microscope glass slides (25 mm × 70 mm). The reactor could be purged with different gases, was cooled with tap water and had on-line measuring capability of the UV-Vis spectra of the solution. The as-prepared titania films were kept in deionised water prior to the photocatalysis experiments. A 10 mm thick solution of NaBr (110 g) and Pb(NO₃)₂ (0.69 g) in water (230 g) was used as a 335 nm cut-off filter in front of the photocatalytic cell and a 125 W Xe lamp (Cermox xenon parabolic lamp) as a radiation source. A titania film on one side of a silica covered glass support was immersed in the dye solution next to the wall of the photocatalytic cell and irradiated (surface 23 mm × 23 mm) along the normal direction. The dye solution (aqueous solution (4.8 mL) of Plasmocorinth B (40 mg L⁻¹), see its chemical formula on Figure 12C) was continuously purged with oxygen during the irradiation. A peristaltic pump (Heidolph PD 5001) with a silicon hose was used to drive the solution from the photocatalytic cell to the cell positioned in the UV-Vis spectrophotometer for on-line absorbance measurements and back to the photocatalytic cell at a flow rate of 10 mL min⁻¹. One photocatalytic experiment lasted 50 min.

4.1.2.3 Photocatalytic degradation of coumarin in water using monochromatic irradiation

One-sided TiO₂ film, deposited on SiO₂-precoated sodium glass (40 mm x 9 mm) was firstly activated by 1 h irradiation in water with the help of black tubes (polychromatic radiation with the maximum at 365 nm). After pretreatment, TiO₂ film was positioned on the back wall of 4 mL standard fluorescence quartz cell (10 mm x 10 mm) containing the aqueous solution of coumarin (5.0 × 10⁻⁴ M, chemical structure on Figure 12D, Fluka). The solution was then irradiated by a steady-state 365 nm monochromatic radiation, obtained from a 1600 W Xe lamp in conjunction with a high-intensity monochromator (Schoeffel). The half-width was about 10 nm. The solution was also continuously stirred and purged with O₂ during irradiation. The photon flux in the cell was evaluated by potassium ferrioxalate actinometry (Murov et al., 1993: 299), and determined to be 3.0 × 10⁻⁶ einstein L⁻¹ s⁻¹. The temperature was kept constant at 20 °C during the experiment. The samples (0.4 mL) were taken from the cell at different times during the irradiation for analysis with HPLC. The samples were analysed without additional filtration, extraction or centrifugation. The degradation experiments lasted between 30 and 150 min. At least two repetitions with each film were performed to evaluate the reproducibility of the measurements. The cell and the film were washed with deionised water before starting a new experiment.

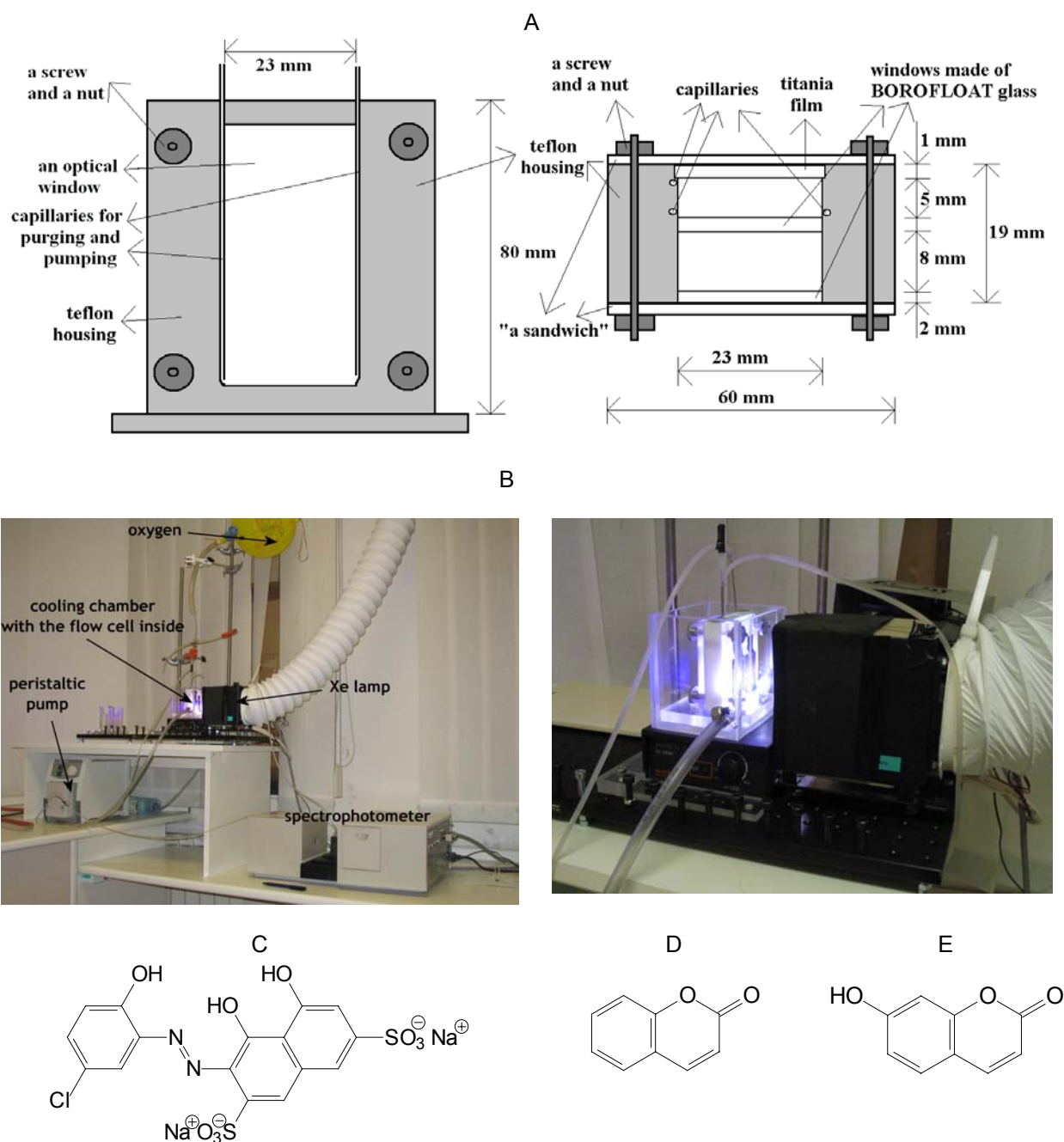


Figure 12: A: The scheme of continuous flow photocatalytic cell with a thin-film TiO_2 catalyst deposited on a microscope glass slide: front view (left) and top view of the reactor (right); B: the photos of continuous flow reactor; C: chemical structure of Plasmocorinth B azo dye; D: chemical structure of coumarin; E: chemical structure of 7-hydroxycoumarin (7OHC)

4.1.2.4 Evaluation of quantum yield of different TiO_2 films

The transmittance (T) and reflectance (R) spectra (300 - 700 nm spectral range) of clean and calcined one-sided TiO_2 films deposited on SiO_2 -precoated sodium glass were recorded on UV-Vis-NIR spectrophotometer Lambda 950 (Perkin Elmer) employing an integration sphere with inner diameter of

150 mm (PELA 1000, Perkin Elmer). When measuring T spectra, the sample was inclined 11° from the normal direction of an incoming radiation beam of a spectrometer with the intention to get the optical interference maxima and minima at exactly the same wavelength values as in reflectance spectra. According to the eq. 4.3, the sum of T and R spectra was subtracted from 1 in order to obtain the real absorption (A) of the investigated TiO_2 film.

$$T + R + A = 1$$

4.3

The rate of absorbed photons by TiO_2 sample was obtained by multiplying the photon flux in the photocatalytic cell with the A at 365 nm. The rate of degradation of coumarin (or the rate of formation of 7OHC) was calculated from the HPLC analysis for each separate TiO_2 sample. In some cases, the formation rates of 7OHC were obtained also from the measurements of fluorescence of the irradiated solution. Finally, the quantum yield for the degradation of coumarin (or formation of 7OHC) at 365 nm was calculated.

4.1.3 Results and discussion

4.1.3.1 Optical properties and porosities of the TiO_2 films

All titania films obtained via sol-gel processing were of a high optical quality. They were crack-free and transparent over the whole visible spectral range (Figure 13A). They were also free of any organic residues, which was confirmed by XPS spectroscopic measurements (Lavrenčič Štangar et al., 2006). As a rule, the presence of a Pluronic F-127 or Brij 56 surfactants in the dip-coating solution increased the thickness of the film (Figure 13B). This is a consequence of increased viscosity of the sol upon an addition of a polymeric templating agent. Film thickness obtained by single dipping ranged from few tens of nm up to 300 nm without deterioration of the optical quality. It increased linearly with the number of dipping and heat-treatment cycles. The type of the substrate (bare glass or SiO_2 -precoated glass used in case of high-temperature film deposition) had no influence on the resulting thickness of the titania film (Figure 13B). Along with a thickness increase, the mass of titania films also increased when using surfactants (Table 3). The macroscopic density of the film, deposited from the sol with added Pluronic F-127, was only half as dense as the film prepared without addition of surfactant. Supposing that the crystallinity was the same in both cases (anatase), which is only a rough approximation since the amount of amorphous phase probably differs, it could be concluded that the film with added Pluronic F-127 was more porous than the others.

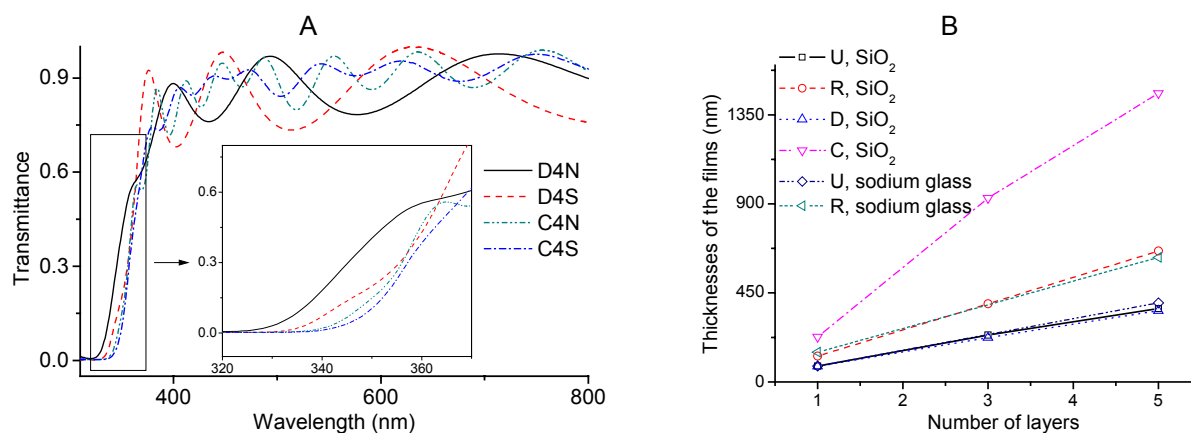


Figure 13: A: UV-Vis transmittance spectra of different one-sided TiO_2 films prepared by high-temperature sol-gel processing; B: The influence of number of TiO_2 layers on thicknesses of the titania films

The difference in porosity was additionally confirmed by nitrogen sorption experiments, which gave the BET (Brunauer, Emmett and Teller) surface area value for C film $75 \text{ m}^2 \text{ g}^{-1}$, while for D film only $5.5 \text{ m}^2 \text{ g}^{-1}$. It must be stressed that in order to be able to measure the nitrogen sorption, the “film powder” samples were obtained from the immobilized thin films. The detailed procedure of obtaining the “film powders” is described in Chapter 3.4.

Table 3: The measured masses, calculated surface densities, macroscopic densities and particle sizes of four-layered titania films; calculated RMS roughnesses of single-layered titania films

Film	Amount of titania (mg)	Surface density (g m^{-2})	Macroscopic density (g L^{-1})	Particle size (from XRD) (nm)	RMS roughness (from AFM)(nm)
U4(1)S	3.0	1.4	4200	18	1.23
R4(1)S	3.6	1.8	3300	11	1.29
D4(1)S	3.0	1.3	4300	19	0.95
C4(1)S	5.8	2.6	2200	10	1.87
R4(1)N	3.6	1.8	3300	15	3.62
D4(1)N	3.0	1.3	4300	17	0.85
C4(1)N	5.8	2.6	2200	13	2.21

The measured T values for a film deposited on the both sides of the glass slide (T_B) were transformed to the transmittance values corresponding to the same film deposited on a single side only (T_S), by using an eq. 4.4 (Sreemany and Sen, 2004). The UV-Vis spectra of the films shown in Figure 13A therefore correspond to the films deposited by 4 coating cycles on one side of the glass substrate, which was either bare (N) or SiO_2 pre-coated (S). All spectra are characterized by interference fringes having lower amplitudes in case of templated films (spectra C4S and C4N). Accordingly, such phenomena in UV-Vis spectra can be ascribed to the thickness of the films and also to the change in density and hence in porosity of the film structure. In addition, interference fringes may vary inside one particular spectrum (C4S) suggesting that films are multilayers with various refractive indices. This may be due to repeated coating-heating cycles, where the first layer underwent longer heat-treatment time than the second one etc. It should be also noted that underlying SiO_2 protective layer may also contribute to the observed amplitude variation.

$$T_S = 2T_B / (1 + T_B) \quad 4.4$$

When comparing spectra of templated films (C4S and C4N) to adequate non-templated ones (D4S and D4N), it is clearly seen that an addition of the template produced a red shift of the absorption edge of the film. The shift can be ascribed to a higher film thickness and to a difference in crystallite size caused by the addition of the template. Absorption of radiation below 370 nm (see insets in Figure 13A) is due to the excitation of electrons from the VB to the CB of TiO_2 and therefore directly responsible for the photocatalytic activity of the films, discussed below in a separate subsection. Higher absorption of UVA radiation in case of templated films, with respect to corresponding non-templated films, is expected to result in their higher photocatalytic activity.

A red shift of the absorption edge of the film was observed systematically also with an increasing number of coating cycles, in agreement with other preparation methods (Yu et al., 2001; Guillard et al., 2004; Yoshitake et al., 2002). A decrease in the band gap energies of TiO_2 with increasing number of coating-heating cycles from 3.48 eV for C1S to 3.28 eV for C7S was calculated from UV-transmittance spectra of the titania films. The difference in the size of the crystallites could be an explanation for this phenomena, because thicker films that underwent longer heat treatment by repeated coating-heating cycles have relatively larger anatase crystallites and this causes the onset of absorption to shift to the red part of the spectrum (Yu et al., 2004). Anyway, the intrinsic absorption of the TiO_2 films at 365 nm, obtained from transmittance and reflection spectra of C and D TiO_2 films increases linearly with the increasing number of TiO_2 layers for C and D films (Table 5 in Chapter 4.1.3.4). This is not in accordance with the decrease of the band gap energies. In order to clarify the confusion, some additional experiment should be performed, but this was out of the scope of my PhD thesis.

There is another factor that influences UVA light absorption properties of the TiO₂ films made by high-temperature processing route (Figure 13A) and this is a type of the substrate. Comparing spectra of the two films D (spectra D4S and D4N), it is clearly evident that the protecting thin silica film underneath also caused a red shift of the absorption edge of the upper titania film. As TiO₂ film thickness was the same in both cases, the shift can be attributed solely to the role of the substrate on the growth of anatase crystallites, influencing radiation absorption efficiency below 370 nm (Figure 13A, inset). In contrast to spectra of films D, the two spectra of films C in Figure 13A do not differ as significantly in the UVA absorption properties (no big shift of the absorption edge). This is because the effect of the substrate is diminished in case of much thicker templated TiO₂ films C4 (1200 nm) compared to non-templated films D4 (300 nm).

4.1.3.2 Structural and morphological properties

X-ray diffraction (XRD) patterns of the most efficient films C are presented in Figure 14A and 14C. The patterns in Figure 14C were obtained directly from C4 films, but the problems of noisy background and small intensities of the peaks are seen. In order to get diffractograms with higher intensities of peaks and therefore better identification of the crystalline phases, they were recorded by using the “film powder” samples. Figure 14A shows that C4 films with high photocatalytic activities consist of a predominant anatase crystalline phase (JCPDS of TiO₂ anatase 21-1272) with one major peak at $2\theta = 25.4^\circ$ which corresponds to (1 0 1) reflections of the anatase phase and which is also supposed to be the most active one for photocatalytic reactions. In addition, the presence of a brookite phase (JCPDS of TiO₂ brookite 29-1360) with a small peak at $2\theta = 30.8^\circ$ is evident in both samples. Films were calcined at 500 °C, which was high enough for the formation of the active anatase phase. For example, films calcined at 350 °C did not show any photocatalytic activity due to an absence of anatase crystalline phase (Černigoj, 2005). Additionally, the conversion to rutile, which is not so photocatalytically active, was negligible at 500 °C. It has been also found that TiO₂ particles immobilized on the quartz support during calcination remained in the anatase form even at 800 °C, whereas self-supported TiO₂ particles in powders were more easily converted into the rutile form starting already at 500 °C (Martyanov and Klabunde, 2004). Accordingly, we observed 5-30% of rutile phase relative to anatase when the samples were calcined in a powder form at 500 °C (Černigoj et al., 2006a).

Similarly to UV-Vis and photocatalytic results, the XRD patterns of both C4 films (Figures 14A and 14C) show only small differences. The effect of the glass support on relatively thick TiO₂ coatings (1200 nm) was minor: even the most developed anatase-TiO₂ (101) peak at $2\theta=25.4^\circ$ is comparable in its intensity in C4N and C4S samples.

The films D4 were characterized by XRD only as thin films (immobilized on the support) (Figure 14B) and not in film powder form, as in the case of C4 films. There are mainly two reasons for this: (i) their thickness is four times lower and the collecting of powder would be very time consuming, (ii) the adherence of films D to the glass support is very high and therefore the mechanical scratching extremely difficult. XRD measurements were done directly on immobilized films resulting in less intense diffraction peaks and noisy patterns. Despite this the significant differences between D4N and D4S films are evident. The crystallization of anatase in case of D4N is considerably less developed, i.e. the amorphous-anatase TiO₂ transition is incomplete. This is in a good correlation with photocatalytic inactivity of D4N films (Table 4).

$$L = K\lambda/\beta\cos\theta$$

4.5

The use of surfactant contributed to the formation of highly oriented anatase phase along the (1 0 1) crystallographic plane and to the smaller mean grain size. The grain size, i.e. the effective size of coherently scattering domains, was calculated from the (1 0 1) peak of anatase using the Scherrer's equation (eq. 4.5) (Klug and Alexander, 1973: 687). Here λ is the wavelength of X-rays (1.54 Å for Cu K α radiation), K is a constant taken to be 0.9 (assuming no crystal distortion in the lattice), β is the full width at half maximum of the signal in radians corrected for the instrumental broadening (0.07°), and θ is the diffraction angle in degrees. In order to obtain comparable results between C and D films, the grain sizes

were calculated from diffractograms by measuring directly immobilized thin films C and D (Figure 14B and C). A crystallite size of 10-11 nm on SiO₂-glass and 13-15 nm on bare glass support was thereby estimated for films prepared with surfactant (Table 3). The slightly larger anatase grains of films deposited on bare glass substrates may be a consequence of the higher concentration of Na⁺ ions diffused from the substrate.

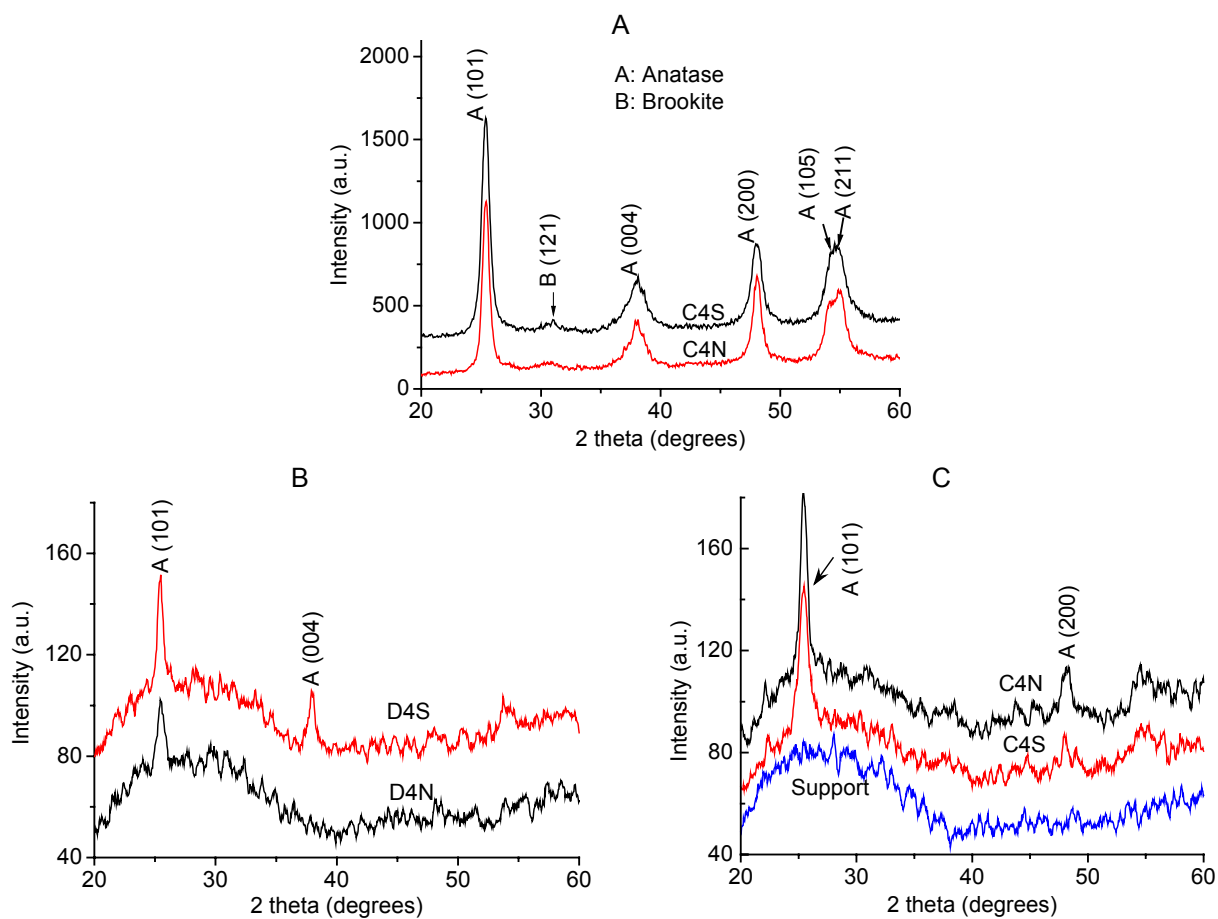


Figure 14: A: XRD patterns of TiO₂ film powder samples; B and C: four-layered thin film samples

We verified the influence of the substrate on thinner C1 films (deposited by only single dipping, film thickness ~ 300 nm) by atomic force microscopy (Figure 15A and B). The AFM images undoubtedly prove the effect of the substrate on the crystal growth. Sodium ions migration from the substrate without a barrier film in the interior of TiO₂ film (C1N) prevented the formation of granular surface with well-resolved nanoparticles as it was in the case of using substrate with a silica barrier film (C1S). The presence of Na⁺ ions caused the agglomeration/aggregation of particles, which resulted in lower contact surface area and also this could lead to lower photodegradation rates. The positive effect of adding the surfactant in the sol is however seen by comparing the images B and C in Figure 15, representing templated and non-templated TiO₂ film, respectively, both deposited on the top of silica barrier layer. The surface of non-templated D1S film is ill-defined and more flat (RMS roughness: 0.95 nm) than the surface of templated C1S film, which is rougher (RMS roughness: 1.87 nm) and well-structured with clear interstices between the particles (their estimated size from AFM is in the range 10-20 nm) (Table 3). The differences in AFM images agree with differences observed in the UV-Vis spectra, reflecting the influence of both experimental parameters, type of the substrate and surfactant assistance, on the related morphological and optical properties of the films.

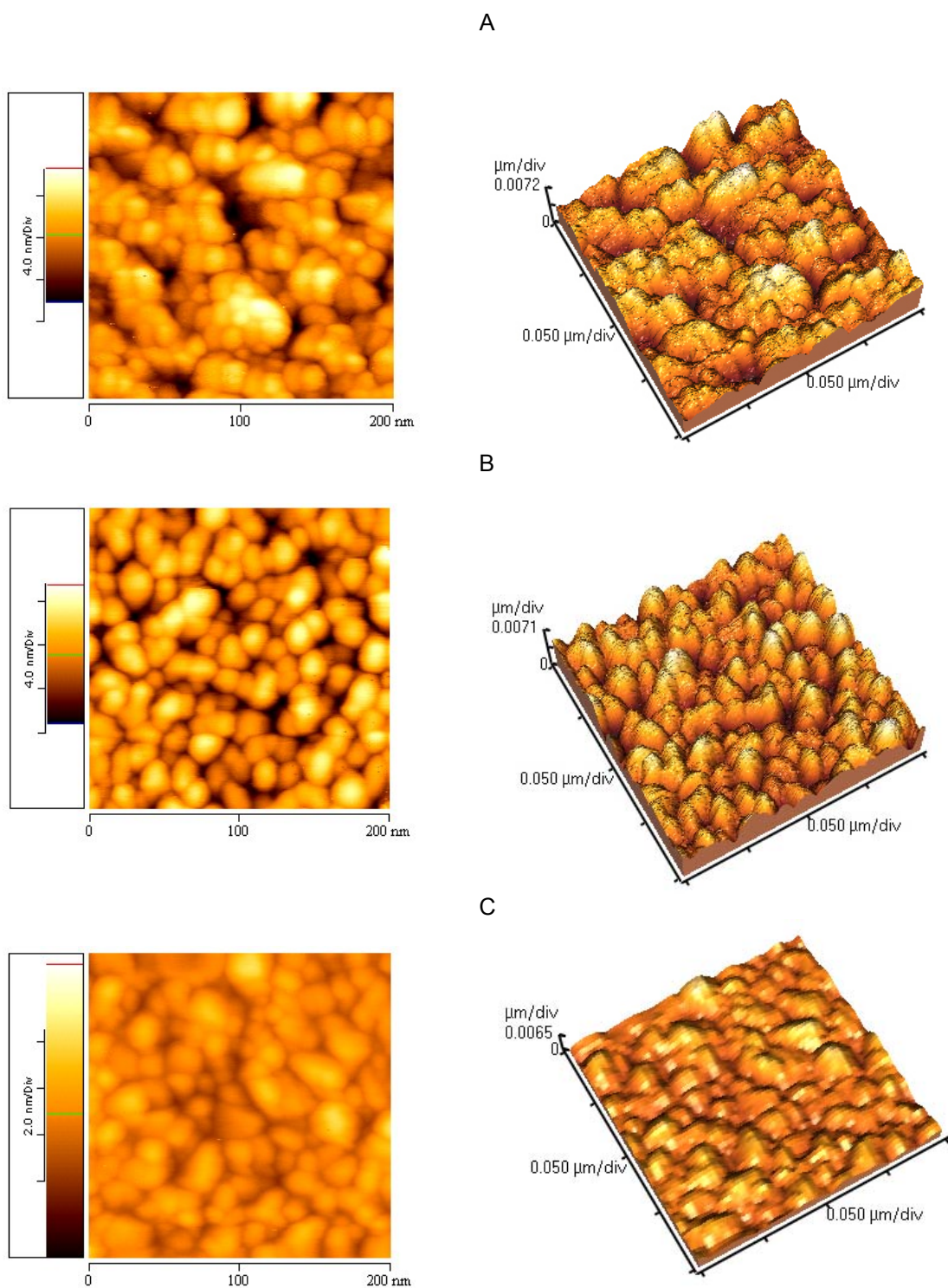


Figure 15: AFM 2- and 3D images of the surface of TiO_2 films; A: C1N, B: C1S and C: D1S

The surface and in-depth composition of films D1N, D1S and C1S were analyzed also by XPS. The aim of the analysis was to investigate the chemical composition of the deposited layers, their possible intermixing (in the case of S substrates) as well as the interdiffusion of sodium in the coatings (Lavrenčič Štangar et al., 2006). Only some relevant conclusions are given here as this part of work was already out of scope of my PhD thesis. By comparing D1N and D1S samples, the most evident difference was the different

amount of detected sodium. While in D1N the atomic percentage of Na was quite high (ca. 5-6%) and constant along the titania layer, in the sample D1S sodium content was lower than 0.5%, proving the effectiveness of silica barrier film. As far as the sample C1S is concerned, the XPS in-depth profile again revealed the presence of a compositionally pure and completely Na-free titania layer, while the underlying silica layer is characterized by a presence of sodium ranging between 1-2% at. All these results are in accordance with XRD and UV spectroscopic results.

Our results confirm that sodium ions impurities have a negative influence on the crystallization of TiO_2 , which is otherwise very important for photocatalysis utilizing the semiconducting properties of the material. We agree with somehow contradictory explanation that sodium ions retard the formation of the anatase phase and increase the particle size (Nam et al., 2004) in sense that Na^+ ions inhibit anatase crystallization and cause agglomeration of TiO_2 particles. However, investigation on our films did not give evidence that sodium ions would stimulate the crystallization of any other phase. Brookite phase was found in the thin film samples regardless of the type of the substrate.

4.1.3.3 Photocatalytic activity

The first goal using different TiO_2 films was to define their photocatalytic properties for degradation of a stable organic molecule. Stable azo dyes were the logical choice for this purpose because it is easy to measure their decolorisation on-line with the help of the spectrometer. The breakage of the azo group of an azo dye is the main reason for bleaching of the coloured aqueous solution. This is not the only mechanism of degradation/oxidation of an azo dye and there are other primary oxidative pathways as hydroxylation of aromatic ring etc., which mainly do not lead to the bleaching. Anyway, the quantification of the bleaching at the beginning of the experiment is proportional to the oxidation of the molecule. Therefore monitoring of the bleaching of a stable azo dye was chosen as a suitable method for evaluation of photocatalytic activities of TiO_2 films due to simplicity of on-line measuring of the absorption of the aqueous solution with the help of a spectrophotometer. Suitable azo compounds for photodegradation studies should fulfill several requirements:

- A dye must be stable when irradiated without the presence of a photocatalyst.
- Coloured degradation products are not desired, because the UV-Vis measurement (as a tool to define the degree of dye decolorisation and degradation) becomes then useless.
- A dye must absorb as little as possible of UV radiation, used in the experiments (in my case between 335 and 390 nm).
- A dye should not adsorb extensively on the photocatalyst film in order to relate the photobleaching of the solution with the photocatalytic process.

The experiment using the aqueous solution of methylene blue (which is a representative of thiazin group of the dyes) was not appropriate for my photocatalytic studies due to a strong adsorption on the surface of catalyst and due to its instability under UV irradiation even in the absence of the photocatalyst. Methyl orange was the next choice, but different coloured degradation products were generated during the photocatalytic degradation which disabled the simple measuring of bleaching as a tool for evaluation of photocatalytic degradation. Acid Orange 7 satisfied all above criteria, if it was irradiated in a batch reactor. When the experiments were performed in a continuous flow reactor, the dye became unstable during irradiation even without the photocatalyst. Plasmocorinth B was found to satisfy all four criteria described above when used in a continuous flow reactor. Also the reproducibility of results of photodegradation with equal films was good. Therefore Plasmocorinth B was chosen as a model compound to define the photocatalytic efficiencies of prepared films (Černigoj, 2005).

The photocatalytic activity of as-prepared films towards the Plasmocorinth B dye in water was tested in the home-made continuous flow cell (Figure 12A) with on-line connection to the UV-Vis spectrophotometer measuring the decrease in the absorbance of the solution at 527 nm. Figure 16 represents the degradation curves of the dye solution catalyzed by four-layered TiO_2 films deposited on SiO_2 support. The same experiments were done also with one-, two-, three- and five- layered films, deposited on SiO_2 support, and with one- and four-layered films, deposited on sodium glass support. All degradation curves indicate first-order kinetics, therefore they were fitted as first order reactions regarding the decrease of

absorbance at 527 nm. The mean half-lives and standard deviations were calculated for each catalyst separately. Some of the results are included in Table 4.

Table 4: The calculated half-lives and rate constants of photodecolorisation of aqueous Plasmocorinth B solutions using calcined TiO₂ films (1 and 4 layers)

	Film	Half-time (min) -mean value	Rate constant (min ⁻¹ x 10 ⁻³)
1	U1S	108	6.42
2	U1N	∞	0
3	R1S	108	6.42
4	R1N	∞	0
5	D1S	108	6.42
6	D1N	∞	0
7	C1S	62	11.2
8	C1N	107	6.48
9	U4S	37	18.9
10	U4N	∞	0
11	R4S	29	23.7
12	R4N	38	18.5
13	D4S	36	19.3
14	D4N	∞	0
15	C4S	19	36.2
16	C4N	22	32.0

Temperature of calcination of the films was 500 °C, which is the optimal temperature for sodium glass substrate. Lower temperatures of annealing resulted in lower photocatalytic activity of photocatalyst, because anatase is not yet developed in the films suspecting to lower annealing temperatures. Higher temperature would result in melting of sodium glass support. Time of calcination was 30 minutes, which was long enough to degrade the organic residues captured in the film. The highest degradation rates were achieved when the solution was purged with oxygen during the experiment. Purging with argon or no purging resulted in lower degradation rates. This is logical, if the O₂ acts as an acceptor of photogenerated electrons. The recombination of holes and electrons prevailed, when only Ar was present.

The films deposited from the same sol on both substrates were compared (Table 4, Figure 16B). Na⁺ cations from the glass substrate diffuse into the TiO₂ film's grains during the thermal treatment with an adverse effect on the photocatalytic activity. This was truly noticed also in our experiments. The only photocatalytically active one-layered titania film was the one deposited from sol with added Pluronic F-127. Its photocatalytic activity was also lower than the activity of the same film, deposited on SiO₂ support (C1S and C1N in Table 4). Similar observations were noticed also with four-layered films. The films deposited from sols D and U (U4N and D4N in Table 4) were still not photocatalytically active. The other two films (R4N and C4N in Table 4) showed some activity against the photodecolorisation of Plasmocorinth B, but this again was still lower than with the same films, deposited on SiO₂ support. This is an excellent agreement with the results, obtained by UV spectroscopy (Figure 13A), where a significant blue shift of the absorption edge of D4N film is noticed when compared to D4S film, but almost no shift is noticed between C4N and C4S films. The shift could be attributed to lower crystallinity of thin samples deposited on sodium glass support (Figures 14B and C).

By increasing the thickness of the deposited films obtained by performing multiple dipping cycles, the effect of sodium diffusion diminishes and the upper part of the TiO₂ film becomes more or less free of sodium ions impurities and the films become photocatalytically active. Accordingly, a set of experiments was performed with different films deposited on SiO₂ support. Results presented in Table 4 show that the photocatalytic activity of the films when deposited on the glass slides with the SiO₂ protective layer

increases with the film thickness (Figure 13B) in all cases. On the other hand it is shown that when comparing different films with the same number of layers of TiO₂, the addition of Pluronic F-127 has a noticeable effect on the increasing photocatalytic activity of the films.

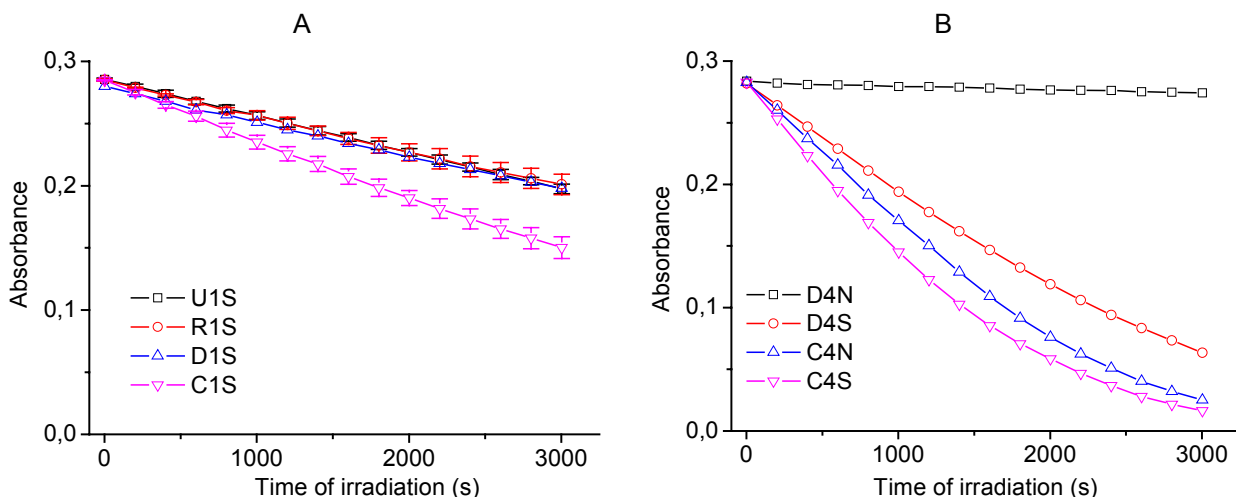


Figure 16: A: The influence of addition of surfactants in sols on photodecolorisation of Plasmocorinth B solution with one-layered TiO₂ films deposited on SiO₂ support. B: The influence of the support on photodecolorisation of Plasmocorinth B solution with different four-layered films.

Our photodegradation studies showed that photocatalytic activity of the films increases with the film thickness and consequently with the TiO₂ amount irrespective of addition of surfactants into the sols (Figure 17). The relation between the thickness (the number of layers, the amount of titania film) and the degradation rate is quite linear for films, deposited from sols U, R and D. This could be simply accounted for by the increase in the number of active sites and in the amount of photons absorbed by TiO₂. A proof for this experimental fact could be found in transmittance UV-Vis spectra of studied films, but interference fringes between 340 and 400 nm disabled the exact calculations of absorbed radiation in this UV range.

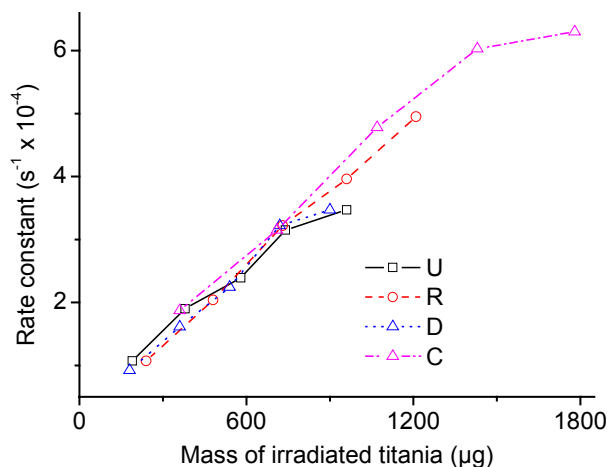


Figure 17: The influence of irradiated amount of titania on the rate constant for the photodecolorisation of aqueous solution of Plasmocorinth B; SiO₂ support

The rate constants of films, deposited from sol C, increase linearly with the number of coatings until the mass of titania about 1500 µg, after this the bleaching rate becomes relatively independent on the amount of additional TiO₂ (Figure 17). Films from sol C are thicker than films deposited from sols U and D and photogenerated holes and electrons from the bottom of the films could not reach the surface of the films,

where they can react with the organic molecule. Therefore the photocatalytic activity cannot correlate indefinitely with the film thickness. It could be expected from Figure 17 that an additional increasing of thicknesses of films R, D and U would also lead to the same nonlinear behaviour of degradation rate constants as it is seen in the case of films C.

The different amounts of irradiated titania films are involved also when comparing different TiO₂ films with the same number of layers and their photodegradation rates. It was calculated from degradation rates that one-layered TiO₂ film deposited from sol C (surfactant Pluronic F-127) is twice more photocatalytically active than similar film deposited from sol D (without surfactant). The mass of the first film is 360 µg, the mass of the second is 180 µg. Higher mass leads to more photoactive sites and more efficient absorption of radiation and consequently higher number of reactive species on the surface of the film capable of reacting with azo dye. It seems from the Figure 17 that the mass of titania is the decisive parameter defining the final photocatalytic activity, because all deposited films have similar photocatalytic activity per unit of mass. This was not expected, because it was believed that also surface structure and the porosity of the film could be involved in improving the photocatalytic activity. In the next subchapters, the influence of a intrinsic absorbance of the films on the photocatalytic activity is studied and explained in more detail.

4.1.3.4 Evaluation of quantum yields of photocatalytically active surfaces

The information on photocatalytic activities obtained from the results above were supplemented by determination of quantum yields. It was necessary to compare our films with some standard material to obtain the intrinsic value of the new material. Therefore C and D films deposited on SiO₂-precoated glass were compared with the Degussa P25 films. Degussa P25, a commercially available TiO₂, is still the most widely used standard TiO₂. It was deposited on glass slides via sedimentation process from aqueous suspension of Degussa P25 powder. White, non-transparent film of different thicknesses (and consequently masses) were obtained. It should be stressed that films prepared by described procedure could not be used in industrial applications because of low physical adhesion of the catalyst. In our experiments they served only as model films for comparison of photocatalytic activities between different types of catalysts. The surface densities of all deposited TiO₂ are collected in Table 5.

It was shown in previous chapters that the Φ is the only truly relevant value for comparison of different photocatalytically active surfaces, therefore I decided to evaluate it for all three types of deposited films. When evaluating Φ , standard and reproducible conditions are of high importance. Temperature was kept constant at 20 °C and the solution was always saturated with O₂. To get rid of problems with mass transfer to the surface of titania, constant stirring was applied to the system. Aqueous solution of coumarin was chosen as a degradation medium because of the characteristics described in the Chapter 4.1.1. Additionally, the concentration of coumarin was relatively high (5 x 10⁻⁴ M) with the intention to monitor only the degradation of 10 % (or even less) of the initial coumarin, present in the cell. With this we could assure that the majority of formed hydroxyl radicals reacted with the parent molecule and not with its degradation products or via some other mechanisms. Monochromatic radiation was used in the experiments, because otherwise quantum yield could not be defined. The wavelength at 365 nm was chosen because: (i) it is within the UVA region, which is also within the solar spectrum; (ii) TiO₂ is excited at this wavelength; (iii) coumarin does not absorb at 365 nm and consequently it cannot be degraded by the direct radiation; (iv) due to completely transparent medium at 365 nm all the incident photons in the cell reach the TiO₂ surface.

The intrinsic absorption (*A*) of the TiO₂ films cannot be evaluated directly from the transmittance (*T*) spectra, such as those presented in Figure 13A. If the value of the *A* at the desired wavelength is taken out of the *T* spectrum, then this value corresponds to the sum of the true absorbed light and of the reflected light. The reflection on transparent films (in our case films C and D) is a consequence of optical interference due to different refraction indexes of TiO₂, air and substrate, on the contrary, the reflection on non-transparent films (in our case Degussa P25 films) results from scattered and reflected radiation on macroscopic particles. In any case, the reflection on prepared films must be evaluated and the sum of *T* and reflectance (*R*) spectra enable the calculation of the true *A* of TiO₂ at the certain wavelength.

Table 5: Different parameters of TiO₂ films, needed for the calculation of quantum yield

Film	Surface density ($\mu\text{g cm}^{-2}$)	A at 365 nm (%)	Coumarin degradation: $v = -dc/dt$ ($\text{mol L}^{-1} \text{min}^{-1} \times 10^{-7}$)	RSD (%)	Φ_{365} (coumarin) (%)	7OHC formation: $v = dc/dt$ ($\text{mol L}^{-1} \text{min}^{-1} \times 10^{-9}$)	RSD (%)	Φ_{365} (7OHC) (%)
P1	60	19	9.1	6.5	2.7	28.6	0.4	0.08
P2	210	44	15.6	0.7	2.0	60.2	1.2	0.08
P3	250	46	16.1	4.0	1.9	60.6	2.4	0.07
P4	471	56	20.6	3.6	2.0	76.9	0.7	0.08
P5	690	67	25.1	4.1	2.1	98.7	2.2	0.08
P6	915	72	23.5	3.2	1.8	108	3.5	0.08
P7	1910	68	22.1	1.0	1.8	91.0	0.5	0.07
D1S	29	2.9	1.4	2.8	2.7	4.9	3.1	0.09
D2S	62	7.9	2.0	8.8	1.4	6.7	2.0	0.05
D3S	93	9	2.3	2.5	1.4	7.5	4.9	0.05
D4S	123	11	3.0	5.4	1.5	9.3	4.0	0.05
D6S	191	15	2.0	9.5	0.7	6.2	4.2	0.02
D9Sa ^a	281	22	4.4	8.9	1.1	14.7	6.4	0.04
D9Sb ^a	281	22	3.9	4.0	1.0	10.9	7.2	0.03
C1S	62	5.6	1.8	0.6	1.8	6.2	0.3	0.06
C2S	112	12	3.5	10.7	1.6	10.6	3.2	0.05
C3S	191	15	5.0	2.7	1.9	14.3	3.4	0.05
C4S	244	22	5.5	2.1	1.4	16.7	2.9	0.04
C7Sa ^a	430	39	6.7	7.7	1.0	21.5	9.3	0.03
C7Sb ^a	430	39	5.1	8.0	0.7	15.5	4.0	0.02

^a a and b denote two films, prepared under exactly the same experimental conditions from the same sol.

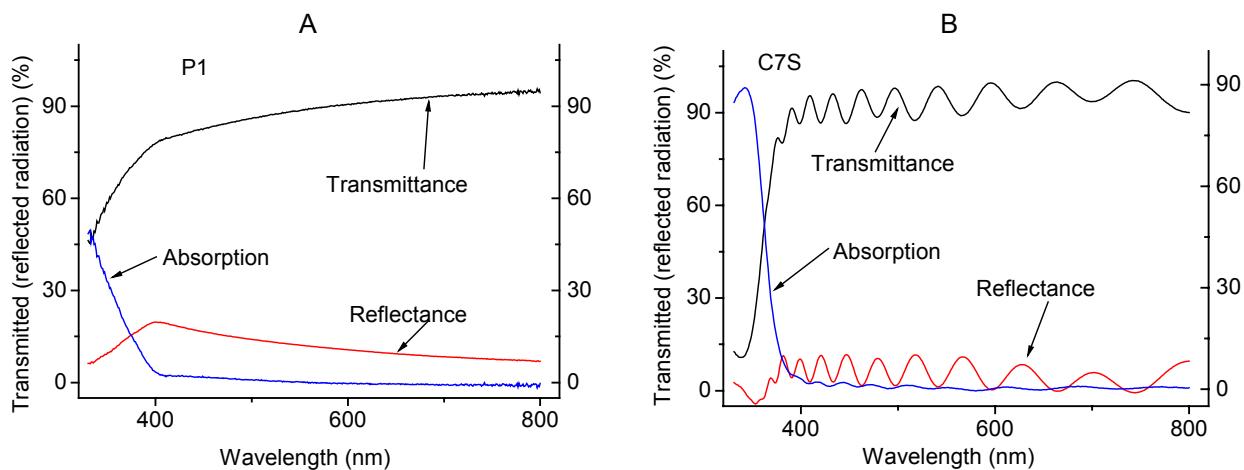


Figure 18: Optical properties and evaluation of the intrinsic absorption of TiO₂ films; A: Degussa P25 film; B: C7S film

Figure 18A and 18B present the *T*, *R* spectra and the sum of both spectra for P1 Degussa P25 film and for C7S film, respectively. The same measurements were done also for other films and the intrinsic percentages of absorbed radiation at 365 nm for all the studied films are given in Table 5. Interestingly, the absorption of the radiation on C and D films linearly increased with the number of layers (and consequently with the mass of the deposited catalyst). The trend was not the same on Degussa P25 films,

where the A rose till certain value and then it was constant or even it decreased a little bit from that point forward. The reason could be in the non-transparency of the material, so higher thickness of titania leads to the absorption of the photons only by the upper layers, meanwhile the reflectance was the same or it was even higher on less transparent films. This was not observed in case of transparent TiO_2 films.

If a fresh film was directly used for photocatalytic degradation of coumarin, the rate of coumarin degradation was in the first repetition considerably lower than in the second or in the third. The same phenomena were known also from the experiments with Plasmocorinth B and methyl orange with polychromatic light sources (Černigoj, 2005). Therefore the films were firstly immersed in water and preactivated by UVA illumination for around 60 min. Such films showed stable and reproducible photocatalytic activities during the next few hours. I did not explore the activation phenomena in detail, but two possible reasons could be outlined. The first is the adsorption of organic and/or inorganic impurities from the atmosphere on the TiO_2 surface, thus decreasing its photocatalytic efficiency by blocking the active sites. The second is so called photo-induced superhydrophilicity (PSH). It is a process, where surface trapped holes weaken the bond between O and Ti and as a result, at such a weakened site, O_2 is released creating an oxygen vacancy, followed by the dissociative adsorption of water at the site to render it more hydroxylated. Such surface becomes superhydrophilic, the contact angles between water droplets and the surface are much lower than before the irradiation. PSH surface is restored to its original form when stored for long periods in the dark. Anyway, it is possible that an increase in the degradation rate is affected by the PSH.

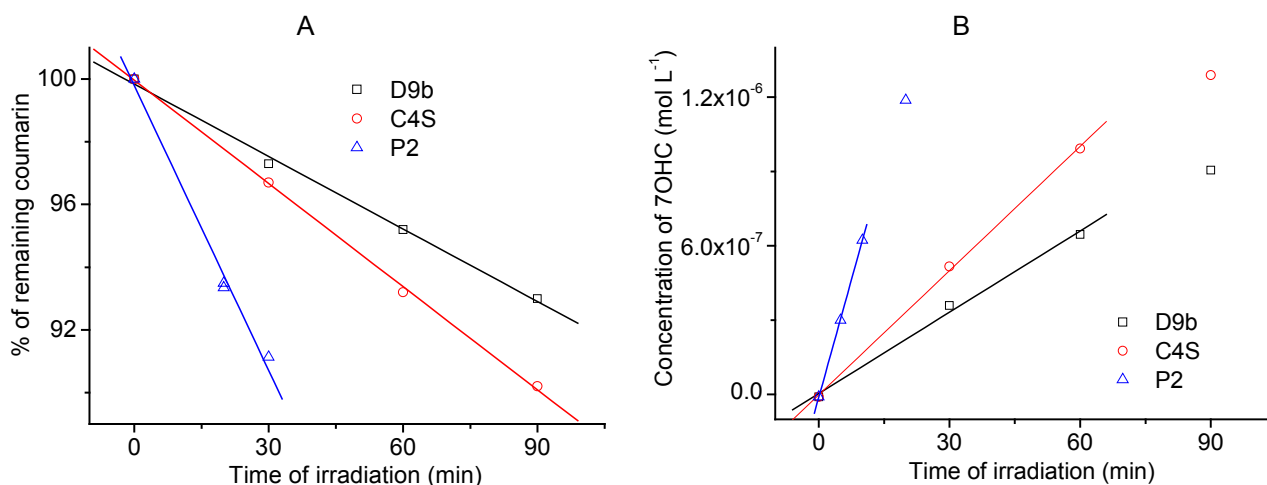


Figure 19: Photocatalytic experiments with coumarin; A: degradation of coumarin, monitored by HPLC-UV detector at 275 nm; B: formation of 7OHC, monitored by HPLC-FLD at 456 nm

As it was mentioned before, both the degradation of parent coumarin and the formation of 7OHC were monitored with HPLC analysis. Some representative experiments with different types of films are presented on Figure 19A (degradation) and B (formation). The amount of 7OHC increases linearly only until its concentration reaches 10^{-6} M, afterwards the rate of its formation starts to decrease. Therefore the degradation and formation rates were calculated only from the starting linear region. All the results together with the relative standard deviations (RSD) of degradation and formation rates are summarized in Table 5. Degradation of the parent molecule and the rate of formation of 7OHC correlate within different experiments. When the degradation rate gets higher, also the formation rate linearly follows the degradation rate (Figure 20A). Additionally, the error (RSD values) connected with measuring the fluorescence is smaller than in case of measuring the degradation of coumarin. An additional simplification could be on-line use of spectrofluorimeter instead of time-consuming HPLC-FLD system to evaluate the formation rate of 7OHC. The preliminary results obtained with Degussa P25 films confirmed the advantage of such type of measurement (Figure 20B), because the values obtained with spectrofluorimeter completely correlate with the concentrations of 7OHC, obtained with HPLC-FLD.

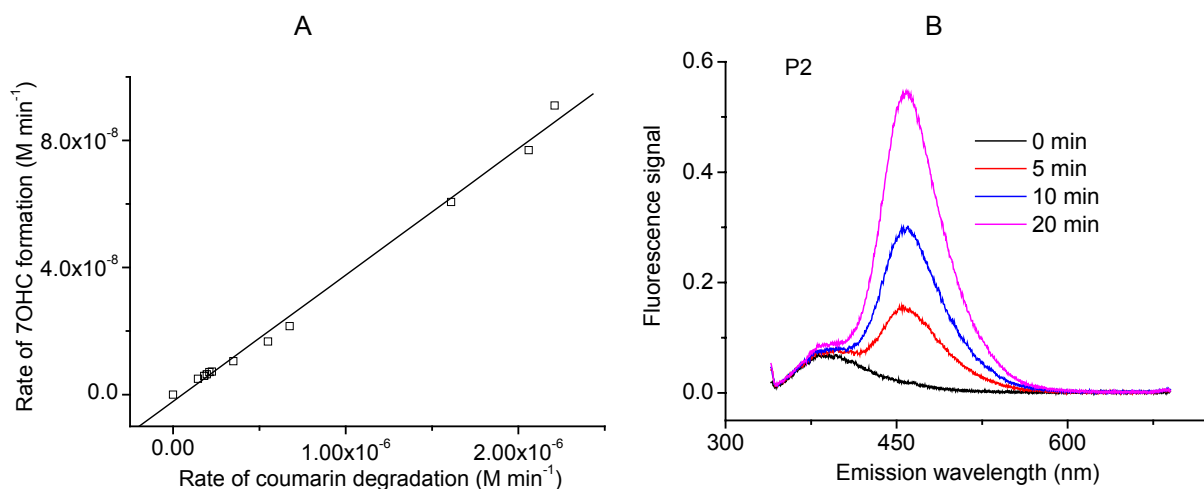


Figure 20: A: A correlation between the formation rates of 7OHC, evaluated with HPLC-FLD, and degradation rates of coumarin, evaluated with HPLC-UV; B: Fluorescence measurements (spectrofluorimeter) of irradiated solution of coumarin; catalyst Degussa P25 P2 film

Degussa P25 films are much more photocatalytically active compared to the sol-gel films with the same amount of titania. For example, comparing the rate of formation of 7OHC on two films with the same surface density of titania, the rate of formation on P1 is $28.6 \times 10^{-9} M \text{ min}^{-1}$, on the other hand the rate of formation on D2S is $6.7 \times 10^{-9} M \text{ min}^{-1}$, which is approximately 4 times slower. Figure 21 shows the correlation between the formation rates and the absorbed radiation by the titania films for non-transparent Degussa P25 and transparent C and D films. There is a linear dependence when studying this effect on non-transparent films. With other words, the percentage of recombined photogenerated electrons and holes is the same regardless the amount of the catalyst. The shadowed TiO_2 particles in the interior of the films do not absorb the radiation and cannot participate in the photocatalytic reactions.

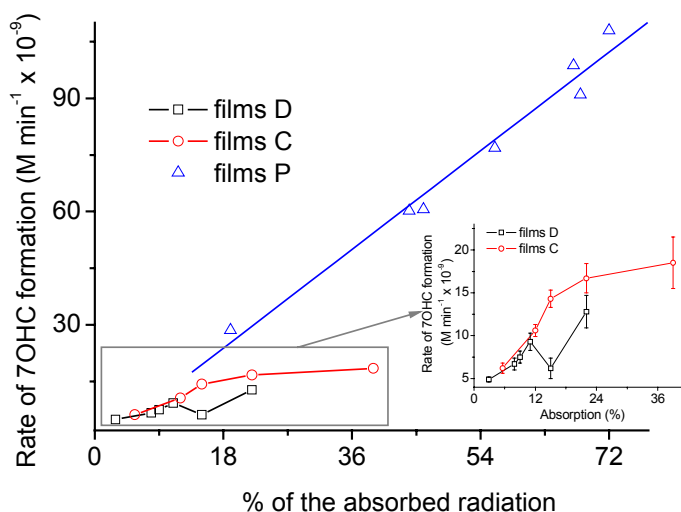


Figure 21: A correlation between formation rates of 7OHC and the absorption (in %) at 365 nm by the TiO_2 films

The story is much more complex in case of transparent films. As it was already explained, the absorption of radiation by transparent titania films increased linearly with the number of layers, e.g with the amount of titania. Additionally, C and D films have almost the same absorption at 365 nm per amount of the catalyst

independently of the number of layers (Table 5). Concluding from these facts, it was supposed that the amount of crystalline anatase phase per amount of the catalyst was similar for both types of films. It seemed that the added surfactant in the preparation of films C did not hinder as well as accelerate the crystallization of anatase phase. In the next step, the influence of surfactant on the photocatalytic properties was evaluated. If the surfactant had the influence on photocatalytic properties, the degradation rates of coumarin per unit of absorbed radiation at 365 nm would differ for C and D films. However, the degradation rates are comparable for the first four deposited layers (inset in Figure 21). The same trend was obtained already with Plasmocorinth B and polychromatic radiation, what was shown in Chapter 4.1.3.3 (Figure 17). It seems that the surfactant truly does not have an impact on photocatalytic activity when the films are thin enough. It seems from the results as though the number of active sites on the surface is similar regardless the use surfactant, what is somehow non-logical, if we take into account that the films C have half lower macroscopic density and 14 times higher BET surface area compared to films D.

With increasing the number of layers from 4 to 9, the degradation rates do not follow linearly the absorption properties of C as well as D films anymore. Photogenerated holes and electrons from the bottom of the films could not reach the surface of the films, where they can react with the organic molecules. Therefore the photocatalytic activity cannot correlate indefinitely with the film thickness. Regarding the fact that films C have 14 times higher BET surface area, they are more porous and consequently even the photogenerated holes and electrons in the interior of the film should easier reach the interfacial catalyst/liquid surface than in case of D, what results also in lower recombination. Based on this, the thick C films (more than 4 layers) should show higher rates compared to the thick D films (more than 6 layers) with the same amount of the catalyst, e.g., with the same absorption properties. Figure 21 confirms a difference between both types of thick films, if the average rates are taken into account. But unfortunately, when depositing more than four layers, the reproducibility between the samples became low. For instance, 2 studied D9S films (or C7S) prepared under identical conditions, show formation rates, which differ one from another for 15 % in D9S (16 % in C7S). The other outstanding result is presented with D6S, which differs enormously from the trend. The reasons for such high deviations with thick films are not known, but it clearly indicates the importance of also other parameters (besides absorbance and amount of catalyst) on photocatalytic activity of the material.

The quantum yields for degradation of coumarin (and for formation of 7OHC) were calculated according to the equation 4.6, where Φ_{365} is quantum yield at 365 nm, $-dn(\text{coumarin})/dt$ is number of degraded coumarin molecules per unit time, $dn(7\text{OHC})/dt$ is number of formed 7OHC molecules per unit time and Φ_p^{abs} is absorbed photon flow at 365 nm. Φ_p^{abs} is calculated by multiplying the whole photon flow in the cuvette and the A of TiO_2 film. The results are presented in Table 5. The correlation between the quantum yields of different films and the amount of irradiated catalyst are shown in Figure 22. Again, there is very evident correlation between the Φ_{365} s of coumarin degradation (Figure 22A) and of 7OHC formation (Figure 22B). Calculated from presented values, during the first steps of coumarin degradation, 100 degraded parent molecules gave rise to approximately 3 fluorescent 7OHC molecules under conditions used.

$$\Phi_{365}(\text{coumarin}) = \frac{-dn(\text{coumarin})/dt}{\Phi_p^{abs}} \quad (\Phi_{365}(7\text{OHC}) = \frac{dn(7\text{OHC})/dt}{\Phi_p^{abs}}) \quad 4.6$$

First of all, it is almost impossible to compare the calculated Φ_{365} with the literature data due to the reasons described in previous chapters. It could be said that according to the literature the values between 1 and 10 % were expected, therefore the obtained values seem reasonable. Surprisingly, the differences in Φ_{365} between Degussa films and sol-gel processed films are smaller than expected. According to the fact that Degussa P25 films showed approximately 4 times higher degradation rates when the same amount of titania is studied, also the 4 times higher Φ_{365} was expected. But Figure 22 shows that the Degussa P25 has only twice higher Φ_{365} (in the range of the titania amount between 60 and 300 $\mu\text{g cm}^{-2}$) when the surface density of TiO_2 between compared samples is similar. This means that the recombination rate of photogenerated holes and electrons is similar in all three types of the films. The

phenomena could be explained by higher absorbance of Degussa P25 films per amount of the catalyst, what could be the consequence of its more crystalline structure (higher amount of anatase per amount of TiO_2) compared to my sol-gel films. The second obvious observation is that in all three cases the decrease of quantum yield is noticed with the increase of the film thickness. This slope is the steepest in the case of D films (and similar also in the case of films C) and the gentlest in the case of Degussa P25 films. Higher the thickness, more pronounced is the recombination of holes and electrons, before they could be trapped by the organic substrate. In the case of Degussa P25 films, the decrease is not distinctive, because of the same reasons, which were already explained. On the other hand, the decrease is steeper in the case of both denser, transparent films, what is also in accordance with the observations in Figure 21.

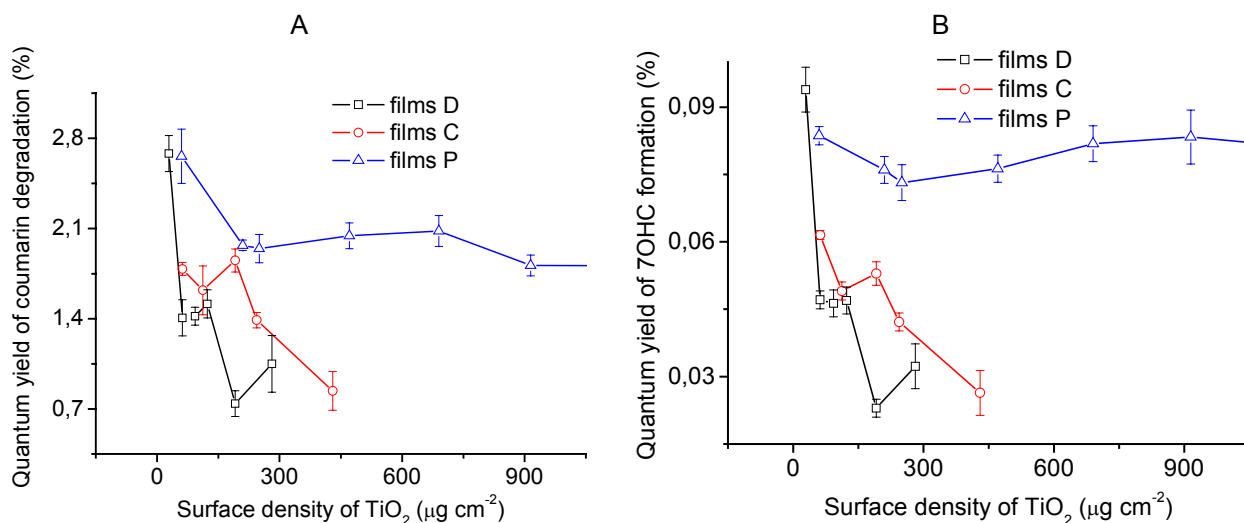


Figure 22: Calculated Φ_{365} for A: degradation of coumarin; B: formation of 7OHC

Despite noticeable influence of the adding surfactant in the sol on different characteristics of deposited films the films C are not photocatalytically distinctively superior to films D. The organised mesoporous TiO_2 films were not prepared and even in that case the higher efficiency is not predictable since it was shown that porosity (higher BET surface area) is not directly correlated with the photocatalytic activity. However, the main advantage of films C is that higher amount of TiO_2 could be deposited within one dip-coating cycle and consequently higher photocatalytic activity of the deposited film is achieved.

An extensive knowledge about TiO_2 photocatalysis was obtained through the described research work and photocatalytically active films were successfully prepared and evaluated. If such immobilized material is intended to be used in real applications, the development of an efficient reactor system is of great importance, therefore the construction and evaluation of a novel reactor for immobilized TiO_2 became my subsequent issue.

4.2 PART 2: Evaluation of a novel Carberry type photoreactor for the degradation of organic pollutants in water and studying the effect of ozone on TiO₂ photocatalysis (Černigoj et al., 2007a, 2007b and unpublished results)

4.2.1 State of the art

4.2.1.1 Photocatalytic reactors

Problems of a construction of the efficient photocatalytic reactor and information on solar photocatalytic reactors have been already introduced in the Chapter 2.3.6. Besides the types of reactors already mentioned (mostly for solar photocatalysis), many other reactors for degradation of organic molecules in aqueous media have already been constructed and tested on laboratory or pilot plant scale level.

Already in 1995, Bideau et al. reviewed the literature on different types of reactors based on immobilized TiO₂. TiO₂ was often immobilized (i) on the wall of the glass spiral, where the light source was put in the middle; (ii) on the internal walls of the tubing; (iii) on fiber cloth or optical fibre; (iv) on the glass beads, which are placed on the bottom of the reactor (fixed-bed); etc.

More recent literature on the topic of photocatalytic reactors is presented here. Ray and Beenackers (1998) proposed the distributive type of photoreactor in which catalyst was fixed to a structure in the form of hollow glass tubes inside the reactor, as the most perspective for scaling up. The hollow glass tubes served as light conductors and distributors to the photocatalyst. The reactor configuration increased the surface-to-volume ratio while eliminating the possibility of radiation loss by absorption and scattering of the reaction medium.

Fountain photocatalytic reactor, an innovative slurry-type reactor was presented by Li Puma and Yue (2001). The basic concepts of this reactor centers on the design of a special nozzle that provides a thin film in the form of a fountain in continuous flow exposed to a light source, which is situated above the water fountain. The design is particularly suitable for large-scale solar applications. Such a reactor configuration allows a very high photocatalyst activation, a high O₂ mass transfer rate and does not suffer from the filming problem. The main drawback is a slurry system.

Fluidized-bed reactors are based upon the TiO₂ immobilized on small macroscopic particles (i.e. sand), which readily settle down when added to water (Haarstrick et al., 1996). The flow of the liquid keeps these immobilized TiO₂ fluidizing and mixing in the water, but when the flow is stopped, all the particles settle down, keeping the water clean and without any suspended particles. Compared to fixed-bed photoreactors, fluidized-bed photoreactors can offer superior mass transfer efficiency and light transmission (Nelson et al., 2007). It has been reported that the annular-type fluidized-bed configuration could enable the most efficient use of the light source in photochemical reactions. One of the problems of fluidized-bed photocatalytic reactors is attrition of the TiO₂ particles at high flow rates of the medium.

Optical fibers were also used as both light distributors and support for photocatalysis. One example of using optical fibers for a construction of photoreactor was presented by Danion et al. (2004). Their preliminary results with a single-optical fiber reactor showed the feasibility of a multi-fiber reactor for water treatment. One disadvantage of such reactor could represent light transmission discontinuity due to break of a coated optical fiber.

Rotating disc photocatalytic reactor was another innovative reactor, where TiO₂ was immobilized on the rotating disc (Dionysiou et al., 2000; Hamill et al., 2001). The lower part of the rotating disc was immersed in the solution of the pollutant, the upper part was opened to the atmosphere. When the radial section of the disc emerged from the liquid during the rotation, it carried a thin film of liquid, which was irradiated by UV radiation. There are no problems with the mass transfers limitations because of a thin layer of liquid,

which is constantly replaced by a fresh one. It is also not difficult to scale up such reactor. One big disadvantage is that only artificial light sources could be effectively employed.

The corrugated plate photocatalytic reactor was found to be up to 150 % faster and more energy-efficient than the usual thin-film-fixed-bed reactor (TFFBR) for the degradation of 4-chlorophenol (Zhang et al., 2004). Its efficiency was estimated to be close to that of the slurry system. The superior performance of the corrugated plate reactor is due primarily to its large illuminated catalyst surface area and its capacity for transport of reactants and efficient capture of photons on the catalyst surface.

The large-scale cylindrical circulating photoreactor, which incorporated the flexible fiberglass cloth support with immobilized TiO_2 and radiation source positioned in the center of the photoreactor was constructed by Horikoshi et al. (2002) to detoxify wastewater. Very efficient Taylor vortex reactor was presented by Dutta and Ray (2004). It is based on the Taylor-Couette flow, which generates circulation of fluid continually between the bulk and the rotating illuminated catalyst coated inner cylindrical surface; thereby minimizing the external mass transfer resistance. The experimental results demonstrated that Taylor vortex reactor could be useful for water purification even when catalyst is fixed, because there were no significant difference in overall degradation rate between slurry and immobilized system. Its drawback is mechanical complexity due to the requirement of the rotation of the inner cylinder.

The spinning disc reactor is another type of the reactor, developed also for photocatalysis (Yatmaz et al., 2001). The thin liquid films produced in these reactors possess high turbulence and hence correspondingly high values of the rate of transfer of organic material to the surface of the supported TiO_2 .

Two innovative ideas of efficient photocatalytic reactors were realized by a group of Morawski (Grzechulska and Morawski, 2003; Mozia et al., 2005). One is the labyrinth flow reactor with immobilized catalyst bed. It resembles corrugated plate reactor and DSSR (double skin sheet reactor), so its advantage is possibility of using the solar energy as a source of irradiation. The second one is based on coupling of photocatalysis and direct contact membrane distillation. The membrane plays both the role of a simple barrier for the photocatalyst (slurry) and of a selective barrier for the molecules to be degraded. The membrane distillation process may be utilized for the preparation of ultrapure water as well as separation and concentration of organic matter, acids and salt solutions. One of drawbacks of presented reactor is a need to heat the feed solution, because the driving force of the membrane distillation is a process of evaporation of feed volatile components through a porous hydrophobic membrane.

Despite so much effort in development of new reactors, it is still necessary to improve the existed technologies or to develop new types of reactors with the objective of increasing their efficiency, which would end up in commercialization of this technology. My attempt was to combine the existing knowledge on TiO_2 photocatalysis and reactor engineering and to develop a simple, efficient photoreactor with immobilized TiO_2 , which could utilize solar as well as artificial light sources. The removal of 4-chlorophenol (intermediates in dyestuffs and in the manufacture of higher chlorinated phenols) by TiO_2 photocatalytic oxidation has been studied in details (Konstantinou and Albanis, 2003; Kormali et al., 2006), therefore 4-chlorophenol was chosen as a model organic compound for evaluation of the novel photocatalytic system. Afterwards the suitability of the photoreactor for the degradation of a variety of organic compounds was tested.

4.2.1.2 The influence of ozone on TiO_2 photocatalysis

Despite several advantages of using ozone, there are a few disadvantages, which limit the application of ozone in water treatment technology. These include high cost of ozone production and only partial degradation of organic molecules present in water. Ozone is in aqueous solution a moderately stable molecule with a $t_{1/2}$ of more than 10^4 s under pH 5 (Hoigne, 1998). Therefore mostly selective oxidations of organic molecules with molecular ozone and not hydroxyl radical mediated reactions are expected at acidic pHs. At alkaline pH, where the concentration of hydroxide anions gets higher, ozone is efficiently decomposed (eq. 4.7), generating different reactive species and hydroxyl radicals (eqs. 4.8-4.10), which consequently accelerate the degradation of organic pollutant (Hoigne, 1998).



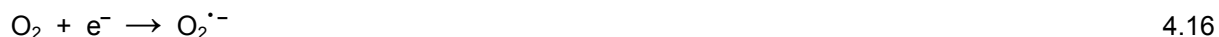
Ozone absorbs UV radiation below 320 nm and it is consequently efficiently degraded under irradiation with UVC or UVB photons. The primary product is atomic oxygen (eq. 4.11). It then reacts with water forming H_2O_2 (eq. 4.12). In the subsequent reactions, new reactive species are formed from H_2O_2 , and this enhances the degradation of the organic substrate.



On the other hand, TiO_2 photocatalysis ($\text{O}_2/\text{TiO}_2/\text{UV}$) has a great potential for the removal of organic pollutants from wastewater, although it is still not used in practice because of the low efficiency of the process. A combination of photocatalysis together with ozone is reasonable for the treatment of organic molecules since it has already been shown that photocatalytic ozonation ($\text{O}_3/\text{TiO}_2/\text{UV}$) is a more powerful process than the sum of ozonation coupled with UV radiation (O_3/UV) and $\text{O}_2/\text{TiO}_2/\text{UV}$ (Agustina et al., 2005). Three possible reasons for synergistic effects of O_3/UV and $\text{O}_2/\text{TiO}_2/\text{UV}$ were proposed. First, ozone as a stronger oxidant than oxygen is more easily reduced by a photogenerated conduction electron from TiO_2 (eqs. 4.13 and 4.14), producing ozonide radical anion, which in the next steps generates a hydroxyl radical (eqs. 4.15, 4.10) (Sanchez et al., 1998; Hernandez-Alonso et al., 2002). Due to more efficient trapping of photogenerated electrons by ozone also the recombination between holes and electrons is minimized.



Moreover, even if molecular oxygen accepts the photogenerated electron, a resulting superoxide radical anion can react with ozone to give in subsequent steps a hydroxyl radical (eqs. 4.16, 4.17, 4.15, and 4.10) (Kopf et al., 2000).



The use of $\text{O}_3/\text{TiO}_2/\text{UV}$ has recently been studied in a liquid phase to treat inorganic anions, such as cyanide ions (Hernandez-Alonso et al., 2002), simple organic molecules, such as monochloroacetic acid (Kopf et al., 2000), oxalate anions (Addamo et al., 2005) or formic acid (Wang et al., 2002). Besides the investigations of degradation of these relatively simple molecules, a few studies were also performed on environmentally problematic organic compounds, such as pesticides and their precursors (Farre et al., 2005; Beltran et al., 2005; Muller et al., 1998; Li et al., 2005). In all cases a significant improvement of oxidation process performance was reported as the mineralization rate of organic substances was greatly enhanced. In some papers the effects of pH and ozone dosage on $\text{O}_2/\text{TiO}_2/\text{UV}$ were studied (Muller et al.,

1998; Li et al., 2005; Tong et al., 2005), but no profound investigation and explanation of the effects of both parameters on O₃/TiO₂/UV were carried out.

According to the results presented in Chapter 4.2.3.6 stabilities of thiacloprid and imidacloprid under UVA radiation (O₂/UV) were studied in detail. Their chemical stabilities in different aqueous solutions were evaluated and compared. Next, O₃ treatment and three different photochemical advanced oxidation processes, namely O₃/UV, O₃/TiO₂/UV and O₂/TiO₂/UV were applied to assess the suitability of these processes to promote the degradation and mineralization of thiacloprid in water at different pH values. In all photochemical processes, only the light source emitting predominately in UVA range was applied. The effect of ozone dosage on TiO₂ photocatalysis was evaluated and explained.

4.2.2 Experimental part

4.2.2.1 Preparation of the catalyst

Degussa P25 slurries: The appropriate amount of Degussa P25 powder was weighed and added to the aqueous solution of organic pollutant (samples A-E). The biphasic system was mixed thoroughly before the degradation experiment to homogenize the suspension and to prevent the settling of the catalyst.

Table 6: Characteristics of different photocatalytic systems and calculated half-lives of 4-chlorophenol for each configuration

Config-uration	Catalyst	Number of glass slides	Average amount of TiO ₂ on each slide [mg]	The total surface area covered with TiO ₂ [cm ²]	Weight concentration of TiO ₂ in the solution of pollutant [mg L ⁻¹]	Half-life of 4-chlorophenol [min]
A	P25	0	slurry	slurry	148	3.5
B	P25	0	slurry	slurry	300	2.9
C	P25	0	slurry	slurry	720	2.5
D	P25	0	slurry	slurry	1000	2.4
E	P25	0	slurry	slurry	1440	2.3
F	P25	6	5.3	262	160	13.5
G	P25	6	9.2	262	275	8.5
H	P25	6	26.3	262	790	6.6
I	P25	6	36.5	262	1095	6.9
J	P25	6	52.5	262	1575	6.7
K	P25	2	71	87	710	16.9
L	P25	1	148	44	740	24.9
M	P25	12	35	524	2100	4.4
N	sol-gel	6	1.8	262	55	52.8
O	sol-gel	6	11.1	262	333	29.7
P	sol-gel	6	18.3	262	550	23.4
R	sol-gel	6	25.5	262	764	24.7
T	sol-gel	12	18.3	524	1100	not measured
S	blank	6	0	0	0	245

Degussa P25 films: The commercially available Degussa P25 TiO₂ was used as a test photocatalyst. The immobilized particulate TiO₂ layers were prepared on glass slides (175 mm x 12.5 mm x 2 mm) by sedimentation from aqueous suspension of TiO₂ P25 (10 g L⁻¹) for different periods of time as it is described in Chapter 3.3.2. The sedimentation was also repeated on the other side of the glass slide. The

amount of immobilized TiO_2 was determined by weighing and the results are given in Table 6 (samples F-M).

Sol-gel derived TiO_2 films (sol C): In contrast with opaque P25 films, transparent TiO_2 -anatase films deposited on both sides of SiO_2 -precoated soda-lime glass slides (175 mm x 12.5 mm x 2 mm) were produced by the sol-gel processing route described in detail already in Chapters 3.2 and 3.3.1. The amount of the catalyst on a glass slide was determined by weighing and the results are given in Table 6 (samples N-T).

4.2.2.2 Photocatalytic cell and photoreactor

The photocatalytic cell consists of a DURAN glass tube (240 mm, inner diameter 40 mm), which is closed on the lower side with a glass frit and the valve for purging with gas (Figure 23A). The effective volume of the glass tube is 250 mL. The spinning basket is made exclusively of Teflon (Figure 23B) and fits into the photocatalytic cell. Up to 12 glass slides with immobilized catalyst were fastened around the axis (10 mm in diameter, Figure 23C) with the help of two holders. The glass slides and the axis are not joined together, there is a gap of 1.5 mm in between to enable homogeneous mixing of the solution in all segments of the cell. The spinning basket with the immobilized TiO_2 placed in the glass tube can freely rotate around its axis. The novel reactor was named as a Carberry-type photoreactor (CTP).

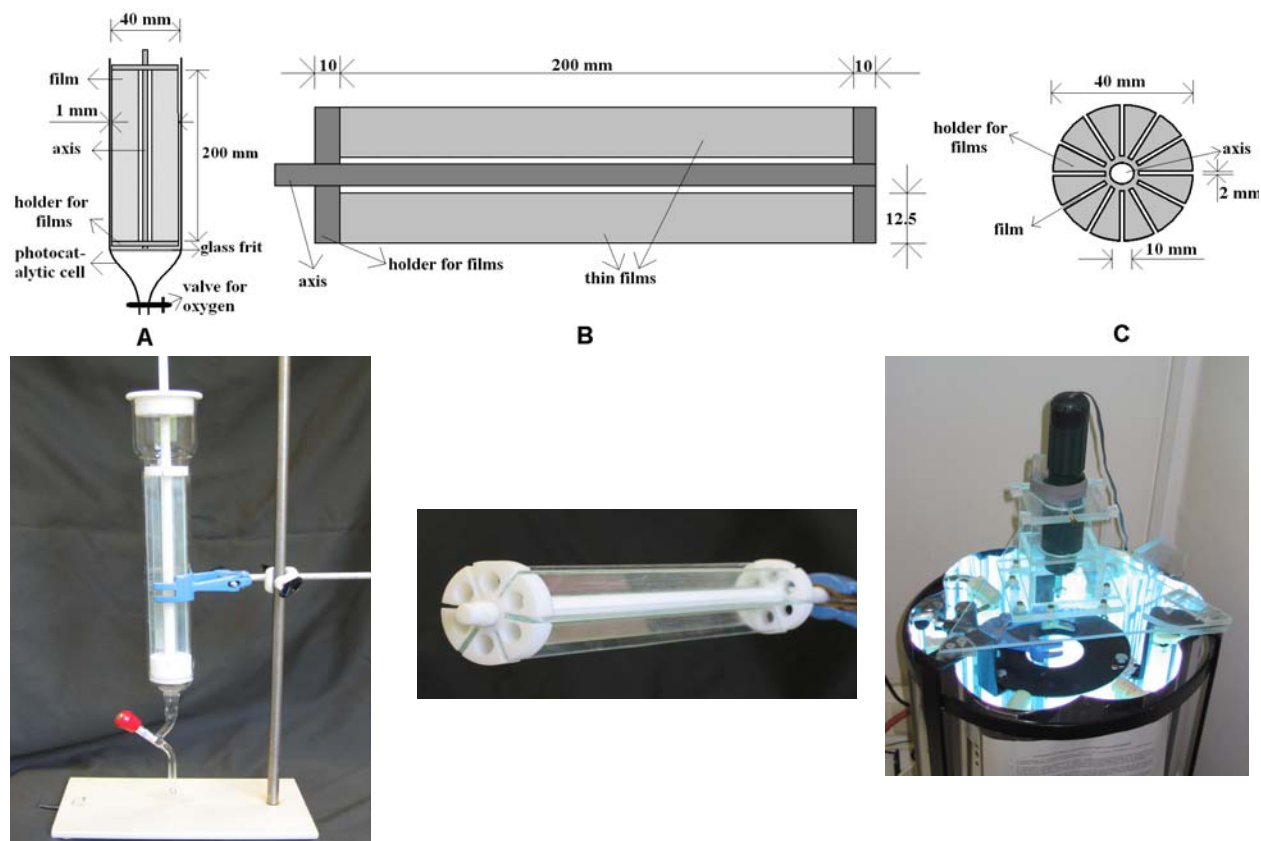


Figure 23: Top: the photocatalytic cell with the spinning basket inside; A: the spinning basket is placed into the tube with an inner diameter of 40 mm; B: longitudinal section of the spinning basket; C: cross-section of the spinning basket. Bottom: Photos of photocatalytic cell (left), spinning basket with immobilized catalyst (middle) and of the upper part of a photoreactor (right)

The photocatalytic activity of the as-prepared films were evaluated in a tailor-made chamber photoreactor using 6 low-pressure mercury fluorescent lamps as a UVA radiation source (CLEO 20 W, 438 mm x 26 mm, Philips; broad maximum at 355 nm). The lamps in the periphery of the photoreactor are positioned on a circular line and the reflective surface of polished aluminium is placed behind them. The photocatalytic cell is put in the center of the circle. The motor on the top of the reactor rotates the spinning basket with variable speeds (between 0 and 300 rpm).

4.2.2.3 Degradation experiments

4.2.2.3.1 Evaluation of the CTP

Aqueous solution (200 mL) of 4-chlorophenol, myclobutanil, sulfathiazole, sulfamethoxazole, thiacloprid or imidacloprid (15 mg L^{-1}) were used as a photodegradation medium in the evaluation experiments of the novel reactor. All mentioned chemicals except thiacloprid and imidacloprid were used as received. The procedure of obtaining pure neonicotinoids is described in detail in Chapter 3.1. The photocatalytic degradations were performed with: (i) the P25 TiO_2 slurries; (ii) 1, 2, 6 or 12 glass slides with immobilized P25 TiO_2 and (iii) 6 or 12 glass slides with immobilized sol-gel derived TiO_2 . Blank experiments were performed in the same way, but without TiO_2 on the glass plates. At least two repetitions with each configuration were performed to evaluate the reproducibility of measurements. During the irradiation, the solution was constantly purged with oxygen (10 L h^{-1}), keeping the solution saturated with dissolved oxygen during the whole irradiation time. The effect of rotation on photocatalytic activities was also evaluated. The temperature was kept constant at $30 \text{ }^\circ\text{C}$ during the experiment. The photon flux in the cell was evaluated by potassium ferrioxalate actinometry (Murov et al., 1993), and determined to be $4.2 \times 10^{-5} \text{ einstein L}^{-1} \text{ s}^{-1}$. The solution of organic pollutant was left rotating and purging with oxygen 30 min in the dark prior to irradiation. Samples of 2 mL were taken from the cell at different times during the irradiation and analyzed by HPLC. Except the samples taken from TiO_2 slurry (these samples were centrifuged at 13200 rpm for 15 min and then the supernatant was collected for chromatographic analysis), they were analyzed without additional filtration, extraction or centrifugation. All disappearance curves indicate first-order kinetics, therefore they were fitted as first-order reactions. The TiO_2 -coated slides and the photocatalytic cell were washed with deionised water after the experiment. Before starting the next one, the cell was washed and filled with the new solution of the pollutant.

4.2.2.3.2 Determination of neonicotinoid's stabilities in aqueous solutions in dark

Pure thiacloprid or imidacloprid were dissolved in deionised water or tap water (50 mg L^{-1}). The hydrochloric acid or sodium hydroxide were added to obtain the appropriate pH value of the solution. The solutions were kept in dark at room temperature for at least half a year. Samples (1 mL) were taken twice a month and analysed by HPLC.

4.2.2.3.3 Comparison of photocatalysis with other AOPs

Ozone was bubbled into the bottom of the CTP through the glass frit. Ozone was generated by Pacific Ozone Technology equipment (model LAB21) fed with pure oxygen (99.5 %) and its concentration was determined by iodometric titration (Taras et al., 1974: 271). The applied specific ozone dose for experimental time of 120 min varied from 1.6 mg ozone per 1 mg of the pollutant (at the flow rate of ozone 0.04 g h^{-1}) to 60 mg ozone per 1 mg of the pollutant (at the flow rate of ozone 1.5 g h^{-1}). The total gas flow rate was constant (10 L h^{-1}) during the experiment

Thiacloprid or imidacloprid solutions (100 mL , 50 mg L^{-1}) were used in degradation experiments. The starting pH of the aqueous solution was regulated by adding hydrochloric acid, sodium hydroxide, sodium bicarbonate or sodium dihydrogenphosphate/disodium hydrogenphosphate buffer. The temperature was

kept constant at 30 °C during the experiment. CTP was used in all performed experiments. The samples (4 mL or 35 mL) were taken from the cell at different times during the degradation experiments for HPLC, ionic chromatography (IC), total organic carbon (TOC) and total nitrogen (TN) analyses. The samples were analysed without additional filtration, extraction or centrifugation. The degradation experiments lasted between 100 and 150 min. At least two repetitions with each configuration were performed to evaluate the reproducibility of measurements. Some experimental specifications of each type of experiment are given below.

O₂/UV: The pesticide solution was treated by UVA radiation under constant purging with oxygen. O₃: The pesticide solution was constantly purged with ozone during the degradation experiment. O₃/UV: The pesticide solution was exposed to UVA radiation under constant purging with ozone. O₂/TiO₂/UV and O₃/TiO₂/UV experiments were performed with twelve glass slides with immobilized TiO₂ (configuration T in Table 6) under otherwise similar conditions as in O₂/UV and O₃/UV, respectively.

4.2.3 Results and discussion

4.2.3.1 Photocatalytic degradation of 4-chlorophenol with different reactor's configurations

When considering solar photocatalytic pilot plants, two different types of reactors are mostly used: CPCRs (compound parabolic collecting reactor) with TiO₂ slurries or TFFBRs. We combined the advantages of both systems, i.e. compact and convenient compound parabolic collectors with glass tubes and turbulent flow from CPCRs, and immobilized catalysts from TFFBRs. The tube with the central axis through it, on which long slides of immobilized catalyst are positioned radially, meets the above criteria. To our knowledge, there is only one scientific publication discussing the use of the principle of the spinning basket with immobilized TiO₂ for photocatalytic reactor (a Carberry type photoreactor = CTP) (Marci et al., 2003). That photoreactor, however, is not intended for CPCs and aqueous solutions.

In our photocatalytic cell, the irradiated area of TiO₂ film is 15 cm² per 1 cm of tube length, when 6 glass slides are used. If we take into account the fact that the aperture of a standard compound parabolic collector is 9.25 cm (Blanco et al., 1999) and if we presume that the tube is placed in the standard CPC, we are able to irradiate a 1.62 times higher surface area of the catalyst in a novel CTP than in a fixed-bed reactor on the same projected area. The magnification is even higher when more glass slides with immobilized catalyst are positioned into the cell.

As we do not have a CPR yet, all our experiments were performed in the chamber photoreactor, where the photocatalytic cell is placed in the center of irradiation in order to equally irradiate the tube from all sides (approximation to CPC). First we compared the rate of disappearance of 4-chlorophenol catalyzed by different configurations of immobilized Degussa P25 TiO₂ films, while keeping the amount of TiO₂ the same in all cases (Figure 24). Degussa P25 was chosen for evaluation purposes of the novel photoreactor for two reasons. Firstly, it is used worldwide as a standard TiO₂ photocatalyst and its characteristics are known. Secondly, since we were able to prepare pure Degussa P25 films, a direct comparison between the photocatalytic activity of a slurry and immobilized system could easily be evaluated. It should be stressed that films prepared by the procedure described above could not be used in industrial applications because of low physical adhesion of the catalyst. In our experiments, they only served as model films for comparison of photocatalytic activities between slurry and immobilized systems.

When working with Degussa P25 films, the problem of losing the catalyst from the films has to be evaluated. 2±1 mg of TiO₂ was lost from the first to the second experiment when 6 TiO₂ films were used (configuration H). The differences between the calculated half-lives of the first three repetitions using the same films were lower than 5 % in all configurations. After using the films constantly for some days (20 repetitions or more), the layers of TiO₂ (not powder) were detached from the surface and fell to the bottom of the cell. Nevertheless, the novel CTP worked as an immobilized system and not as a slurry one. At the end of the experiment, only up to 3 mg of suspended TiO₂ was measured in the solution, which represents a maximal concentration of 15 mg L⁻¹ of TiO₂ in the solution at the end of the experiment, i.e. 10 times lower than in the configuration A. The beginning of the experiment was however always devoid of

suspended TiO_2 as 3 mg of TiO_2 were found exclusively at the end of the experiment. Most of detached TiO_2 was not even in the form of milky suspension, since the catalyst detached in form of bigger aggregates with a low surface area to volume ratio. The solution of the pollutant under investigation was always clear (not turbid) with new films (first 5 repetitions). When changing the spinning rate, no increase in photocatalytic activity was measured. If the system had worked as a slurry one, the increased spinning (300 rpm) would certainly have resulted in higher degradation because of the more pronounced detachment of the catalyst.

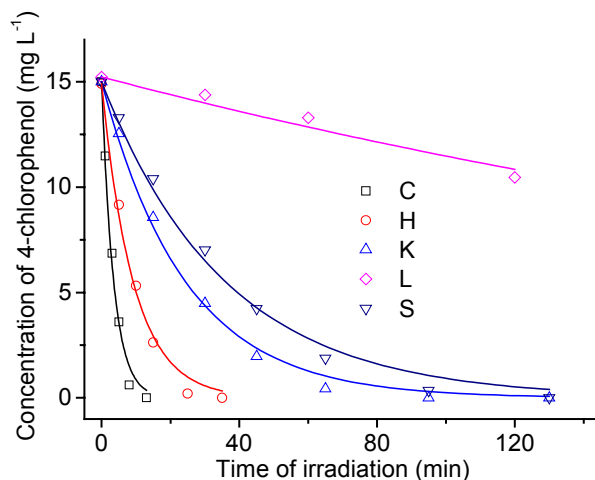


Figure 24: Photocatalytic degradation of 4-chlorophenol; spinning rate 100 rpm; configurations from Table 6

No measurable dark adsorption of the parent molecules on TiO_2 particles was noticed before the irradiation. The photodegradation of 4-chlorophenol in the absence of TiO_2 (curve S in Figure 24) was much slower than in photocatalytic experiments, where four different photocatalytic systems were used to evaluate the photoreactor (C, H, K, L in Figure 24 and Table 6).

The disappearance rate was highest when TiO_2 slurry instead of thin films was used (curve C in Figure 24). This is because in a slurry system the transport processes are facilitated by the high liquid-solid interface between the TiO_2 particles and the pollutant solution. The disappearance rate of 4-chlorophenol during the run with the system in the configuration H, with 6 glass slides and 790 mg of TiO_2 , is ca. 2.6 times higher than that of the system in configuration K, 2 slides and 710 mg of TiO_2 (see Figure 24). The magnification of the disappearance rate should ideally have been 3 (instead 2.6), since the surface area was 3 times higher in H than in K. The difference between the real and the ideal system is expected due to the effect of additional shading in the configuration where six instead of two slides are used. Despite this, the result is very promising and was additionally improved by placing 12 slides with immobilized TiO_2 in the cell (Chapter 4.2.3.4).

4.2.3.2 The influence of spinning on photocatalytic activity

The intense spinning of the TiO_2 films should provide better (more turbulent) mixing of the solution of 4-chlorophenol and consequently better transportation of molecules to the surface of the catalyst. Interestingly, when performing the experiment with configuration H (Table 6), no differences in disappearance rates were noticed at different spinning rates. Even in the absence of rotation, the disappearance rate was the same. It seems that purging with oxygen from the bottom of the cell through the glass frit generates a degree of mixing which is high enough for the reaction not to be diffusion-controlled. In order to confirm this hypothesis, two experiments were carried out by bubbling oxygen for 10 s every 5 min; the first one maintaining the slides in rotation and the second one with the system working

as a fixed bed (Figure 25). In the last case the disappearance rate was 1.25 times slower than in the case of continuous spinning. The same effect was also noticed with the configuration K (2 TiO₂ films).

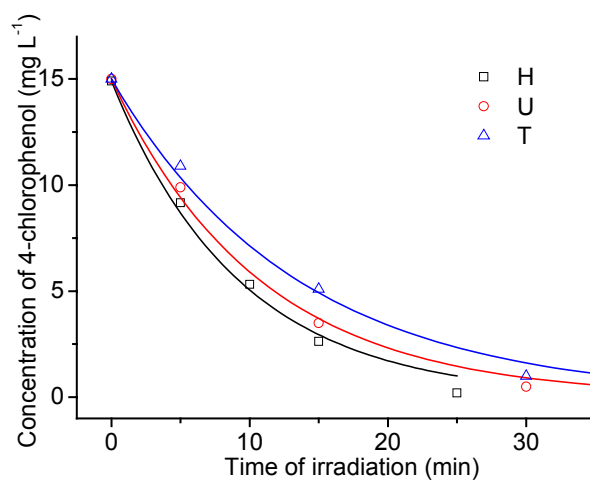


Figure 25: Photocatalytic degradation of 4-chlorophenol; configuration H from Table 6; (□) constant purging with O₂ during the irradiation, spinning rate 100 rpm; (○) purging with O₂ for 10 s every 5 min, spinning rate 100 rpm; (△) purging with O₂ for 10 s every 5 min, no rotation

As it can be seen from Figure 25, the disappearance rate of 4-chlorophenol in a system, where purging with oxygen for 10 s each 5 min was applied together with continuous rotation was only slightly slower than in the system with continuous purging with oxygen. It can be concluded from this result that the flow rate of oxygen was unnecessarily high in configuration H, since 1 min of purging led to almost the same result as 30 min of purging with the same oxygen flow rate in the configuration H. Lowering of the oxygen flow rate for 50 times while purging through the whole experiment would still be enough for the solution to remain saturated with the oxygen during the experiment. But in this case the spinning of the solution would become necessary, otherwise the kinetic-controlled regime would turn into the diffusion-controlled one.

When studying the possibility of installing a novel CTP type into CPC system, it must be stressed that the CPCRs generally work in total recirculation configuration and the flow inside the tubes is highly turbulent. In such case the spinning of the films would not be necessary. But another characteristic of CPCs is that the tube is irradiated from all sides, not only from the top or bottom. Therefore we find such configuration of TiO₂ slides, which is used in our novel CTP reactor, convenient and promising for the application in the CPCs, as a very large surface of immobilized TiO₂ could be efficiently irradiated.

4.2.3.3 The effect of the amount of TiO₂ on photocatalytic activity

In slurry and in immobilized photocatalytic processes, the amount of photocatalyst is an important parameter, which can affect the disappearance rate of organic compounds. The optimal catalyst concentrations reported in literature for TiO₂ Degussa P25 range from 100 to 5000 mg L⁻¹, depending on the nature of the compounds and the photoreactor geometry (Parra et al., 2004).

The aim of the experiments was to determine the optimal amount of the catalyst used in our photocatalytic cell. The photocatalytic efficiencies of the suspended as well as of the immobilized catalyst through the whole range of TiO₂ concentrations were evaluated and compared. The spinning rate was 100 rpm and the solution was purged with oxygen during the whole experiment. Figure 27A shows a plot of the half-lives (min) of 4-chlorophenol as a function of Degussa P25 concentration. It is observed that the initial disappearance rate increases with TiO₂ concentration both for slurry and immobilized system until it

reaches a plateau, indicating a progressive saturation of the photonic absorption by the catalyst for a given incident radiation flux. The initial rate of oxidation of 4-chlorophenol is not affected above 900 mg L^{-1} of TiO_2 . The increase of the disappearance rate between 100 and 800 mg L^{-1} of TiO_2 is more pronounced in an immobilized system. Both phenomena were discussed in detail in Chapter 4.1.3.4. In a slurry system, the outer layer of the suspended catalyst absorbs the majority of photons and the core of the tube is actually non-irradiated yet at low concentrations of catalyst. An additional amount of TiO_2 therefore does not improve the photocatalytic activity. On the contrary, the radiation can penetrate all the way to the center of the tube in case of immobilized TiO_2 catalyst.

4.2.3.4 Optimizing the configuration of the photocatalytic system

The optimal configuration of our photocatalytic system was determined on the basis of the results, obtained in experiments described in the previous subchapters. The spinning rate was 100 rpm and the solution was purged with oxygen during the whole experiment. The average amount of TiO_2 on each slide was around 36 mg . Lower amounts would have resulted in lower photocatalytic efficiencies while higher amounts would not have brought any significant benefits to the improved photocatalysis. Figure 24 shows that more slides with immobilized catalyst resulted in higher efficiencies and that the plateau (maximal disappearance rate with immobilized TiO_2) has still not been reached with 6 TiO_2 films. Therefore another 6 slides with immobilized catalyst were incorporated in the photocatalytic cell, which increased the surface area of the slides by a factor of 2 (configuration M from Table 6).

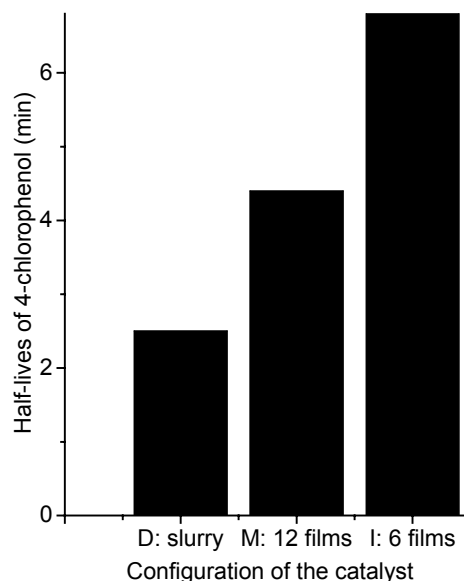


Figure 26: Graphical comparison between the most efficient slurry and immobilized configurations

The configuration M was compared to configuration I, which had 6 TiO_2 slides with the TiO_2 amount on one slide similar to that in configuration M. As a third reference, a slurry system with the highest photoactivity was chosen (configuration D). Indeed, the disappearance of 4-chlorophenol was 1.45 times faster when 12 glass slides (half-life 4.4 min) were used instead of 6 (half-life 6.9 min) (Table 6 and Figure 26). Our optimized photocatalytic system with the immobilized catalyst was in this way only 1.8 times slower than the slurry system (half-life 2.4 min). A difference between slurry and immobilized systems was expected, but it is known from the literature (Zertal et al., 2004) that usually the kinetics of immobilized TiO_2 systems is more than 10 times slower than the kinetics of comparable slurry systems. Moreover, our results are comparable to the most efficient laboratory scale reactors with immobilized TiO_2 (Dutta and Ray, 2004; Horikoshi et al., 2002; Zhang et al., 2004).

These results suggest that more than 12 glass slides would still enhance the disappearance rate, but it is physically almost impossible to fasten more 2 mm-thick glass slides onto the holder. However, it remains a challenge for me to further improve the configuration of the photocatalytic system by increasing the illuminated surface of the immobilized catalyst.

4.2.3.5 Comparison of photocatalytic activities between Degussa P25 and sol-gel thin films

A set of experiments with a novel photoreactor was therefore performed in order to obtain additional information on our sol-gel films. The configuration with 6 glass supports was used for this purpose. The TiO₂ thin films were deposited on both sides and the amount of TiO₂ was regulated by the number of dipping-heating cycles. Figure 27B confirms that our sol-gel films have considerably lower activity than Degussa P25 TiO₂ films. The obtained results are also in accordance with the results presented in Chapter 4.1.3.4.

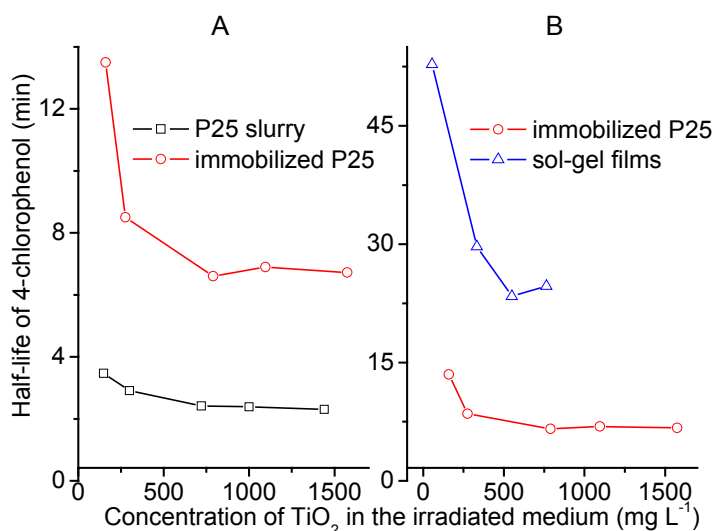


Figure 27: The influence of the amount of the irradiated catalyst on half-life of 4-chlorophenol; A: half-life in the range 0-14 min; B: half-life in the range 0-50 min; (□) the configurations from A to E in Table 1; (○) the configurations from F to J in Table 6; (△) the configurations from N to R in Table 6

Besides the physical and chemical differences in TiO₂ crystalites, one of the main reasons for the remarkable difference could again be the solid-liquid interface between the TiO₂ particles and the aqueous solution. The P25 films consisted of very slightly physically adsorbed TiO₂ aggregates (0.1 μm in diameter; the BET surface area of these aggregates is 55±12 m² g⁻¹) on glass surface. This is not a dense, adhesive structure, but rather a structure with a large contact area of TiO₂. Sol-gel deposited film had a much denser structure, individual crystallites were connected and consequently the contact area between the TiO₂ and the solution was lower. Therefore fewer holes and electrons reached the surface and the disappearance rate was slower. It was also observed that the disappearance rate increased only up to TiO₂ concentration of 550 mg L⁻¹ in sol-gel immobilized system, while in Degussa system the plateau was reached at approximately 800 mg L⁻¹. The holes and electrons, formed in deeper layers of the sol-gel prepared films were caught in the crystal lattice defects and they recombined before reaching the surface of the catalyst. This also lowered the photocatalytic activity of the catalyst. But the advantage of presented sol-gel films in comparison with Degussa films is their better adhesion to the substrate. They are not detached from the substrate during the photocatalytic experiments (spinning, washing, irradiating) and they did not lose their photocatalytic activity within our experimental period.

4.2.3.6 Suitability of the reactor for the degradation of POPs other than 4-chlorophenol

To prove the general usefulness of the constructed CTP, the degradation of different POPs with the help of 6 TiO₂ films, prepared via sol-gel method (sol C), was tested (configuration O in Table 6). The attention was paid to the chemicals, which are widely used and released into the environment and which have not been yet deeply studied in photocatalytic experiments.

Neonicotinoid insecticides represent the fastest growing class of insecticides introduced to the market since the launch of pyrethroids. Imidacloprid, the member of the first generation of neonicotinoids, is the best selling insecticide worldwide (Meienfisch et al., 1999), while thiacloprid belongs to the second generation of neonicotinoid insecticides and is replacing the members of the first generation of the neonicotinoids. Both of them are among the active substances authorised for use in plant protection products (Annex I of Council Directive 91/414/EEC). Several studies of environmental behaviour of both compounds were performed in the past (Roberts et al., 1999:107; Krohn, 2001) and it was shown that both molecules are resistant to the degradation in water by hydrolysis at neutral or acidic pH values. The photodegradation of imidacloprid resulted in the quantitative transformation of the molecule using the high pressure Hg lamp ($\lambda > 290$ nm) as a radiation source (Moza et al., 1998). Additionally, it is well-known that O₂/TiO₂/UV is an effective process for the degradation of imidacloprid (Aguera et al., 1999; Malato et al., 2001), while, to our knowledge, the photocatalytic degradation of thiacloprid in the presence of oxygen or ozone has not been studied yet. Since thiacloprid exhibits at least as high threat for the aquatic systems as imidacloprid, it is of great importance to find the effective method for its elimination from aquatic systems.

Antibiotics represent an important group of pharmaceuticals in today's medicine. In addition to the treatment of human infections, they are also used in veterinary medicine. Recently, there has been a growing interest in the presence of pharmaceutical substances in the aquatic environment (Hirsch et al., 1999). Already very low antibiotics concentration in the environment are suspected to induce resistances in bacterial strains causing a serious threat for public health as more and more infections can no longer be treated with the presently known antidotes. Sulfonamides belong to one of the most important class of antibiotics and they are often found in aqueous environment (Andreozzi et al., 2003). According to the literature, sulfamethoxazole and sulfathiazole, two members of the sulfonamides, were chosen as appropriate candidates for testing the novel CTP. While sulfathiazole has already been a subject of photocatalytic studies (Calza et al., 2004), to my knowledge no scientific publications exist about the photocatalytic degradation of the sulfamethoxazole.

Triazoles as well as the structurally related imidazole fungicides are used as clinical drugs and as agricultural pesticides, including applications for the treatment and protection of cereals, soybeans, and a variety of fruits (Roberts and Hutson, 1999). Their fungicidal effect is a result of the inhibition of cytochrome (CYP) P-450 dependent C14 demethylation of lanosterol, an intermediate in ergosterol biosynthesis (Roberts and Hutson, 1999). Myclobutanil is a moderately toxic compound in toxicity class II and it is sparingly soluble in water (142 mg L⁻¹). It degrades in aqueous solutions on exposure to light, but it is stable to hydrolysis at pH 5–9. It does not degrade under anaerobic conditions. It has medium toxicity against animals. Its LD₅₀ is 290 mg kg⁻¹ for female rats and it is not mutagenic in the Ames test (Athanasopoulos et al., 2003). Because it is widely used herbicide in European vineyards and because its photocatalytic treatment in aqueous solutions has not been reported yet, it was chosen as another compound for evaluation of the CTP.

HPLC was chosen as a method for monitoring the disappearance of parent organic molecules. Additionally, IC was chosen for determination of inorganic anions, which were generated during the degradation of organic substrate. Monitoring these anions helped me to obtain some information about the mineralization of the organic matter. Plots representing photolytic and photocatalytic disappearance and mineralization of sulfamethoxazole are included in Figure 28. The disappearance of sulfamethoxazole and consequent formation of sulphate(VI) and chloride anions followed the first-order kinetics (Figure 28), therefore the formation curves were fitted as such. Similar experiments were performed also with other selected POPs and Table 7 combines all the calculations obtained from the degradation experiments of mentioned compounds.

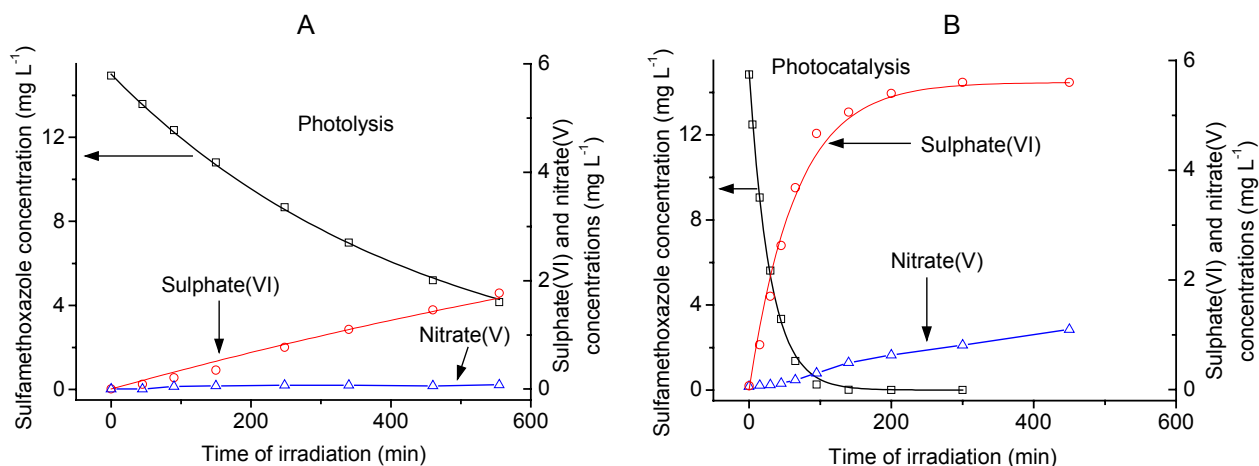


Figure 28: Photolytic (A) and photocatalytic (B) degradation and mineralization of aqueous solution of sulfamethoxazole (15 mg L^{-1})

All studied molecules were slowly degraded also under the UVA irradiation, but the kinetics of the decomposition of different compounds differed considerably (Table 7). Photolytic decomposition depends on the chemical nature of the molecules and on absorption properties of the molecules dissolved in water. Therefore the UV-Vis spectra of aqueous solutions of selected compounds (10.5 ppm) were obtained to get the information on their absorption characteristics in UVB and UVA range (Figure 29). The correlation between UV-Vis absorption properties and the kinetics of the photolytic degradation exists when the molecules with similar chemical structures are compared. For instance, imidacloprid was highly susceptible to the degradation under UVA radiation, while thiacloprid was much more photostable. Both molecules absorb radiation with the absorbance maximum in the UVC range, but the absorption spectra of the studied molecules extend far to the UVB range. The applied UVA light source emits radiation down to approx. 300 nm and this is the reason that imidacloprid as well as thiacloprid were slowly degraded within the O_2/UV process irrespective of pH. While thiacloprid has an absorbance maximum at 242 nm , imidacloprid has one at 270 nm . When exposing imidacloprid to UV radiation, the photons are more efficiently absorbed by imidacloprid and therefore faster degradation kinetics was observed for imidacloprid.

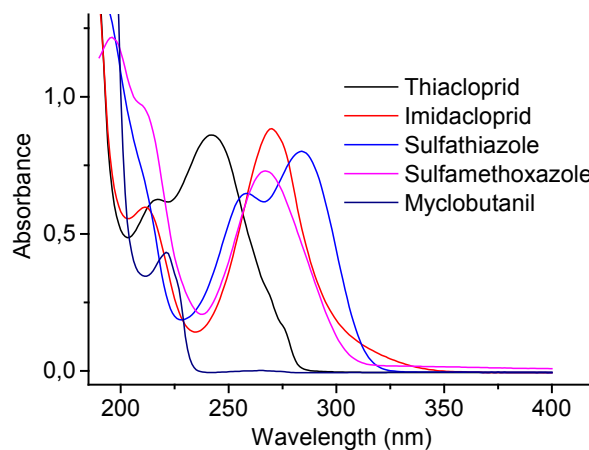
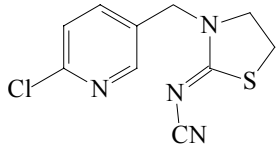
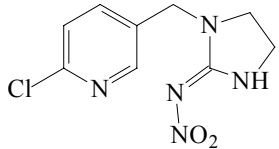
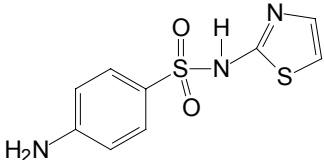
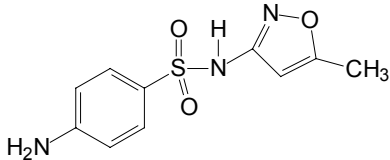
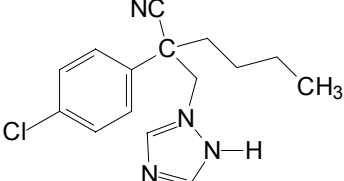


Figure 29: UV spectra of aqueous solutions (10.5 mg L^{-1}) of different POPs

The mineralization of the selected compounds followed by IC follows the same trend than decomposition of the parent compounds, but the kinetics is slower. The stoichiometric evolution of chloride, sulphate(VI)

and nitrate(V) anions were not achieved during my photolytic experiment. Nitrogen atom was more stable against the oxidation compared to the sulphur atom. The only photolytic experiment with relatively fast conversion of nitrogen to nitrate(V) was the degradation of imidacloprid. The reason is nitro group in the molecule of imidacloprid, which is relatively easy photolytically cleaved, forming nitrate(III), which is consequently oxidized to nitrate(V). The presence of nitrate(III) and its oxidation to nitrate(V) was also proven by IC. According to the photolytic degradation of selected compounds, photocatalysis as an AOP could be useful for the treatment of at least thiacloprid, which shows high photostability. But if the total mineralization is the main goal of the treatment of these molecules, the photocatalysis is the possible choice also for the other POPs.

Table 7: Chemical structures of five treated organic molecules and the results regarding their disappearance and mineralization during photocatalytic and photolytic experiments

Pollutant	Chemical structure		O ₂ /TiO ₂ /UV - Half-life (min)	O ₂ /UV - Half-life (min)
Thiacloprid		Disappearance	15.6	810
		Formation of chloride	35	>> 1000
		Formation of sulphate(VI)	50	>> 1000
		Formation of nitrate(V)	130 for 10 %	>> 1000
Imidacloprid		Disappearance	13.5	77
		Formation of chloride	33	190
		Formation of nitrate(V)	130 for 30 %	150 for 10 %
Sulfathiazole		Disappearance	13.8	510
		Formation of sulphate(VI)	33	>> 1000
		Formation of nitrate(V)	400 for 20 %	>> 1000
Sulfamethoxazole		Disappearance	20.3	300
		Formation of sulphate(VI)	45	1080
		Formation of nitrate(V)	130 for 10 %	>> 1000
Myclobutanil		Disappearance	17.5	420
		Formation of chloride	35	2000
		Formation of nitrate(V)	250 for 10 %	>> 1000

Using the described experimental procedures (configuration O from Table 6), all studied molecules were efficiently photocatalytically decomposed with the half-lives that do not differ very much from one to another. Similar rate of decomposition of the studied molecules could be assigned to the similar reactivity of the molecules toward the HO[•] attack. Comparing these half-lives with the one obtained in the photocatalytic degradation of 4-chlorophenol under the same experimental conditions (O in Table 6), the higher stability of 4-chlorophenol is noticed. This was somehow expected due to a lower number of reactive points in the molecule of 4-chlorophenol, where the reaction with HO[•] radical is possible. Also the mineralization is considerably faster in photocatalytic experiments compared to photolytic ones. The

formation of sulphate(VI) and chloride anions are quantitative in all cases, on the contrary this is not so with the oxidation of nitrogen to nitrate(V). Evidently longer irradiation times would be necessary for complete mineralization of selected compounds.

According to the presented photocatalytic experiments, the novel CTP could be used efficiently for treatment of different aqueous solutions of POPs. In order to evaluate its possible commercial applicability, also its comparison with other AOPs is a logical continuation of my research. The choice of an appropriate model compound used for desired purposes is of a great importance. According to the conclusions introduced in presented subchapter neonicotinoid pesticides (imidacloprid and thiacloprid) were chosen to deepen the knowledge on recently developed photocatalytic system.

4.2.3.7 Stability of two neonicotinoid pesticides in aqueous solutions

At first, some stability tests of thiacloprid and imidacloprid in aerated aqueous solution at different pHs were performed. Both molecules have been stable for months at neutral and acidic conditions without any hydrolysis or oxidation products (Table 8). At pHs above 9.0 decomposition of both molecules was noticed. Approximately 10 % of thiacloprid was degraded after 6 months. There is one main degradation product, which was analysed by HPLC-MS and it was found to be the molecule where the sulphur atom in thiacloprid is oxidized to sulphoxide group (m/z : 269 [M+1], 229 [M+1-(N-C≡N)], 201). No degradation as a result of hydrolysis was noticed. On the contrary, imidacloprid is susceptible for the attack of hydroxide anions, resulting in hydrolytic decomposition of the molecule at alkaline pH (Guzsvany et al., 2006). In our experiment, $t_{1/2}$ of imidacloprid was around 1.5 month at pH 10. Comparing the stabilities of both neonicotinoids in water, it is clearly concluded that thiacloprid is more stable in aqueous solution than imidacloprid, which undergoes a moderately fast hydrolytic degradation at alkaline conditions.

Table 8: Comparison of stabilities of thiacloprid and imidacloprid in aqueous solutions at different experimental conditions

Experimental conditions	Stability of the pesticide	
	Thiacloprid	Imidacloprid
Aerated H ₂ O, acidified to pH 3.5	<1 % degradation in 12 months	<1 % degradation in 12 months
Tap water (pH = 8.1)	<1 % degradation in 6 months	<1 % degradation in 6 months
Aerated H ₂ O, alkalinized to pH 10.0	10 % degradation in 6 months	$t_{1/2} = 1.5$ month
Oxygenated deionised water and UVA irradiation	$t_{1/2} = 810$ min	$t_{1/2} = 77$ min
Ozonated deionised water (the flow rate of ozone 1.5 g h ⁻¹)	$t_{1/2} = 24$ min	$t_{1/2} = 3.6$ min
Ozonated tap water (pH = 8.1, the flow rate of ozone 1.5 g h ⁻¹)	$t_{1/2} = 2.0$ min	$t_{1/2} \sim 0.6$ min

The reasons for higher photostability of thiacloprid compared to imidacloprid are explained already in Chapter 4.2.3.6. Also ozonation experiments confirmed the higher chemical stability of thiacloprid both in acidic and in neutral solutions. The $t_{1/2}$ of thiacloprid was found to be at least 4 times longer than $t_{1/2}$ of imidacloprid under the same experimental conditions.

Considering the photo- and chemical stabilities of the pesticides as one of the important parameters in determining their impact on the environment, I decided to focus further only to the degradation of the more stable thiacloprid by different AOPs.

4.2.3.8 Degradation of thiacloprid by O₃, O₃/UV, O₃/TiO₂/UV and O₂/TiO₂/UV

Configuration T from Table 6 was used in all described O₃/TiO₂/UV and O₂/TiO₂/UV experiments. The first experiments were performed with thiacloprid dissolved in deionised water. However, unbuffered solution with the initial pH of 6.2 led to gradual decrease in pH, because organic and inorganic acids were generated during the oxidative degradation of organic molecules (Oppenländer, 2003: 197). After applying any AOP for 100 min, the final pH was around 3.2. Additionally, the kinetics of all degradation processes performed in deionised water was similar (only slightly faster) compared to the kinetics obtained in diluted hydrochloric acid. This is also an indication that the pH of deionised water dropped fast after the start of the degradation experiment and the acidification of the solution resulted in slower degradation of selected compounds. According to the fact that pH decrease reduces the decomposition rate of ozone, which consequently results in lower amount of some active species as hydroxyl radicals, the low degradation efficiency of neonicotinoid pesticides in deionised water was a consistent result.

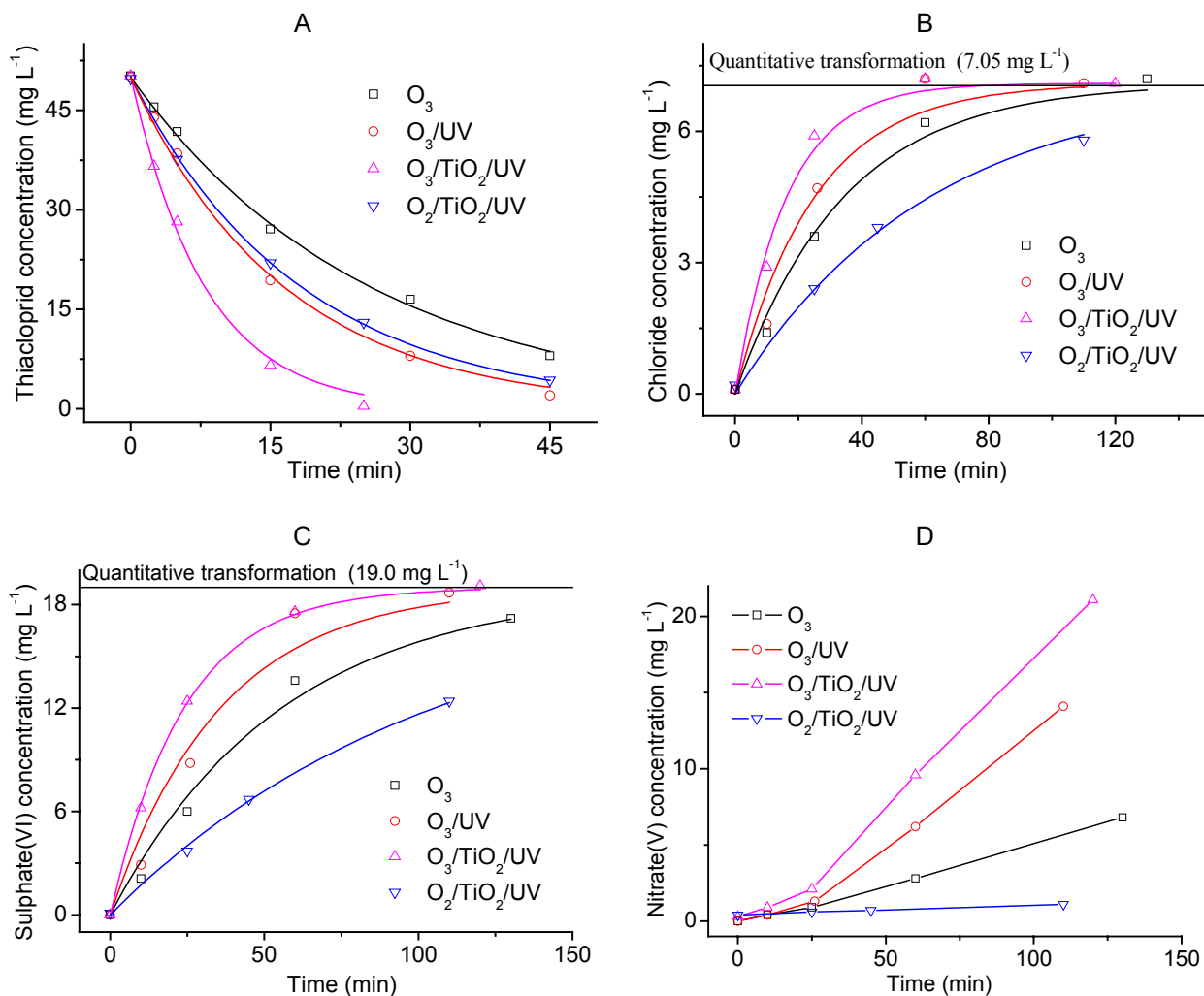


Figure 30: Degradation of thiacloprid with different AOPs at pH 8.1; A – disappearance of thiacloprid; B – formation of chloride; C – formation of sulphate(VI); D – formation of nitrate(V). The flow rate of ozone was 0.11 g h⁻¹

Subsequent experiments were therefore performed at more controlled pHs, so that the real effects of ozonation on the degradation rate could be studied. Four different initial pHs were chosen and maintained by different pH buffers/modifiers: i) pH 3.2, hydrochloric acid, ii) pH 5.6, a phosphate buffer, iii) pH 8.1,

sodium bicarbonate, iv) pH 11.0, sodium hydroxide. Both bicarbonate as well as phosphate buffers act as free radical scavengers and thus stabilize ozone or compete with water and organic molecules for hydroxyl radicals in all applied processes. This may affect the reaction rates and pathways. The second-order rate constants for the reaction between hydroxyl radicals and bicarbonate anions ($8.5 \times 10^6 \text{ L mol}^{-1} \text{ s}^{-1}$), phosphate anions ($<10^7 \text{ L mol}^{-1} \text{ s}^{-1}$), phosphoric acid ($4.2 \times 10^4 \text{ L mol}^{-1} \text{ s}^{-1}$) are at least 100 times lower compared to the rate constants with organic molecules, similar to the pollutants used in the experiments (more than $10^9 \text{ L mol}^{-1} \text{ s}^{-1}$) (Oppenländer, 2003: 180). The initial concentration of neonicotinoid pesticides in my experiments was around $2 \times 10^{-4} \text{ M}$, which is approximately 10 times lower than the concentration of bicarbonate or phosphate buffers (1.7 mM). According to the rate constants and to the concentrations of buffers and pollutants, it can be concluded that the reaction rate between hydroxyl radicals and the organic compounds should be much faster (at least 10 times) than the reaction rate between bicarbonate (phosphate) anions and hydroxyl radicals. The pH values at the end of the experiments were the following: i) 3.0, ii) 4.3, iii) 8.1 and iv) 9.6, with respect to different pH buffers/modifiers. The chosen flow rate of ozone was 0.11 g h^{-1} , because the degradation rates were easily monitored at this flow rate and the error due to the sampling was lower than in case, where the flow rate of ozone was around 1 g h^{-1} (which was found to be an optimal ozone flow rate under my experimental conditions as it is discussed in Chapter 4.2.3.9).

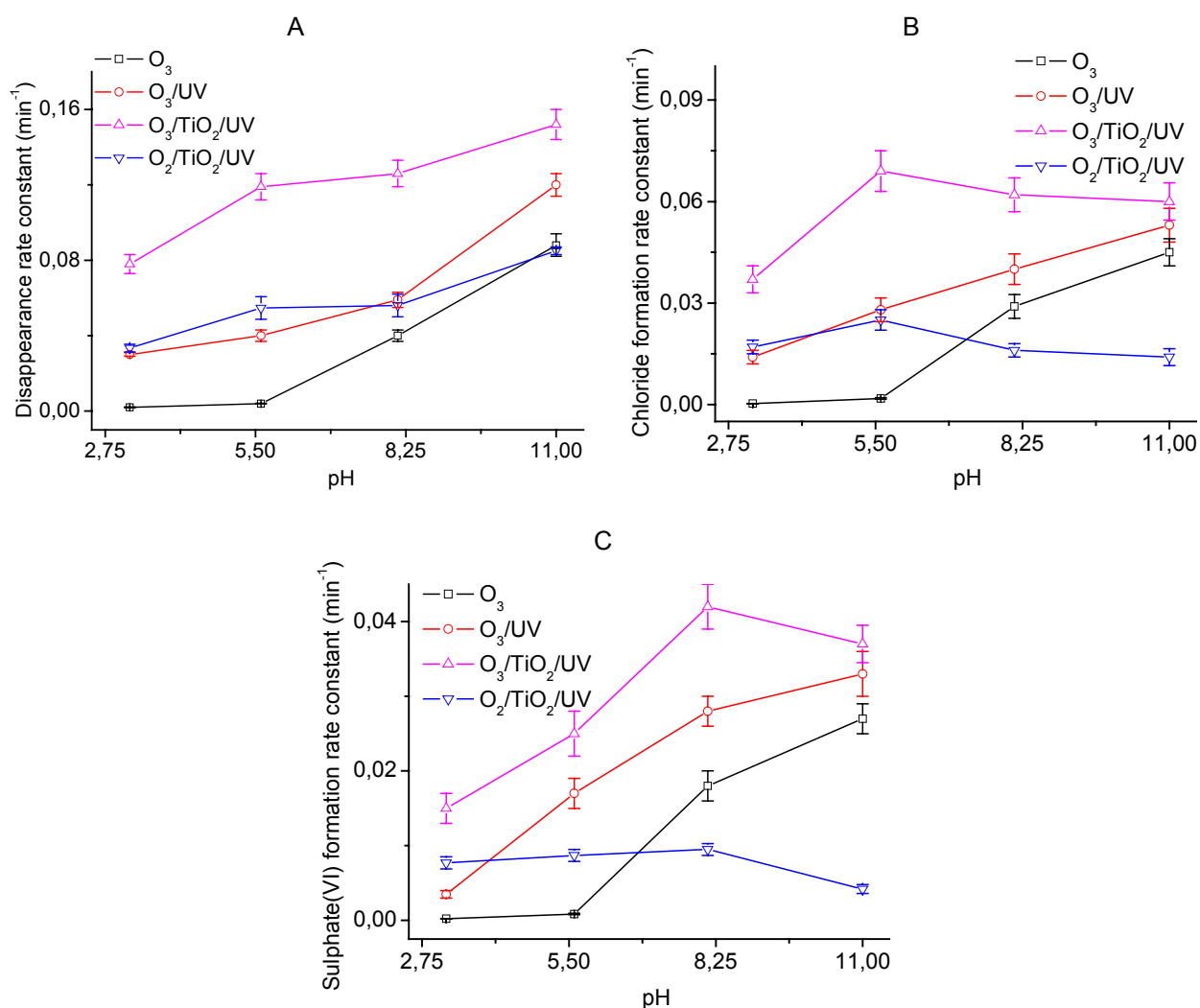


Figure 31: The influence of pH on disappearance rate constants of thiachloprid (A) and on formation rate constants of chloride (B) and sulphate(VI) (C). The flow rate of ozone was 0.11 g h^{-1}

All disappearance curves indicate first-order kinetics, therefore they were fitted as first-order reactions and disappearance rate constants were calculated. Figure 30A shows the disappearance curves for thiacloprid solution with different AOPs at pH 8.1. Similar curves were obtained also at the other pH values and the results are summarized in Figure 31A. The first noticeable characteristic is that whenever the ozone is included in the process, the degradation becomes much faster with the increase of pH. This could be easily explained by the lower stability of ozone at higher pHs, when various reactive species are produced (eqs. 4.7-4.10) and accelerate the degradation of organic molecules.

An obvious difference between O_3 and O_3/UV processes is the consequence of the photodegradation of ozone molecules by UV irradiation. Although UVA light source was used, a part of its radiation also lies between 300 and 320 nm, where ozone absorbs some of the incoming photons, leading to its degradation to atomic $O(^1D)$ and consequently to the other reactive oxygen species (eqs. 4.11 and 4.12).

It is clearly seen that irrespective of the pH of the solution, the $O_3/TiO_2/UV$ was the most efficient AOP. However, the question arises whether this is just a consequence of two independent AOPs ($O_2/TiO_2/UV + O_3/UV$) contributions or there are some synergistic effects of ozone and $O_2/TiO_2/UV$. If the sum of disappearance rate constants of $O_2/TiO_2/UV + O_3/UV$ are smaller than disappearance rate constants of $O_3/TiO_2/UV$, the synergistic effect of ozone would be easily proven. Figure 32 clearly shows that the synergistic effect was present in the pH range between 3 and 8.5, but the synergism was completely lost at higher pH values. It could also be said that the optimal pH (with the most pronounced synergistic effect) is at pH below 7, where ozone is mainly present in its molecular form, which is capable of extracting the electrons from the conduction band of TiO_2 . The total loss of synergism at more alkaline pH could be explained by faster self-decomposition of ozone, so that the actual concentration of molecular ozone in the solution is lower than the ozone dosage. The second possible reason could be also nonfavourable adsorption of ozone on titania surface at alkaline pHs.

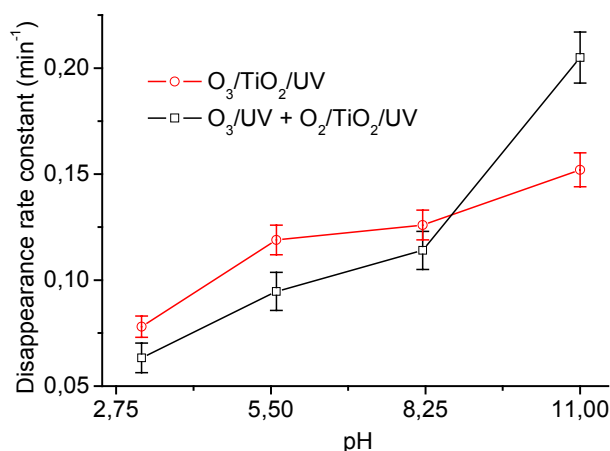


Figure 32: The influence of pH to the synergistic effect of ozone on $O_2/TiO_2/UV$. The flow rate of ozone was 0.11 g h^{-1}

IC was chosen as a method for determining inorganic anions, which were generated during the degradation of organic substrate. Monitoring these anions helped me to obtain some information about the mineralization of the organic matter. Formation curves of chloride and sulphate(VI) anions at pH 8.1 for different AOPs are presented in Figure 30B and 30C. The formation of sulphate(VI) and chloride anions followed the first-order kinetics (Figures 30B and 30C), therefore the formation curves were fitted as such. Similar curves were obtained also at the other pHs and all the results are summarised in Figure 31B and 31C. As expected, the evolution of both anions was slower than the disappearance of thiacloprid. Sulphur from thiacloprid was oxidized quantitatively to sulphate(VI) in all AOPs and no other anions containing sulphur were observed.

On the contrary, chlorine atom was first transformed to chloride in all experiments where the degradation was evident, but afterwards the oxidation of chloride anion to chlorate(V) was noticed in $O_3/TiO_2/UV$ and in O_3/UV processes at acidic pH (Figure 33A and B). It is clearly seen from Figure 33B that the concentration of chloride decreased between 25 and 110 min of irradiation, while at the same time the chlorate(V) with the retention time 9.8 min appeared. The oxidation was more efficient in $O_3/TiO_2/UV$ process and the increase of ozone dosage further accelerated the oxidation. No chlorate(V) was observed in O_3 and $O_2/TiO_2/UV$ system at similar conditions. According to my knowledge, no scientific publication that would deal with the oxidation of chloride to chlorate(V) in the presence of TiO_2 has appeared yet. The mechanism is probably similar to bromide oxidation to bromate(V) (von Gunten, 2003).

The consequences of the presence of chlorate(V) on quality of treated water could be positive or negative. This anion is not naturally present in clean surface water bodies and therefore its presence is not desired. On the other hand, in the process of disinfection of drinking water it is important to have a residual oxidant in the waterworks to protect the subsequent bacterial contamination. In the disinfection processes, where ozone is used, chlorine must be added separately to provide this protection, because ozone itself is not an appropriate choice due to its too low stability in water (Baird, 1999: 475). My experiments revealed that ozone could also be used for »in situ« production of reactive chlorine species, which could simplify the process of disinfection of drinking water.

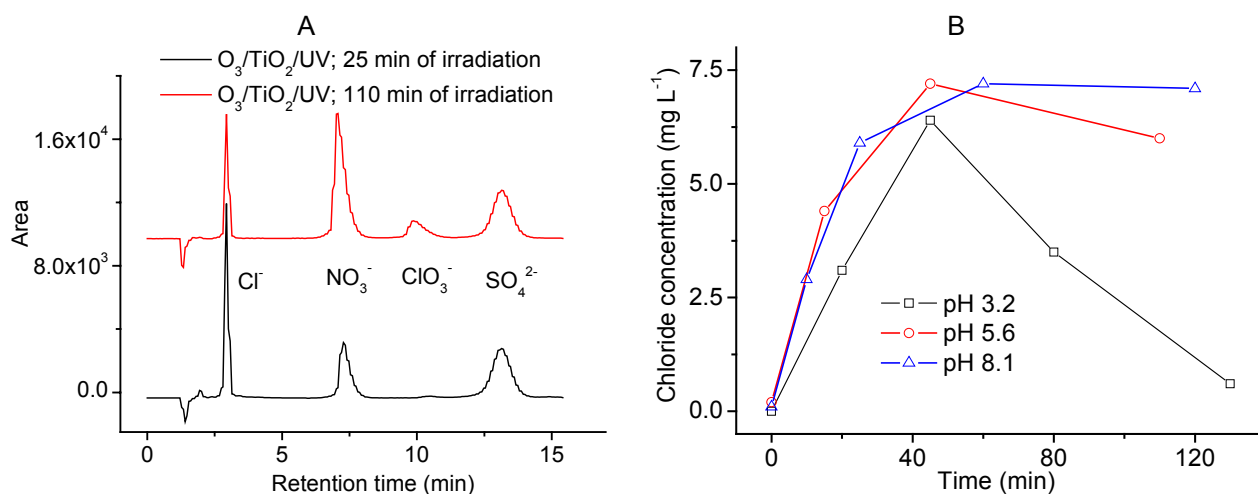


Figure 33: A: Evolution of inorganic anions from thiachloprid solution in deionised water after 25 min and 110 min of irradiation. The flow rate of ozone was 1.4 g h^{-1} . B: Evolution of chloride during the $O_3/TiO_2/UV$ at different pHs and further disappearance of chloride in acidic solution. The flow rate of ozone was 0.11 g h^{-1} .

The formation of nitrate(III) was not noticed during the experiments. The formation of nitrate(V) was a slower process than formation of chloride and sulphate(VI) and it was not formed quantitatively in any of AOP during my experiment (Figure 30D and Table 9). After 6 hours of $O_3/TiO_2/UV$ experiment with the flow rate of ozone 1.4 g h^{-1} at pH 11.0, the transformation of nitrogen to nitrate(V) was 81 % (Figure 34). The reason for not having observed the quantitative mineralization of nitrogen could also be the formation of ammonium ion (Klare et al., 1999) (which was not monitored), formation of molecular nitrogen or volatile organic compounds containing nitrogen (Karkmaz et al., 2004) (which could escape from the liquid medium to the atmosphere) or the formation of some recalcitrant nitrogen containing intermediates (Konstantinou et al., 2001). In order to get at least some information on the exposed problem, the TOC and TN measurements of the $O_3/TiO_2/UV$ experiment (the flow rate of ozone 1.4 g h^{-1} at pH 11.0) were performed. The obtained TN value fluctuated around the theoretical value of $11 \pm 0.5 \text{ mg L}^{-1}$ within 6 hours of irradiation (Figure 34). It means that all released nitrogen or nitrogen containing compounds stayed in the aqueous phase also after 6 hours of irradiation. No molecular nitrogen or volatile nitrogen containing compounds were released to the atmosphere. TOC value decreased during the degradation process from 23.7 mg L^{-1} (also a theoretical value) to 5.6 mg L^{-1} after 6 hours of irradiation (Figure 34). The decreasing

of TOC correlates well with the increasing of nitrate(V) – fast changes during first 2 hours of experiment and then slower mineralization. Obviously, the mineralization was not completed even after such long treatment. 23 % of the initial organic carbon remained in the solution. It seems that some recalcitrant molecules, some of which containing also nitrogen, were formed during the $O_3/TiO_2/UV$ treatment and the occurrence of such compounds slows down the rate of mineralization of the organic matter.

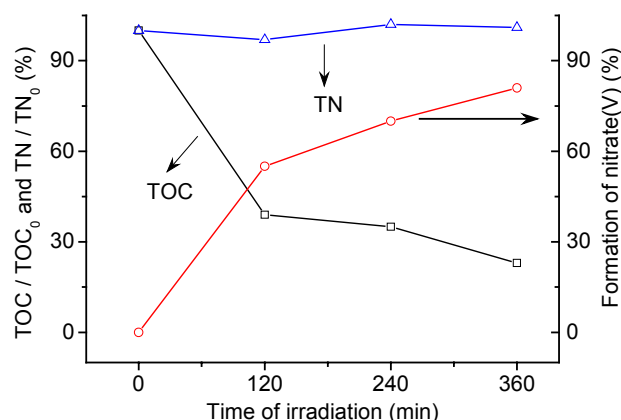


Figure 34: Monitoring of TOC, TN and evolution of nitrate(V) during the $O_3/TiO_2/UV$ treatment at $pH = 11.0$. The flow rate of ozone was $1.4 g h^{-1}$.

The cyanide anions could be also the intermediate products of degradation of thiacloprid. However, we were unable to monitor their formation by IC. Due to the fact that they are easily degraded by O_3 process (Barriga-Ordóñez et al., 2006) and also by $O_2/TiO_2/UV$ and $O_3/TiO_2/UV$ systems (Hernandez-Alonso et al., 2002) (the second-order rate constant between hydroxyl radicals and cyanide anions is $7.6 \times 10^9 L mol^{-1} s^{-1}$ (Oppenländer, 2003: 180)), we did not perform additional analyses of the monitoring of cyanide anions.

The formation of nitrate(V) did not follow the first-order kinetics. The oxidation is in all experiments slower at the beginning of the AOPs and it is accelerated in the continuation of the experiment. It seems that some intermediate molecules containing nitrogen have to be formed first. Consequently, nitrogen in the new molecules is more easily oxidized by ozone and other reactive oxygen species. We also observed that $O_2/TiO_2/UV$ process was to a great extent less efficient process for mineralization of nitrogen than the other three AOPs, which are based on ozonation. For example, at $pH 8.1$ the mineralization in $O_2/TiO_2/UV$ system was 15 times slower than in O_3/UV at $pH 8.1$ or in O_3 systems at $pH 11$, although the disappearance rates of thiacloprid in these three processes were similar. According to these findings I conclude that degradation products were more susceptible to ozone attack than the parent molecule and therefore the ozone accelerated the mineralization more than it was observed only from HPLC analysis. For example, oxidation of the primary amines (as possible degradation products) at the N-atom by ozone can lead to an increased formation of nitrate(V) (Klare et al., 1999).

Table 9: The influence of pH on formation of nitrate(V). The flow rate of ozone was $0.11 g h^{-1}$.

AOP	Time for 10 % conversion of organic nitrogen to NO_3^- (min)		
	$pH 3.2$	$pH 8.1$	$pH 11$
O_3	> 10000	96	53
O_3/UV	130	52	48
$O_3/UV/TiO_2$	47	38	37
$O_2/UV/TiO_2$	300	800	8600

In general, $O_2/TiO_2/UV$ process is not as pH dependant process as ozone based AOPs. Nevertheless, it showed approximately twice higher disappearance rate at alkaline pH compared to the acidic pH . This behaviour could depend on the type of interactions between thiacloprid molecules and the catalyst surface (Carrier et al., 2006). Thiacloprid is a neutral molecule – and within the used pH range it does not form

distinct charged species as a consequence of acid-base equilibriums. This was proven by UV-Vis spectroscopy, where the spectra of aqueous solution of thiacloprid did not change with changing the pH of the solution. It seems that negatively charged TiO_2 surface at alkaline conditions (Ti-O^-) favours the interaction between the surface and the parent molecule. On the contrary, although the disappearance rates of thiacloprid increased with the increase of pH both in $\text{O}_2/\text{TiO}_2/\text{UV}$ and $\text{O}_3/\text{TiO}_2/\text{UV}$ systems, the rate of mineralization for all three anions decreased or did not significantly change within the same experiments (Figure 31, Table 9). Intermediates which are formed from the organic molecules are more polar and often negatively charged molecules (organic acids and their anions) (Oppenländer, 2003: 197), and we suppose that the interactions between the catalyst surface and intermediates are therefore retarded. Consequently the complete oxidation to inorganic anions becomes slower at alkaline conditions. In AOPs where no TiO_2 was present, this trend was not observed.

4.2.3.9 Effect of ozone dosage on the degradation of thiacloprid

According to the literature data (Li et al., 2005; Giri et al., 2007), the increase of the ozone dosage results in more efficient degradation of organic pollutants in $\text{O}_3/\text{TiO}_2/\text{UV}$ and in O_3/UV processes. But the optimal ozone dosage was not proposed, therefore I decided to perform series of experiments aiming to get additional information about the influence of ozone dosage on the degradation rates.

The solution with pH 8.1 was chosen, because it represents the optimal pH value. At this pH, the synergistic effect of ozone on TiO_2 photocatalysis is still present (Figure 32) and on the other hand, the degradation of organic pollutants as a result of a self-decomposition of ozone is already obvious (Figures 30 and 31). Also the mineralization rate is very high at chosen conditions. Because of the dissolved bicarbonate and consequently slightly alkaline pH, such water resembles real water flowing over limestone regions.

Figure 35 shows the results of both $\text{O}_3/\text{TiO}_2/\text{UV}$ and O_3/UV processes. The linear trend is obvious in both cases, when the flow rate of ozone was below 1 g h^{-1} , indicating that both systems followed pseudo-first-order kinetics. The first-order kinetics was expected, as the concentration of ozone during the degradation experiment was constant due to continuous purging of the solution ($-\text{d}[\text{thiacloprid}]/\text{dt} = k' [\text{thiacloprid}]$, where $k' = k'' [\text{O}_3]$; $k'' =$ second-order reaction rate constant, $k' =$ pseudo-first order reaction rate constant).

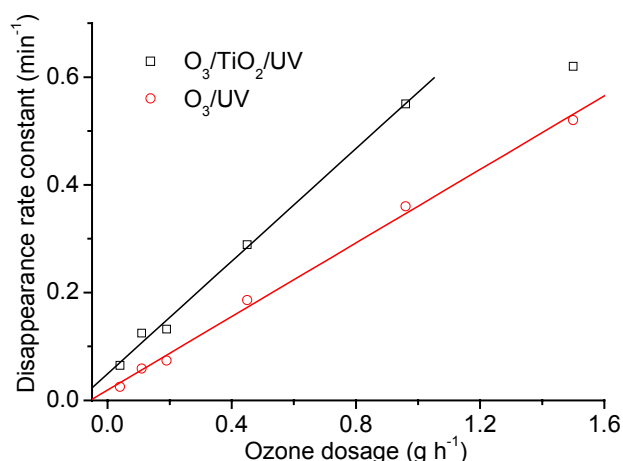


Figure 35: The influence of the flow rate of ozone on disappearance rate constants of thiacloprid at pH 8.1

The calculated slope of the fitted linear line presenting the $\text{O}_3/\text{TiO}_2/\text{UV}$ system is $0.52 \text{ h min}^{-1} \text{ g}^{-1}$, which is 1.5 times higher than in the case of O_3/UV system ($0.35 \text{ h min}^{-1} \text{ g}^{-1}$). If no synergistic effect of ozone was present, the slope would stay the same. This is another proof of the synergism between ozone and $\text{O}_2/\text{TiO}_2/\text{UV}$. According to the linear fit of $\text{O}_3/\text{TiO}_2/\text{UV}$ system kinetics, the calculated disappearance rate constant at the flow rate of ozone of 1.5 g h^{-1} should be 0.83 min^{-1} , but the experimentally obtained value

was only 0.62 min^{-1} . I explain the deviation from the linearity at the flow rates of ozone higher than 1 g h^{-1} by the fact that at this point the number of ozone molecules was already high enough to extract completely the photogenerated electrons from the catalyst surface. The additional increase of the flow rate of ozone could no longer contribute to linear increase of the disappearance reaction rate constant.

When dealing with ozone-based AOPs, the optimal flow rate of ozone could be defined in the range, where the disappearance rate per unit ozone consumption is the highest. This is not appropriate in my case because I took as a reference the $\text{O}_2/\text{TiO}_2/\text{UV}$ process, which would be the most efficient AOP according to such definition. In fact, the degradation rate is small in such system and therefore $\text{O}_2/\text{TiO}_2/\text{UV}$ process is still nowadays rarely used worldwide in real applications. On the other hand, too high flow rates of ozone (above 1 g h^{-1}) is also not the best option due to a loss of a synergism (Figure 35). Therefore the optimal flow rate of ozone lies slightly below 1 g h^{-1} , where the synergism is still fully expressed and the degradation rate is high.

There is one more point that proceeded from the measurements and is worth to be mentioned. Generally, when defining the photocatalytic activities of thin films, one of the main problems is how to separate the role of the thickness of the film (absorption characteristics) and the role of the surface (active sites) on the photocatalytic activity (Černigoj et al., 2006a, 2006b). For instance, a thick film with a low surface area shows comparable photocatalytic activity to a thin film with more active sites on the surface. The differences in slopes, when plotting the disappearance rate constants as a function of the flow rate of ozone (Figure 35) could be possibly used for characterizing different TiO_2 surfaces, independently of the film thickness (absorption characteristics). I suppose that TiO_2 with a higher surface area would result in a more pronounced effect of ozone and therefore the slope would be steeper. This kind of experiment could represent an alternative route to evaluate the availability of the catalyst surface for photocatalytic reactions (the property of a certain catalytic material, regardless of its quantity) and I keep it in mind for my future work.

5 CONCLUSIONS

The focus of my research was the improvement of the efficiency of the photocatalytic process starting from the preparation and evaluation of a new inorganic material, continuing with the design and the evaluation of a new reactor and rounding up the work with a comparison and coupling of the TiO₂ photocatalysis with other AOPs.

1. Nanostructured and transparent titania films with anatase grain sizes of as small as 10 nm were deposited on SiO₂ pre-coated soda-lime glass substrates in order to enhance their activity for the photocatalytic degradation of an azo-dye (Plasmocorinth B). The use of the templating agent in a surfactant-assisted sol-gel process reduced the number of dip coatings necessary to obtain a sufficient titania loading with a photocatalytically active surface area. Increased thickness (mass) of titania films means more efficient absorption of light and consequently a higher number of reactive species of the film capable of reacting with azo dye. The results also reveal that the surface morphology of the films depends on the templating agent used and on the substrate. The films were immersed in the colored solution and photobleaching was followed in-situ with the newly developed continuous-flow reactor. The titania catalyst can easily be removed from the solution, which is one of the principal advantages of using the immobilized films as catalysts rather than titania powders.

The usage of the surfactant in the preparation of sol-gel derived films increases the BET surface area considerably, although ordered mesoporous TiO₂ thin films were not prepared. According to the differences in BET surface area and other physico-chemical characteristics of prepared TiO₂ films it is illogical that the amount of titania is the decisive parameter defining the final photocatalytic activity. These results show the importance of careful and detailed evaluation of the new photocatalytic material, because concluding too fast often leads to misleading information, what is especially not desired in the scientific world.

My results regarding the preparation of the TiO₂ thin films on sodium glass support confirmed that sodium ions impurities had a negative influence on the crystallization of TiO₂, which is otherwise very important for photocatalysis utilizing the semiconducting properties of the material. A somehow contradictory explanation from the literature that sodium ions retard the formation of the anatase phase and increase the particle size could be interpreted in the sense that Na⁺ ions inhibit anatase crystallization and cause agglomeration of TiO₂ particles. However, investigation on my films did not give evidence that sodium ions would stimulate the crystallization of any other phase. The brookite phase was found in the thin film samples regardless of the type of the substrate. The negative influence of sodium cations could also be observed in UV spectra of prepared films, where those films deposited on sodium glass support absorb much less UV light than the films deposited on SiO₂ support.

I succeeded in evaluating the quantum yield for different photocatalytically active surfaces. The proposed method for the evaluation of photocatalytic activity based on the measuring of the fluorescence of 7OHC seems to be simple and relevant. Surprisingly, the differences in Φ_{365} between Degussa P25 and sol-gel processed films are smaller than expected. Although Degussa P25 films showed approximately 5 times higher degradation rates compared to sol-gel processed films with the same amount of the catalyst, the quantum yield of Degussa P25 was only two to three times higher. This means that the recombination of photogenerated holes and electrons is similar in all three types of the films. The phenomena could be explained by higher absorbance of Degussa P25 films per amount of the catalyst, which could be the consequence of its more crystalline structure (higher amount of anatase per amount of TiO₂) compared to my sol-gel films. According to these results it could also be concluded that the evaluation of the quantum yield is not the only relevant quantity for different photocatalytic surfaces. The main problem of calculating the quantum yield is that no information on the absorption characteristics of the material per unit of mass of the catalyst is included in the calculation. Therefore it is always important not only to define the quantum yield, but also to define the correlation between the degradation rate and the irradiated amount of the catalyst. However, some additional experiments should be done to investigate the influence of pH, photon flux and concentration of coumarin on the degradation rate and on formation rate of 7OHC.

2. A novel CTP for the photocatalytic degradation of organic molecules in water has been constructed and evaluated for the photocatalytic degradation of aqueous solutions of organic pollutants. The more glass slides (up to 12 in our experiments) with immobilized TiO_2 were incorporated in the cell, the faster was the photocatalysis (keeping all other parameters the same). The advantage of such a system compared to a classic fixed-bed system is its compactness. A very large surface of immobilized TiO_2 could be efficiently irradiated in a unit of the projected area. Another advantage is that such a reactor might be suitable for the installation in the CPCs, which are at the moment mostly reserved for TiO_2 slurries. I compared both systems (immobilized and slurry TiO_2) and when 12 slides of immobilized TiO_2 were used, the reaction rate was only 1.8 times slower than in the slurry system, which is a very promising result. We believe that with some additional improvements we can achieve a similar photocatalytic activity to the one achieved with the TiO_2 slurries.

The suitability of the novel reactor for different types of organic pollutant dissolved in water was proven. In this way five different members of pesticides, antibiotics and fungicides which photocatalytic degradation has not been yet deeply studied were treated and almost completely mineralized. Thiacloprid (the member of the neonicotinoid pesticides) was shown to be the most interesting choice for additional studies due to its wide usage as an agrochemical and its high photo- and chemical stability.

When comparing four different AOPs, the $\text{O}_3/\text{TiO}_2/\text{UV}$ is the most efficient process irrespective of pH of the thiacloprid solution. The synergistic effect of ozone on TiO_2 photocatalysis was noticed at acidic and neutral pH, but the synergism was lost at basic pH probably due to (1) the faster self-decomposition of ozone, so the actual concentration of molecular ozone in the solution was lower than the ozone dosage; (2) nonfavourable adsorption of ozone on titania surface at alkaline pH. Also the mineralization was the most efficient when the $\text{O}_3/\text{TiO}_2/\text{UV}$ process was applied. Mineralization in the $\text{O}_2/\text{TiO}_2/\text{UV}$ system was slower than in O_3/UV and $\text{O}_3/\text{TiO}_2/\text{UV}$ systems under neutral or alkaline conditions, even in cases where the disappearance rates between these processes were similar. Evidently, the degradation products were more susceptible to the attack of ozone and ozone-generated oxygen species compared to the parent molecule and therefore the mineralization was accelerated more than it was observed only from HPLC analysis.

The oxidation of chloride anions to chlorate(V) was noticed in $\text{O}_3/\text{TiO}_2/\text{UV}$ and in O_3/UV processes at acidic pH. The oxidation was more efficient in $\text{O}_3/\text{TiO}_2/\text{UV}$ process and the increase of the flow rate of ozone additionally accelerated the oxidation.

The synergistic effect of ozone was undoubtedly proven by plotting the disappearance rate constants in the $\text{O}_3/\text{TiO}_2/\text{UV}$ and O_3/UV systems as the function of ozone dosage. The slope of the linear fit of the $\text{O}_3/\text{TiO}_2/\text{UV}$ was 1.5 times steeper than the slope of the O_3/UV system. If no synergistic effect was present, no differences in slopes would be noticed. The linearity in the $\text{O}_3/\text{TiO}_2/\text{UV}$ system was lost only at very high ozone dosages. Under my experimental conditions, the optimal flow rate of ozone lies slightly below 1 g L^{-1} , where the synergism of ozone and photocatalysis is still fully expressed and the degradation rate is also high.

Some novel improvements towards achieving higher efficiency of TiO_2 photocatalysis have been shown and described throughout the thesis. In order to implement the research activities performed during my PhD, a transfer to an application scale level would round up the studied topics. I believe that such a stage has been reached, when a photocatalytic pilot plant based on the novel achievements could be designed and applied to the treatment of real contaminated waters.

6 REFERENCES

- Abdel-Aziz M.M., Yahia I.S., Wahab L.A., Fadel M., Afifi M.A. 2006. Determination and analysis of dispersive optical constant of TiO₂ and Ti₂O₃ thin films. *Applied Surface Science*, 252: 8163-8170
- Addamo M., Augugliaro V., Garcia-Lopez E., Loddo V., Marci G., Palmisano L. 2005. Oxidation of oxalate ion in aqueous suspensions of TiO₂ by photocatalysis and ozonation. *Catalysis Today*, 107-108: 612-618
- Agüera A., Almansa E., Malato S., Maldonado M.I., Fernandez-Alba A.R. 1998. Evaluation of photocatalytic degradation of imidacloprid in industrial water by GC-MS and LC-MS. *Analisis*, 26: 245-251
- Agustina T.E., Ang H.M., Vareek V.K. 2005. A review of synergistic effect of photocatalysis and ozonation on wastewater treatment. *Journal of Photochemistry and Photobiology C: Photochemical Reviews*, 6: 264-273
- Alberius P.C.A., Frindell K.L., Hayward R.C., Kramer E.J., Stucky G.D., Chmelka B.F. 2002. General predictive syntheses of cubic, hexagonal, and lamellar silica and titania mesostructured thin films. *Chemistry of Materials*, 14: 3284-3294
- Andreozzi R., Raffaele M., Nicklas P. 2003. Pharmaceuticals in STP effluents and their solar photodegradation in aquatic environment. *Chemosphere*, 50: 1319-1330
- Arabatzi I. M., Stergiopoulos T., Andreeva D., Kitova S., Neophytides S.G., Falaras P. 2003. Characterization and photocatalytic activity of Au/TiO₂ thin films for azo-dye degradation. *Journal of Catalysis*, 220: 127-135
- Asmus K.-D., Mockel H., Henglein A. 1973. Pulse radiolytic study of the site of hydroxyl radical attack on aliphatic alcohols in aqueous solution. *Journal of Physical Chemistry*, 77: 1218-1221
- Athanasopoulos P.E., Pappas C.J., Kyriakidis N.V. 2003. Decomposition of myclobutanil and triadimefon in grapes on the vines and during refrigerated storage. *Food Chemistry*, 82: 367-371
- Bahnemann D. 2004. Photocatalytic water treatment: solar energy applications. *Solar Energy*, 77: 445-459
- Bahnemann D.W., Hilgendorff M., Memming R. 1997. Charge carrier dynamics at TiO₂ particles: reactivity of free and trapped holes. *Journal of Physical Chemistry B*, 101: 4265-4275
- Baird C. 1999. *Environmental chemistry*, 2nd edition. New York, Freeman and Company
- Barriga-Ordóñez F., Nava-Alonso F., Uribe-Salas A. 2006. Cyanide oxidation by ozone in a steady-state flow bubble column. *Minerals Engineering*, 19: 117-122
- Bavcon Kralj M., Černigoj U., Franko M., Trebše P. 2007. Comparison of photocatalysis and photolysis of malathion, isomalathion, malaoxon, and commercial malathion – Products and toxicity studies. *Water Research*, in press
- Beltran F.J., Rivas F.J., Gimeno O. 2005. Comparison between photocatalytic ozonation and other oxidation processes for the removal of phenols from water. *Journal of Chemical Technology and Biotechnology*, 80: 973-984
- Bettoni M., Del Giacco T., Rol C., Sebastiani G.V. 2004. True quantum yields and adsorption constants as tools for a mechanistic study of the TiO₂-sensitized photooxidation of benzylic derivatives. *Journal of Photochemistry and Photobiology A: Chemistry*, 163: 481-487
- Bideau M., Claudel B., Dubien C., Faure L., Kazouan H. 1995. On the “immobilization” of titanium dioxide in the photocatalytic oxidation of spent waters. *Journal of Photochemistry and Photobiology A: Chemistry*, 91: 137-144
- Blanco J., Malato S., Fernandez P., Vidal A., Morales A., Trincado P., Oliveira J.C., Minero C., Musci M., Casalle C., Brunotte M., Tratzky S., Dischinger N., Funken K.-H., Sattler C., Vincent M., Collares-Pereira M., Mendes J.F., Rangel C.M. 1999. Compound parabolic concentrator technology development to commercial solar detoxification applications. *Solar Energy*, 67: 317-330
- Bosc F., Edwards D., Keller N., Keller V., Ayrál A. 2006. Mesoporous TiO₂-based photocatalysts for UV and visible light gas-phase toluene degradation. *Thin Solis Films*, 495: 272-279
- Brinker C. J., Scherer G. W. 1990. *Sol-gel science. The physics and chemistry of sol-gel processing*. London, Academic Press
- Bu S.J., Jin Z.G., Liu X.X., Yang L.R., Cheng Z.J. 2004. Synthesis of TiO₂ porous thin films by polyethylene glycol templating and chemistry of the process. *Journal of the European Ceramic Society*, 25: 673-679

- Calza P., Medana C., Pazzi M., Baiocchi C., Pelizzetti E. 2004. Photocatalytic transformations of sulphonamides on titanium dioxide. *Applied Catalysis B: Environmental*, 53: 63-69
- Carp O., Huisman C.L., Reller A. 2004. Induced reactivity of titanium dioxide. *Progress in Solid State Chemistry*, 32: 33-177
- Carrier M., Perol N., Herrmann J.-M., Bordes C., Horikoshi S., Paise J.O., Baudot R., Guillard C. 2006. Kinetics and reactional pathway of Imazapyr photocatalytic degradation: influence of pH and metallic ions. *Applied Catalysis B: Environmental*, 65: 11-20
- Chitose N., Ueta S., Seino S., Yamamoto T.A. 2003. Radiolysis of aqueous phenol solutions with nanoparticles. 1. Phenol degradation and TOC removal in solutions containing TiO₂ induced by UV, γ -ray and electron beams. *Chemosphere*, 50: 1007-1013
- Choi W., Hoffmann M.R. 1995. Photoreductive mechanism of CCl₄ degradation on TiO₂ particles and effects of electron donors. *Environmental Science and Technology*, 29: 1646-1654
- Colombo D.P., Bowman R.M. 1996. Does interfacial charge transfer compete with charge carrier recombination? A femtosecond diffuse reflectance investigation of TiO₂ nanoparticles. *Journal of Physical Chemistry*, 100: 18445-18449
- Correia V.M., Stephenson T., Judd S.J. 1994. Characterisation of textile wastewaters. A review. *Environmental Technology*, 15: 917-929
- Crepaldi E.L., Soler-Illia G.J. de A.A., Grosso D.D., Cagnol F., Ribot F., Sanchez C. 2003. Controlled formation of highly organized mesoporous titania thin films: from mesostructured hybrids to mesoporous nanoanatase TiO₂. *Journal of American Chemical Society*, 125: 9770-9786
- Černigoj U. 2005. Preparation and characterization of TiO₂ films and their applications in photodegradation of aqueous solutions of azo dyes and pharmaceuticals residues. Argumentation for the doctoral dissertation theme, Nova Gorica Polytechnic
- Černigoj U., Lavrenčič Štangar U., Trebše P. 2007a. Evaluation of a novel Carberry type photoreactor for the degradation of organic pollutants in water. *Journal of Photochemistry and Photobiology A: Chemistry*, 188: 169-176
- Černigoj U., Lavrenčič Štangar U., Trebše P. 2007b. Degradation of neonicotinoid insecticides by different advanced oxidation processes and studying the effect of ozone on TiO₂ photocatalysis. *Applied Catalysis B: Environmental*, 75: 231-240
- Černigoj U., Lavrenčič Štangar U., Trebše P., Opara Krašovec U., Gross S. 2006a. Photocatalytically active TiO₂ thin films produced by surfactant-assisted sol-gel processing. *Thin Solid Films*, 495: 327-332.
- Černigoj U., Lavrenčič Štangar U., Trebše P., Rebernik Ribič P. 2006b. Comparison of different characteristics of TiO₂ films and their photocatalytic properties. *Acta Chimica Slovenica*, 53: 29-35
- Danion A., Disdier J., Guillard C., Abdelmalek F., Jaffrezic-Renault N. 2004. Characterization and study of a single-TiO₂-coated optical fiber reactor. *Applied Catalysis B: Environmental*, 52: 213-223
- Davis R.J., Gainer J.L., O'Neal G., Wu I.-W. 1994. Photocatalytic decolorization of wastewater dyes. *Water Environment Research*, 66: 50-53
- Devipriya S., Yesodharan S. 2005. Photocatalytic degradation of pesticide contaminants in water. *Solar Energy Materials & Solar Cells*, 86: 309-348
- Dillert R., Vollmer S., Schober M., Theurich J., Bahnemann D.W., Arntz H.-J., Pahlmann K., Sager G. 1999. Photocatalytic treatment of an industrial wastewater in the double-skin sheet reactor, *Chemical Engineering & Technology*, 22: 931-934
- Ding Z., Lu G.Q., Greenfield P.F. 2000. Role of the crystallite phase of TiO₂ in heterogeneous photocatalysis for phenol oxidation in water. *Journal of Physical Chemistry B*, 104: 4815-4820
- Dionysios D.D., Balasubramanian G., Suidan M.T., Khodadoust A.P., Baudin I., Laine J.-M. 2000. Rotating disk photocatalytic reactor: development, characterization, and evaluation for the destruction of organic pollutants in water. *Water Research*, 34: 2927-2940
- Dionysios D.D., Suidan M.T., Baudin I., Laine J.-M. 2004. Effect of hydrogen peroxide on the destruction of organic contaminants - synergism and inhibition in a continuous-mode photocatalytic reactor. *Applied Catalysis B: Environmental*, 50: 259-269
- Du Y., Rabani J. 2003. The measure of TiO₂ photocatalytic efficiency and the comparison of different photocatalytic titania. *Journal of Physical Chemistry B*, 107: 11970-11978
- Dutta P.K., Ray A.K. 2004. Experimental investigation of Taylor vortex photocatalytic reactor for water purification. *Chemical Engineering Science*, 59: 5249-5259

- Emeline A., Ryabachuk V., Serpone N. 2000. Factors affecting the efficiency of a photocatalyzed process in aqueous metal-oxide dispersions: prospect of distinguishing between two kinetic models. *Journal of Photochemistry and Photobiology A: Chemistry*, 133: 89-97
- Evans P., Mantke S., Mills A., Robinson A., Sheel D.W. 2007. A comparative study of three techniques for determining photocatalytic activity. *Journal of Photochemistry and Photobiology A: Chemistry*, 188: 387-391
- Farre M.J., Franch M.I., Malato S., Ayllon J.A., Peral J., Domenech X. 2005. Degradation of some biorecalcitrant pesticides by homogeneous and heterogeneous photocatalytic ozonation. *Chemosphere*, 58: 1127-1133
- Fenton H.J.J. 1894. Oxidation of tartaric acid in the presence of iron. *Journal of Chemical Society*, 65: 899-901
- Fernandez-Ibanez P., Blanco J., Sichel C., Malato S. 2005. Water disinfection by solar photocatalysis using compound parabolic collectors. *Catalysis Today*, 101: 345-352
- Fox M.A., Dulay M.T. 1993. Heterogeneous photocatalysis. *Chemical Reviews*, 93: 341-357
- Fujishima A., Rao T.N., Tryk D.A. 2000. Titanium dioxide photocatalysis. *Journal of Photochemistry and Photobiology C: Photochemistry Reviews*, 1: 1-21
- Giri R.R., Ozaki H., Ishida T., Takanami R., Taniguchi S. 2007. Synergy of ozonation and photocatalysis to mineralize low concentration of 2,4-dichlorophenoxyacetic acid in aqueous solution. *Chemosphere*, 66: 1610-1617
- Gogate P.R., Pandit A.B. 2004. A review of imperative technologies for wastewater treatment I: oxidation technologies at ambient conditions. *Advances in Environmental Research*, 8: 501-551
- Gomes A., Fernandes E., Lima J.L.F.C. 2005. Fluorescence probes used for detection of reactive oxygen species. *Journal of Biochemical and Biophysical Methods*, 65: 45-80
- Goslich R., Dillert R., Bahnemann D.W. 1997. Solar water treatment: principles and reactors. *Water Science and Technology*, 35: 137-148
- Goswami D.Y. 1997. Chemically enhanced sunlight for killing bacteria. *Journal of Solar Energy Engineering*, 119: 101-107
- Grzechulska J., Morawski A.W. 2003. Photocatalytic labyrinth flow reactor with immobilized P25 TiO₂ bed for removal of phenol from water. *Applied Catalysis B: Environmental*, 46: 415-419
- Guillard C., Beaugiraud B., Dutriez C., Herrmann J.M., Jaffrezic H., Jaffrezic-Renault N., Lacroix M. 2002. Physicochemical properties and photocatalytic activities of TiO₂-films prepared by sol-gel methods. *Applied Catalysis B: Environmental*, 39: 331-342
- Guillard C., Debayle D., Gagnaire A., Jaffrezic H., Herrmann J.-M. 2004. Physical properties and photocatalytic efficiencies of TiO₂ films prepared by PECVD and sol-gel methods. *Materials Research Bulletin*, 39: 1445-1458
- Von Gunten U. 2003. Ozonation of drinking water: part II. Disinfection and by-product formation in presence of bromide, iodide or chlorine. *Water Research*, 37: 1469-1487
- Guzsvany V., Csanadi J., Gaal F. 2006. NMR study of the influence of pH on the persistence of some neonicotinoids in water. *Acta Chimica Slovenica*, 53: 52-57
- Haarstrick A., Kut O.M., Heinzle E. 1996. TiO₂-assisted degradation of environmentally relevant organic compounds in wastewater using a novel fluidized bed photoreactor. *Environmental Science and Technology*, 30: 817-824
- Hamill N.A., Weatherley L.R., Hardacre C. 2001. Use of a batch photocatalytic contactor for the degradation of organic pollutants in wastewater. *Applied Catalysis B: Environmental*, 30: 49-60
- Hammer M.J., Hammer M.J. (Jr.) 1996. *Water and wastewater technology*, 3rd edition. New Jersey, Prentice-hall
- Haque M.M., Muneer M., Bahnemann D.W. 2006. Semiconductor-mediated photocatalyzed degradation of a herbicide derivative, chlorotoluron, in aqueous suspensions. *Environmental Science and Technology*, 40: 4765-4770
- Hashimoto K., Irie H., Fujishima A. 2005. TiO₂ photocatalysis: a historical overview and future prospects. *Japanese Journal of Applied Physics*, 44: 8269-8285
- Hernandez-Alonso M.D., Coronado J.M., Javier Maira A., Soria J., Loddo V., Augugliaro V. 2002. Ozone enhanced activity of aqueous titanium dioxide suspensions for photocatalytic oxidation of free cyanide ions. *Applied Catalysis B: Environmental*, 39: 257-267
- Herrmann J.-M. 2005. Heterogeneous photocatalysis: state of the art and present applications. *Topics in Catalysis*, 34: 49-65

- Hirsch R., Ternes T., Haberer K., Kratz K.-L. 1999. Occurrence of antibiotics in the aquatic environment. *The Science of the Total Environment*, 225: 109-118
- Houas A., Lacheb H., Ksibi M., Elaloui E., Guillard C., Herrmann J.-M. 2001. Photocatalytic degradation pathway of methylene blue in water. *Applied Catalysis B: Environmental*, 31: 145-157
- Hoffmann A.J., Carraway E.R., Hoffmann M.R. 1994. Photocatalytic production of H₂O₂ and organic peroxides on quantum-sized semiconductor colloids. *Environmental Science and Technology*, 28: 776-785
- Hoffmann M.R., Martin S.T., Choi W., Bahnemann D.W. 1995. Environmental applications of semiconductor photocatalysis. *Chemical Reviews*, 95: 69-96
- Hoigne J., 1998. Chemistry of aqueous ozone and transformation of pollutants by ozonation and advanced oxidation processes. In: *The handbook of environmental chemistry*, Vol. 5, Part C. Hutzinger O. (ed.). Berlin, Springer-Verlag: 84-141
- Horikoshi S., Watanabe N., Onishi H., Hidaka H., Serpone N. 2002. Photodecomposition of a nonylphenol polyethoxylate surfactant in a cylindrical photoreactor with TiO₂ immobilized fiberglass cloth. *Applied Catalysis B: Environmental*, 37: 117-129
- Hu C., Tang Y., Jiang Z., Hao Z., Tang H., Wong P.K. 2003. Characterization and photocatalytic activity of noble-metal-supported surface TiO₂/SiO₂. *Applied Catalysis A: General*, 253: 389-369
- Ince N.H., Tezcanli G., Belen R.K., Apikyan I.G. 2001. Ultrasound as a catalyzer of aqueous reaction systems: the state of the art and environmental applications. *Applied Catalysis B: Environmental*, 29: 167-176
- Ireland J.C., Davila B., Moreno H. 1995. Heterogeneous photocatalytic decomposition of polyaromatic hydrocarbons over titanium dioxide. *Chemosphere*, 30: 965-984
- Ishibashi K., Fujishima A., Watanabe T., Hashimoto K. 2000. Quantum yields of active oxidative species formed on TiO₂ photocatalyst. *Journal of Photochemistry and Photobiology A: Chemistry*, 143: 139-142
- Karkmaz M., Puzenat E., Guillard C., Herrmann J.-M. 2004. Photocatalytic degradation of the alimentary azo dye amaranth. Mineralization of the azo group to nitrogen. *Applied Catalysis B: Environmental*, 51: 183-194
- Kartini I., Meredith P., Diniz da Costa J.C., Riches J.D., Lu G.Q.M. 2004. Formation of mesostructured titania thin films using isopropoxide precursors. *Current Applied Physics*, 4: 160-162
- Kaur S., Singh V. 2007. TiO₂ mediated photocatalytic degradation studies of Reactive Red 198 by UV irradiation. *Journal of Hazardous Materials*, 141: 230-236
- Klare M., Waldner G., Bauer R., Jacobs H., Broekaert J.A.C. 1999. Degradation of nitrogen containing organic compounds by combined photocatalysis and ozonation. *Chemosphere*, 38: 2013-2027
- Klug H.P., Alexander L.E. 1973. *X-Ray Diffraction Procedures*. 2nd edition. New York, John Wiley&Sons
- Konstantinou I.K., Albanis T.A. 2003. Photocatalytic transformation of pesticides in aqueous titanium dioxide suspensions using artificial and solar light: intermediates and degradation pathways. *Applied Catalysis B: Environmental*, 42: 319-335
- Konstantinou I.K., Sakellariades T.M., Sakkas V., Albanis T.A. 2001. Photocatalytic degradation of selected s-triazine herbicides and organophosphorus insecticides over aqueous TiO₂ suspensions. *Environmental Science and Technology*, 35: 398-405
- Kopf P., Gilbert E., Eberle S.H. 2000. TiO₂ photocatalytic oxidation of monochloroacetic acid and pyridine: influence of ozone. *Journal of Photochemistry and Photobiology A: Chemistry*, 136: 163-168
- Kormali P., Triantis T., Dimotikali D., Hiskia A., Papaconstantinou E. 2006. On the photooxidative behaviour of TiO₂ and PW₁₂O₄₀³⁻: OH radicals versus holes. *Applied Catalysis B: Environmental*, 68: 139-146
- Kormann C., Bahnemann D.W., Hoffmann M.R. 1991. Photolysis of chloroform and other organic molecules in aqueous titanium dioxide suspensions. *Environmental Science and Technology*, 25: 494-500
- Krohn J. 2001. Behaviour of thiacloprid in the environment. *Planzenschutz-Nachrichten Bayer*, 54: 281-290
- Kuznetsova I.N., Blaskov V., Stambolova I., Znaidi L., Kanaev A. 2005. TiO₂ pure phase brookite with preferred orientation, synthesized as a spin-coated film. *Materials Letters*, 59: 3820-3823
- Lavrenčič Štangar U., Černigoj U., Trebše P., Maver K., Gross S. 2006. Photocatalytic TiO₂ coatings: effect of substrate and template. *Monatshefte für Chemie*, 137: 647-655

- Lawton L.A., Robertson P.K.J., Cornish B.J.P.A., Jaspars M. 1999. Detoxification of microcystins (cyanobacterial hepatotoxins) using TiO₂ photocatalytic oxidation. *Environmental Science and Technology*, 33: 771-775
- Legrini O., Oliveros E., Braun M. 1993. Photochemical processes for water treatment. *Chemical Reviews*, 93: 671-698
- Levec J., Pintar A. 1995. Catalytic oxidation of aqueous solutions of organics. An effective method for removal of toxic pollutants from waste waters. *Catalysis Today*, 24: 51-58
- Levenspiel O. 1999. *Chemical reaction engineering*. 3rd edition. New York, John Wiley & Sons
- Li D., Guo Y., Hu C., Jiang C., Wang E. 2004. Preparation, characterization and photocatalytic property of the PW₁₁O₃₉⁷⁻/TiO₂ composite films towards azo-dye degradation. *Journal of Molecular Catalysis A: Chemical*, 207: 183-193
- Li L., Zhu W., Chen L., Zhang P., Chen Z. 2005. Photocatalytic ozonation of dibutyl phthalate over TiO₂ film. *Journal of Photochemistry and Photobiology A: Chemistry*, 175: 172-177
- Li Puma G., Yue P.L. 2001. The modeling of a fountain photocatalytic reactor with a parabolic profile. *Chemical Engineering Science*, 56: 721-726
- Liu X., Jin Z., Bu S., Yin T. 2005. Influences of solvent on properties of TiO₂ porous films prepared by a sol-gel method from the system containing PEG. *Journal of Sol-Gel Science and Technology*, 36: 103-111
- Litter M.I. 2005. Introduction to photochemical advanced oxidation processes for water treatment. In: *Environmental photochemistry. Part II*. Boule P., Bahnemann D.W., Robertson P. (eds.). Berlin Heidelberg, Springer-Verlag: 325-366
- Louit G., Foley S., Cabillic J., Coffigny H., Taran F., Valleix A., Renault J.P., Pin S. 2005. The reaction of coumarin with the OH radical revisited: hydroxylation product analysis determined by fluorescence and chromatography. *Radiation Physics and Chemistry*, 72: 119-124
- Malato S., Blanco J., Alarcon D.C., Maldonado M.I., Fernandez-Ibanez P., Gernjak W. 2007. Photocatalytic decontamination and disinfection of water with solar collectors. *Catalysis Today*, 122: 137-149
- Malato S., Blanco J., Vidal A., Richter C. 2002. Photocatalysis with solar energy at a pilot-plant scale: an overview. *Applied Catalysis B: Environmental*, 37: 1-15
- Malato S., Caceres J., Agüera A., Mezcuca M., Hernando D., Vial J., Fernandez-Alba A.R. 2001. Degradation of imidacloprid in water by photo-Fenton and TiO₂ photocatalysis at a solar pilot plant: a comparative study. *Environmental Science and Technology*, 35: 4359-4366
- Maness P.-C., Smolinski S., Blake D.M., Huang Z., Wolfrum E.J., Jacoby W.A. 1999. Bactericidal activity of photocatalytic TiO₂ reaction: toward an understanding of its killing mechanism. *Applied and Environmental Microbiology*, 65: 4094-4098
- Mao Y., Schoneich C., Asmus K.D. 1991. Identification of organic acids and other intermediates in oxidative degradation of chlorinated ethanes on titania surfaces en route to mineralization: a combined photocatalytic and radiation chemical study. *Journal of Physical Chemistry*, 95: 10080-10089
- Marci G., Addamo M., Augugliaro V., Coluccia S., Garcia-Lopez E., Loddo V., Martra G., Palmisano L., Schiavello M. 2003. Photocatalytic oxidation of toluene on irradiated TiO₂: comparison of degradation performance in humidified air, in water and in water containing a zwitterionic surfactant. *Journal of Photochemistry and Photobiology A: Chemistry*, 160: 105-114
- Martyanov I.N., Klabunde K.J. 2004. Comparative study of TiO₂ particles in powder form and as a thin nanostructured film on quartz. *Journal of Catalysis*, 225: 408-416
- Marugan J., Hufschmidt D., Lopez-Munoz M.-J., Selzer V., Bahnemann D. 2006. Photonic efficiency for methanol photooxidation and hydroxyl radical generation on silica-supported TiO₂ photocatalysts. *Applied Catalysis B: Environmental*, 62: 201-207
- Maurino V., Minero C., Pelizzetti E., Piccinini P., Serpone N., Hidaka H. 1997. The fate of organic nitrogen under photocatalytic conditions: degradation of nitrophenols and aminophenols on irradiated TiO₂. *Journal of Photochemistry and Photobiology A: Chemistry*, 109: 171-176
- Meienfisch P., Brandl F., Kobel W., Rindlisbacher A., Senn R. 1999. *Nicotinoid insecticides and nicotin acetylcholine receptor*. Tokyo, Springer
- Mills A., Davies R., Worsley D. 1993. Water purification by semiconductor photocatalysis. *Chemical Society Reviews*, 417-425
- Mills A., Le Hunte S. 1997. An overview of semiconductor photocatalysis. *Journal of Photochemistry and Photobiology A: Chemistry*, 108: 1-35

- Mills A., Lepre A., Elliott N., Bhopal S., Parkin I.P., O'Neill S.A. 2003. Characterisation of the photocatalyst Pilkington Activ™: a reference film photocatalyst? *Journal of Photochemistry and Photobiology A: Chemistry*, 160: 213-224
- Mills A., Elliott N., Parkin I.P., O'Neill S.A., Clark R.J. 2002. Novel TiO₂ CVD films for semiconductor photocatalysis. *Journal of Photochemistry and Photobiology A: Chemistry*, 151: 171-179
- Minabe T., Tryk D.A., Sawunyama P., Kikuchi Y., Hashimoto K., Fujishima A. 2000. TiO₂-mediated photodegradation of liquid and solid organic compounds. *Journal of Photochemistry and Photobiology A: Chemistry*, 137: 53-62
- Minero C., Vione D. 2006. A quantitative evaluation of the photocatalytic performance of TiO₂ slurries. *Applied Catalysis B: Environmental*, 67: 257-269
- Moza P.N., Hustert K., Feicht E., Kettrup A. 1998. Photolysis of imidacloprid in aqueous solution. *Chemosphere*, 36: 497-502
- Mozia S., Tomaszewska M., Morawski A.W. 2005. A new photocatalytic membrane reactor (PMR) for removal of azo-dye Acid Red 18 from water. *Applied Catalysis B: Environmental*, 59: 131-137
- Mukherjee P.S., Ray A.K., 1999. Major challenges in the design of a large-scale photocatalytic reactor for water treatment. *Chemical Engineering and Technology*, 22: 253-260
- Muller T.S., Sun Z., Kumar M.P. G., Itoh K., Murabayashi M. 1998. The combination of photocatalysis and ozonolysis as a new approach for cleaning 2,4-dichlorophenoxyacetic acid polluted water. *Chemosphere*, 36: 2043-2055
- Muneer M., Bahnmann D.W. 2002. Semiconductor-mediated photocatalyzed degradation of two selected pesticide derivatives, terbacil and 2,4,5-tribromoimidazole, in aqueous suspension. *Applied Catalysis B: Environmental*, 36: 95-111
- Murov S.L., Carmichael I., Hug G.L. 1993. *Handbook of photochemistry*, 2nd edition. New York, Marcel Dekker Inc.
- Nam H.J., Amemiya T., Murabayashi M., Itoh K. 2004. Photocatalytic activity of sol-gel TiO₂ thin films on various kinds of glass substrates: the effects of Na⁺ and primary particle size. *Journal of Physical Chemistry B*, 108: 8254-8259
- Navntoft C., Araujo P., Litter M.I. Apella M.C., Fernandez D., Puchulu M.E., Hidalgo M.V., Blesa M.A. 2007. Field tests of the solar water detoxification SOLWATER reactor in Los Pereyra, Tucumán, Argentina. *Journal of Solar Energy Engineering*, 129: 127-134
- Nelson R.J., Flakker C.L., Muggli D.S. 2007. Photocatalytic oxidation of methanol using titania-based fluidized beds. *Applied Catalysis B: Environmental*, 69: 189-195
- Newton G.L., Milligan J.R. 2006. Fluorescence detection of hydroxyl radicals. *Radiation Physics and Chemistry*, 75, 473-478
- Neyens E., Baeyens J. 2003. A review of classic Fenton's peroxidation as an advanced oxidation technique. *Journal of Hazardous Materials*, B98: 33-50
- Nohara K., Hidaka H., Pelizzetti E., Serpone N. 1997. Processes of formation of NH₄⁺ and NO₃⁻ ions during the photocatalyzed oxidation of N-containing compounds at the titania/water interface. *Journal of Photochemistry and Photobiology A: Chemistry*, 102: 265-272
- Nosaka, Y., Ohta N., Miyama H. 1990. Photochemical kinetics of ultrasmall semiconductor particles in solution: effect of size on the quantum yield of electron transfer. *Journal of Physical Chemistry*, 94: 3752-3755
- Obana H., Okihashi M., Akutsu K., Kitagawa Y., Hori S. 2003. Determination of neonicotinoid pesticide residues in vegetables and fruits with solid phase extraction and liquid chromatography mass spectrometry. *Journal of Agricultural and Food Chemistry*, 51: 2501-2505
- Ohko Y., Hashimoto K., Fujishima A. 1997. Kinetics of photocatalytic reactions under extremely low-intensity UV illumination on titanium dioxide thin films. *Journal of Physical Chemistry A*, 101: 8057-8062
- Ollis D.F. 2004. Kinetics of liquid phase photocatalyzed reactions: an illuminating approach. *Journal of Physical Chemistry B*, 109: 2439-2444
- Oppenlander T. 2003. *Photochemical purification of water and air. Advanced oxidation processes (AOPs): principles, reaction mechanisms, reactor concepts.* Weinheim, Wiley-VCH
- Parra S., Stanca S.E., Guasaquillo I., Thampi K.R. 2004. Photocatalytic degradation of atrazine using suspended and supported TiO₂. *Applied Catalysis B: Environmental*, 51: 107-116

- Paz Y., Heller A. 1997. Photo-oxidatively self-cleaning transparent titanium dioxide films on soda lime glass: the deleterious effect of sodium contamination and its prevention. *Journal of Materials Research*, 12: 2759-2766
- Peill N.J., Bourne L., Hoffmann M.R. 1997. Iron(III)-doped Q-sized TiO₂ coatings in a fiber-optic cable photochemical reactor. *Journal of Photochemistry and Photobiology A: Chemistry*, 108: 221-228
- Perret A. 1926. Zinc oxide, a photochemical sensitizer. *Journal de Chimie Physique et de Physico-Chimie Biologique*, 23: 97-129
- Peterson M.W., Turner J.A., Nozik A.J. 1991. Mechanistic studies of the photocatalytic behavior of titania: particles in a photoelectrochemical slurry cell and the relevance to photodetoxification reactions. *Journal of Physical Chemistry*, 95: 221-225
- Piccinini P., Minero C., Vincenti M., Pelizzetti E. 1997. Photocatalytic mineralization of nitrogen-containing benzene derivatives. *Catalysis Today*, 39: 187-195
- Pirkanniemi K., Sillanpaa M. 2002. Heterogeneous water phase catalysis as an environmental application: a review. *Chemosphere*, 48: 1047-1060.
- Pruden A.L., Ollis D.F. 1983. Photoassisted heterogeneous catalysis: the degradation of trichloroethylene in water. *Journal of Catalysis*, 82: 404-417
- Rampaul A., Parkin I.P., O'Neill S.A., DeSouza J., Mills A., Elliott N. 2003. Titania and tungsten doped titania thin films on glass; active photocatalysts. *Polyhedron*, 22: 35-44
- Ray A.K., Beenackers A.A.C.M. 1998. Development of a new photocatalytic reactor for water purification. *Catalysis Today* 40: 73-83
- Rincon A.G., Pulgarin C. 2004. Effect of pH, inorganic ions, organic matter and H₂O₂ on E. coli K12 photocatalytic inactivation by TiO₂: implications in solar water disinfection. *Applied Catalysis B: Environmental*, 51: 283-302
- Roberts T.R., Hutson D.H., Jewess P.J., Lee P.W., Nicholls P.H., Plimmer J.R. 1999. Metabolic pathways of agrochemicals. Part 2: insecticides and fungicides. Cambridge, The royal society of chemistry
- Robertson K.J., Bahnemann D.W., Robertson J.M.C., Wood F. 2005. Photocatalytic detoxification of water and air. In: *Environmental photochemistry. Part II*. Boule P., Bahnemann D.W., Robertson P. (eds.). Berlin Heidelberg, Springer-Verlag: 367-423
- Saaduon L., Ayllón J.A., Jiménez-Becerril J., Peral J., Domènech X., Rodríguez-Clemente R. 1999. 1,2-diolates of titanium as suitable precursors for the preparation of photoactive high surface titania. *Applied Catalysis B: Environmental*, 21: 269-277
- Salinaro A., Emeline A.V., Zhao J., Hidaka H., Ryabchuk V.K., Serpone N. 1999. Terminology, relative photonic efficiencies and quantum yields in heterogeneous photocatalysis. Part II: experimental determination of quantum yields. *Pure and Applied Chemistry*, 71: 321-335
- Sanchez L., Peral J., Domenech X. 1998. Aniline degradation by combined photocatalysis and ozonation. *Applied Catalysis B: Environmental*, 19: 59-65
- Sclafani A., Hermann J.-M. 1996. Comparison of the photoelectronic and photocatalytic activities of various anatase and rutile forms of titania in pure liquid organic phases and in aqueous solutions. *Journal of Physical Chemistry*, 100: 13655-13661
- Serpone N., Lawless D., Khairutdinov R., Pelizzetti E. 1995. Subnanosecond relaxation dynamics in TiO₂ colloidal sols (particle sizes R_p = 1.0-13.4 nm). Relevance to heterogeneous photocatalysis. *Journal of Physical Chemistry*, 99: 16655-16661
- Serpone N. 1997. Relative photonic efficiencies and quantum yields in heterogeneous photocatalysis. *Journal of Photochemistry and Photobiology A: Chemistry*, 104: 1-12
- Serpone N., Salinaro A. 1999. Terminology, relative photonic efficiencies and quantum yields in heterogeneous photocatalysis. Part I: suggested protocol. *Pure and Applied Chemistry*, 71: 303-320
- Shang J., Yao W., Zhu Y., Wu N. 2004. Structure and photocatalytic performances of glass/SnO₂/TiO₂ interface composite film. *Applied Catalysis A: General*, 257: 25-32
- Sichel C., Blanco J., Malato S. Fernández-Ibáñez P. 2007. Effects of experimental conditions on E. coli survival during solar photocatalytic water disinfection. *Journal of Photochemistry and Photobiology A: Chemistry*, in press
- Siffert B., Metzger J. 1991. Study of the interaction of titanium dioxide with cellulose fibers in an aqueous medium. *Colloids and Surfaces*, 53: 79-99
- Sonawane R.S., Kale B.B., Dongare M.K. 2004. Preparation and photocatalytic activity of Fe-TiO₂ thin films prepared by sol-gel coating. *Materials Chemistry and Physics*, 85: 52-57

- Sreemany M., Sen S. 2004. A simple spectrophotometric method for determination of the optical constants and band gap energy of multiple layer TiO₂ thin films. *Materials Chemistry and Physics*, 83: 169-177
- Stathatos E., Tsiourvas D., Lianos P. 1999. Titanium dioxide films made from reverse micelles and their use for the photocatalytic degradation of adsorbed dyes. *Colloids and Surfaces A: Physicochemical and Engineering Aspects*, 149: 49-56
- Stefan M.I., Bolton J.R. 1999. Reinvestigation of the acetone degradation mechanism in dilute aqueous solution by the UV/H₂O₂ process. *Environmental Science and Technology*, 33: 870-873
- Stylidi M., Kondarides I., Verykios X.E. 2002. Pathways of solar light-induced photocatalytic degradation of azo dyes in aqueous TiO₂ suspensions. *Applied Catalysis B: Environmental*, 125: 1-16
- Tanaka K., Capule M.F.V., Hisanaga T. 1991. Effect of crystallinity of TiO₂ on its photocatalytic action. *Chemical Physics Letters*, 187: 73-76
- Taras M.J., Greenberg A.E., Hoak R.D., Rand M.C. 1974. Standard methods for the examination of water and wastewater. Washington, American Public Health Association
- Theurich J., Lindner M., Bahnemann D.W. 1996. Photocatalytic degradation of 4-chlorophenol in aerated aqueous titanium dioxide suspensions: a kinetic and mechanistic study. *Langmuir*, 12: 6368-6376
- Tong S., Xie D., Wei H., Liu W. 2005. Degradation of sulfosalicylic acid by O₃/UV, O₃/TiO₂/UV and O₃/V-O/TiO₂: a comparative study. *Ozone Science and Engineering*, 27: 233-238
- Topalov A.S., Šojić D.V., Molnar-Gabor D.A., Abramović B.F., Čomor M.I. 2004. Photocatalytic activity of synthesized nanosized TiO₂ towards the degradation of herbicide mecoprop. *Applied Catalysis B: Environmental*, 54: 125-133
- Trapalis C.C., Keivanidis P., Kordas G., Zaharescu M., Crisan M., Szatvanyi A., Gartner M. 2003. TiO₂(Fe³⁺) nanostructured thin films with antibacterial properties. *Thin Solid Films*, 433: 186-190
- Turchi C., Ollis D.F. 1990. Photocatalytic degradation of organic water contaminants: mechanisms involving hydroxyl radical attack. *Journal of Catalysis*, 122: 178-192
- Vidal A., Diaz A.I., El Hraiki A., Romero M., Muguruza I., Senhaji F., Gonzales J. 1999. Solar photocatalysis for detoxification and disinfection of contaminated water: pilot plant studies. *Catalysis Today*, 54: 283-290
- Villarreal T.L., Gomez R., Gonzales M., Salvador P. 2004. A kinetic model for distinguishing between direct and indirect interfacial hole transfer in the heterogeneous photooxidation of dissolved organics on TiO₂ nanoparticle suspensions. *Journal of Physical Chemistry B*, 108: 20278-20290
- Wang C.-Y., Pagel R., Bahnemann D.W., Dohrmann J.K. 2004. Quantum yield of formaldehyde formation in the presence of colloidal TiO₂-based photocatalysts: effect of intermittent illumination, platinization, and deoxygenation. *Journal of Physical Chemistry B*, 108: 14082-14092
- Wang C.-Y., Rabani J., Bahnemann D.W., Dohrmann J. 2002. Photonic efficiency and quantum yield of formaldehyde formation from methanol in the presence of various TiO₂ photocatalysts. *Journal of Photochemistry and Photobiology A: Chemistry*, 148: 169-176
- Wang S., Shiraishi F., Nakano K. 2002. A synergistic effect of photocatalysis and ozonation on decomposition of formic acid in an aqueous solution. *Chemical Engineering Journal*, 87: 261-271
- Wiszniewski J., Robert D., Surmacz-Górska J., Miksch K., Malato S., Weber J.-V. 2004. Solar photocatalytic degradation of humic acids as a model of organic compounds of landfill leachate in pilot-plant experiments: influence of inorganic salts. *Applied Catalysis B: Environmental*, 33: 127-137
- Yan X., Ohno T., Nishijima K., Abu R., Ohtani B. 2006. Is methylene blue an appropriate substrate for a photocatalytic activity test? A study with visible-light responsive titania. *Chemical Physics Letters*, 429: 606-610
- Yang Y., Li X.-J., Chen J.-T., Wang L.-Y. 2004. Effect of doping mode on the photocatalytic activities of Mo/TiO₂. *Journal of Photochemistry and Photobiology A: Chemistry*, 163: 517-522
- Yatmaz H.C., Wallis C., Howarth C.R. 2001. The spinning disc reactor – studies on a novel TiO₂ photocatalytic reactor. *Chemosphere*, 42: 397-403
- Yoshitake H., Sugihara T., Tatsumi T. 2002. Preparation of wormhole-like mesoporous TiO₂ with an extremely large surface area and stabilization of its surface by chemical vapor deposition. *Chemistry of Materials*, 14: 1023-1029
- Yoshiya K., Shin-ya M., Hiroshi K., Bunsho O. 2002. Design, preparation and characterization of highly active metal oxide photocatalysts. In: *Photocatalysis: science and technology*. Kaneko M., Okura I. (eds.). Berlin Heidelberg New York, Springer-Verlag: 29-49

- Yu J.C., Wang X., Fu X. 2004. Pore-wall chemistry and photocatalytic activity of mesoporous titania molecular sieve films. *Chemistry of Materials*, 16: 1523-1530
- Yu J., Zhao X., Zhao Q. 2001. Photocatalytic activity of nanometer TiO₂ thin films prepared by the sol-gel method. *Materials Chemistry and Physics*, 69: 25-29
- Yu J.C., Yu J., Zhao J. 2002. Enhanced photocatalytic activity of mesoporous and ordinary TiO₂ thin films by sulfuric acid treatment. *Applied Catalysis B: Environmental*, 36: 31-43
- Yun H., Mijazawa K., Honma I., Zhou H., Kuwabara M. 2003. Synthesis of semicrystallized mesoporous TiO₂ thin films using triblock copolymer templates. *Materials Science and Engineering C*, 23: 487-494
- Zertal A., Molnar-Gabor D., Malouki M.A., Sehili T., Boule P. 2004. Photocatalytic transformation of 4-chloro-2-methylphenoxyacetic acid (MCPA) on several kinds of TiO₂. *Applied Catalysis B: Environmental*, 49: 83-89
- Zhang Z., Anderson W.A., Moo-Young M. 2004. Experimental analysis of a corrugated plate photocatalytic reactor. *Chemical Engineering Journal*, 99: 145-152
- Zhang Z.B., Wang C.C., Zakaria R., Ying J.Y. 1998. Role of particle size in nanocrystalline TiO₂-based photocatalysts. *Journal of Physical Chemistry B*, 102: 10871-10878